NASA/CR-2003-212169

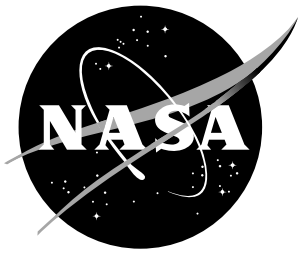

Advanced Energetics for Aeronautical Applications

David S. Alexander
MSE Technology Applications, Inc., Butte, Montana

February 2003

The NASA STI Program Office . . . in Profile

Since its founding, NASA has been dedicated to the advancement of aeronautics and space science. The NASA Scientific and Technical Information (STI) Program Office plays a key part in helping NASA maintain this important role.

The NASA STI Program Office is operated by Langley Research Center, the lead center for NASA's scientific and technical information. The NASA STI Program Office provides access to the NASA STI Database, the largest collection of aeronautical and space science STI in the world. The Program Office is also NASA's institutional mechanism for disseminating the results of its research and development activities. These results are published by NASA in the NASA STI Report Series, which includes the following report types:

- TECHNICAL PUBLICATION. Reports of completed research or a major significant phase of research that present the results of NASA programs and include extensive data or theoretical analysis. Includes compilations of significant scientific and technical data and information deemed to be of continuing reference value. NASA counterpart of peer-reviewed formal professional papers, but having less stringent limitations on manuscript length and extent of graphic presentations.

- TECHNICAL MEMORANDUM. Scientific and technical findings that are preliminary or of specialized interest, e.g., quick release reports, working papers, and bibliographies that contain minimal annotation. Does not contain extensive analysis.

- CONTRACTOR REPORT. Scientific and technical findings by NASA-sponsored contractors and grantees.

- CONFERENCE PUBLICATION. Collected papers from scientific and technical conferences, symposia, seminars, or other meetings sponsored or co-sponsored by NASA.

- SPECIAL PUBLICATION. Scientific, technical, or historical information from NASA programs, projects, and missions, often concerned with subjects having substantial public interest.

- TECHNICAL TRANSLATION. English-language translations of foreign scientific and technical material pertinent to NASA's mission.

Specialized services that complement the STI Program Office's diverse offerings include creating custom thesauri, building customized databases, organizing and publishing research results ... even providing videos.

For more information about the NASA STI Program Office, see the following:

- Access the NASA STI Program Home Page at ***http://www.sti.nasa.gov***

- E-mail your question via the Internet to help@sti.nasa.gov

- Fax your question to the NASA STI Help Desk at (301) 621-0134

- Phone the NASA STI Help Desk at (301) 621-0390

- Write to:
  NASA STI Help Desk
  NASA Center for AeroSpace Information
  7121 Standard Drive
  Hanover, MD 21076-1320

NASA/CR-2003-212169

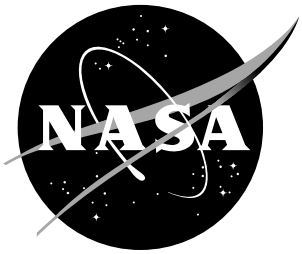

Advanced Energetics for Aeronautical Applications

David S. Alexander
MSE Technology Applications, Inc., Butte, Montana

National Aeronautics and
Space Administration

Langley Research Center
Hampton, Virginia 23681-2199

Prepared for Langley Research Center
under Grant NAG1-02048

February 2003

Acknowledgments

The author would like to extend his appreciation to those who have contributed to this report.

In particular, these include, at NASA Langley Research Center, Dennis Bushnell for his vision and leadership and Mark Guynn for his technical contributions. At MSE Technology Applications Inc. (MSE), Dr. Ying-Ming Lee provided technical contributions; David Micheletti provided project support; and Judy Harvey, Lisa Barker, Julie Wyant, Chuck Clavelot, and Lee Black provided editorial, graphic, and document preparation support.

Work was conducted under Montana Aerospace Development Authority Subcontract No. MADA0001 and National Aeronautics and Space Administration Langley Research Center Grant No. NAG1-02048 at MSE.

Available from:

NASA Center for AeroSpace Information (CASI)
7121 Standard Drive
Hanover, MD 21076-1320
(301) 621-0390

National Technical Information Service (NTIS)
5285 Port Royal Road
Springfield, VA 22161-2171
(703) 605-6000

Contents

Contents (Cont'd)

Contents (Cont'd)

Figures

Tables

Acronyms and Abbreviations

A	ampere(s)
ac	alternating current
AFC	alkaline fuel cell
AIAA	American Institute of Aeronautics and Astronautics
atm	atmosphere (measurement)
B	boron
B^{11}	most common boron isotope with atomic weight 11
BLP	Blacklight Power, Inc.
Btu	British thermal unit(s)
cm	centimeter(s)
CNT	carbon nanotube(s)
dc	direct current
DOT	U.S. Department of Transportation
e_c	Carnot efficiency
e_{TD}	Thermal Diode efficiency
E_{TD}	electricity by Thermal Diodes
EDL	electrical double layer
e-plane	electric plane
e_s	system efficiency
eV	electron volt(s)
FAA	Federal Aviation Administration
FASTec	Foundation for Advancing Science and Technology Education
Fe	iron
FLOPS	Flight Optimization System
ft	foot/feet
g	gram(s)
GaSb	gallium antimonide
GH_2	gaseous hydrogen
GLARE	glass fiber-reinforced aluminum
GTE	gas turbine engine

Acronyms and Abbreviations (Cont'd)

GW	gravitational wave(s)
H^1	hydrogen
Hz	hertz
He^4	helium 4
HEDM	high energy density material
HFC	hydrogen fuel cell(s)
HFGW	high frequency gravitational wave(s)
HIPCO	high-pressure carbon monoxide
hp	horsepower
HTSC	high temperature superconductor/superconductivity
IEC	inertial electrostatic confinement
in	inch/inches
INE	Institute of New Energy
I_{sp}	specific impulse
K	kelvin
KeV	kiloelectron volt
kg	kilogram(s)
kJ	kilojoule
km	kilometers
kW	kilowatt
kWh	kilowatt-hour
lb	pound(s)
L/D	lift-to-drag
LEC	Lattice Energy Corporation
LEO	low Earth orbit
LENR	low energy nuclear reaction
LFC	laminar flow control
LH_2	liquid hydrogen
LHe	liquid helium

Acronyms and Abbreviations (Cont'd)

LiH	lithium hydride
LN_2	liquid nitrogen
LOX	liquid oxygen
LTS	low temperature superconductor
m	meter(s)
mA	milliampere
MCFC	molten carbonate fuel cell
MeV	megaelectron volt
MGTOW	maximum gross takeoff weight
MIT	Massachusetts Institute of Technology
MJ	megajoule
mks	meter-kilogram-second
mm	millimeter
MSE	MSE Technology Applications, Inc.
MW	megawatt
N	newton(s)
NASA	National Aeronautics and Space Administration
NASA-GRC	NASA Glenn Research Center
NASA-JSC	NASA Johnson Space Center
NASA-LaRC	NASA Langley Research Center
NASA-MSFC	NASA Marshall Space Flight Center
Nd	neodymium
NERI	New Energy Research Institute
nm	nanometer(s)
nmi	nautical mile(s)
NMR	nuclear magnetic resonance
OD	outside diameter
PAFC	phosphoric acid fuel cell
PEM	proton exchange membrane
P/P	power/propulsion

Acronyms and Abbreviations (Cont'd)

PPC	Proton Power Cells
psi	pound per square inch
psig	pounds per square inch gauge
PSOFC	planar solid oxide fuel cell
PV	photovoltaic
R	rankine
ROOTS	ROOTS, Inc.
rpm	revolutions per minute
RSSPC	Reference Stirling Space Power Converter
s	second(s)
SBW	strut-based wing(s)
SMES	superconducting magnetic energy storage
SOFC	solid oxide fuel cell
SRI	Stanford Research Institute
SSME	Space Shuttle main engine
T_d	distant thermocouple
TDT	Transdimensional Technologies, Inc.
TOGW	takeoff gross weight
TPV	thermophotovoltaic
T_s	source thermocouple
μA	microampere
U of I	University of Illinois
USAF	U. S. Air Force
V	volt(s)
W	watt(s)
WGF	weight growth factor
Wh	watt hour(s)
WRF	weight reduction factor

Executive Summary

The National Aeronautics and Aerospace Administration (NASA) has identified water vapor emission into the upper atmosphere from commercial transport aircraft, particularly as it relates to the formation of persistent contrails, as a potential environmental problem. Since 1999, MSE Technology Applications, Inc. (MSE) has been working with the NASA Langley Research Center (NASA-LaRC) to investigate the concept of a transport-size emissionless aircraft fueled with liquid hydrogen (LH_2) combined with other possible breakthrough technologies. The goal of the project is to significantly advance air transportation in the next decade and beyond. The power/ propulsion (P/P) system currently being studied would be based on hydrogen fuel cells (HFCs) powering electric motors, which drive fans for propulsion. The liquid water reaction product is retained onboard the aircraft until a flight mission is completed.

As of now, NASA-LaRC and MSE have identified P/P system components that, according to the high-level analysis conducted to date, are light enough to make the emissionless aircraft concept feasible. Calculated maximum aircraft ranges (within a maximum weight constraint) and other performance predictions are included in this report.

Carrying liquid water reaction product onboard for the duration of a flight mission imposes a severe weight penalty. If modeling and experiments show that water may be expelled as liquid droplets of an appropriate size and temperature and will not significantly reevaporate in the higher atmosphere nor freeze and form hailstones when falling through the lower atmosphere, the resulting weight relief would greatly accelerate the practical realization of this project. A preliminary calculation showing the magnitude of the resulting benefit of this weight reduction is included in this report.

Even though near-term technology allows for a plausible concept for an emissionless aircraft and therefore a solution to the high-altitude water vapor problem, more advanced technologies presently being investigated in research laboratories may potentially offer more practical solutions. For example, advanced aerodynamics could potentially extend the fuel efficiency of any aircraft; this report describes some leading examples of this type of research.

In the midterm, recently discovered types of nuclear reactions that do not produce penetrating radiation may offer fuel energy densities approximately one million times greater than that of chemical fuels. Examples of these reactions are described. Additionally, recently discovered methods for converting heat to electricity, transferring heat, and storing energy are discussed.

In the long-term, technologies that can only be described as "breakthrough" may potentially be available for producing energy from the very structure of space-time itself or propelling vehicles without using a material propellant to balance momentum. Present research being conducted at multiple locations around the world indicates such technologies may be possible, and this is presented.

Finally, some topics of "breakthrough physics," which typically precede breakthrough technology, are presented at an introductory level.

1. Potential New Aeronautical Energetic Requirement - The "Emissionless Aircraft"

1.1 Current State-of-the-Art Transport Aircraft

The National Aeronautics and Space Administration Langley Research Center (NASA-LaRC) and MSE Technology Applications, Inc. (MSE) of Butte, Montana, have been working closely regarding aircraft parameters and performance capabilities. NASA-LaRC routinely uses computer codes to estimate aircraft performance for a number of different aircraft types under various technology assumptions. MSE and NASA-LaRC jointly selected as a state-of-the-art technology baseline aircraft for comparison purposes one with the following parameters:

- number of passengers.....300;
- maximum range .....7,500 nautical miles (nmi);
- average cruise velocity.....Mach 0.85; and
- maximum gross takeoff weight (MGTOW) .....655,626 pounds (lb).

1.2 Water Vapor/Cloud Formation Problem (with other pollutants)

NASA has identified water vapor emission into the upper atmosphere from commercial transport aircraft, particularly as it relates to the formation of persistent contrails, as a potential environmental problem. There is growing evidence that contrails and clouds that form where contrails have been located significantly affect the heat balance of the Earth at some locations.

In a recent article (Ref. 1), climate scientists David Travis of the University of Wisconsin in Whitewater, Wisconsin, and Andrew Carleton of Pennsylvania State University in University Park, Pennsylvania, stated that contrails formed by the condensation of water vapor in high-altitude jet aircraft exhaust significantly reduce the daily range in temperature between daytime highs and night lows. These researchers additionally stated that a growth in air traffic and consequently more contrails could disrupt regional ecosystems because "certain trees, crops, and insert species depend on specific daily temperature variations for their survival." The absence of commercial air traffic in the United States after the September 11, 2001, terrorist attacks, when contrails all but disappeared, provided a "zero" baseline that allowed these researchers to be certain that their findings were valid.

NASA-LaRC requested that MSE begin investigating the feasibility of propelling transport aircraft in such a way that no water would be emitted to the upper atmosphere. In addition, the expectation has been that an aircraft power/propulsion (P/P) system revolutionary enough to not emit water vapor would also be emissionless with regard to other combustion/reaction products (e.g., carbon dioxide, carbon monoxide, sulfur dioxide, oxides of nitrogen, unburned hydrocarbons, and particulates).

1.3 Emissionless Approaches

Power required for aircraft flight could theoretically be provided by:

- energy storage by some means, which would presumably be electrical, magnetic, or mechanical;
- energy beamed from a ground (or space) location to the aircraft in flight; and
- onboard power production from a fuel (the oxidizer could be provided by ambient air).

The first two methods will not change aircraft weight during flight. For an emissionless aircraft, the third method will cause the aircraft to gain weight as the fuel reacts with atmospheric oxygen and the reaction product is retained onboard until the completion of a flight mission.

1.3.1 Energy Storage

MSE investigated state-of-the-art methods of energy storage and quickly determined they were not sufficient enough (by orders of magnitude) to provide the energy required to propel a transport aircraft for a practical distance. As a comparison basis, the total combustion of jet fuel with air (which is, of course, not emissionless) will provide approximately 18,585 British thermal units (Btu)/lb (of that fuel). This chemical reaction can be compared with emissionless energy storage systems as seen in Table 1.

Table 1. Energy density (per mass) for state-of-the-art fuels and energy systems.

Fuel or Energy Storage System	Energy Density
Jet fuel combustion	18,585 Btu/lb
Lead acid storage battery	62 Btu/lb
Energy storage flywheels	48 Btu/lb
Superconducting storage	2.1 Btu/lb
Supercapacitor storage	1.1 Btu/lb

1.3.2 Beamed Energy

MSE's experience with energy beams required for hypersonic flight testing was used and it was learned relatively quickly that it would not be feasible to use such beams to transmit the amount of power required to sustain flight. The technical obstacles associated with this are:

- energy absorption (in air);
- beam focusing; and
- beam directing.

1.3.3 Chemical Propulsion

For an ***emissionless*** aircraft that uses ambient air to oxidize an onboard fuel and must store chemical reaction products onboard for the duration of a flight mission, the aircraft will (contrary to conventional aircraft) ***gain weight*** throughout a flight mission. Propulsion system power density, fuel energy density, vehicle weight reduction, and aerodynamics are obviously important for an aircraft. These are of much ***greater*** importance when that aircraft is emissionless and retains reaction products onboard until the completion of a flight mission, as there must be compensation for the continuous ***increase*** in onboard weight. NASA-LaRC and MSE have

identified possible improvements in all of these areas, and these will be described in subsequent sections of this report.

1.4 Energy Conversion Approaches

Unlike the state-of-the-art gas turbine engine (GTE), an emissionless aircraft P/P system must "decouple" the power and propulsion systems. For example, a power production system must be able to retain chemical reaction products onboard the aircraft while providing power to operate a propulsion system. In the near term, MSE and NASA-LaRC believe the propulsion system will be fans, such as are presently driven by the "cores" of turbofan engines.

1.4.1 Heat Engine

1.4.1.1–Heat Engine Limitations Gas turbine engine technology has had much development over many decades, and the baseline aircraft achieves a fuel energy-to-aircraft energy efficiency (cruise phase of flight) of approximately 37%. This is high for a heat engine; yet, it may be slightly increased by using more exotic ultrahigh temperature materials in the combustion section of the GTEs.

The so-called Second Law of Thermodynamics (sometimes referred to as the Carnot Equation) states that the ***upper limit*** of the fraction of heat energy that may be converted to mechanical energy in a heat engine is given by:

$$e = (T_1 - T_2)/T_1$$

where:

e = the conversion efficiency

T_1 = the upper temperature in the engine

T_2 = the lower temperature (of exhaust) from the engine

In this equation, T_1 and T_2 are each expressed on the same absolute temperature scale, [e.g., kelvin (K) or rankine (R)].

In practice, the upper efficiency limit yielded by the Second Law of Thermodynamics is then multiplied by a ***mechanical*** efficiency of the engine, resulting in the overall efficiency that could be obtained.

Representative types of power production (energy conversion) systems investigated by MSE are presented in the following sections.

1.4.1.2–Stirling Engines Basic Stirling engine technology was invented nearly 200 years ago. Heat from an external source causes an internally contained gas to expand and push the "power piston," which is connected to an external workload. The power piston is mechanically coupled

to a second "displacer" piston that pushes the expanded and cooled (because it expanded) gas back to the hot end of the engine where it reabsorbs heat and is ready to repeat the cycle. The working gas does not enter or leave the engine as it is sealed inside. Personnel at the NASA Glenn Research Center (NASA-GRC) have developed an efficient modern version of this engine, which they call the "Reference Stirling Space Power Converter" (RSSPC) and which is described herein (Refs. 2, 3, and 4). This was a "free piston" type of engine, which means there is no mechanical linkage to remove the mechanical power that is produced from heat by the engine. The reciprocating piston is coupled with a "linear alternator" in which permanent magnets are moved back and forth within electric coils to generate electricity. The entire mechanism is hermetically sealed within a metal shell that is filled with the helium gas working fluid at a pressure of 150 atmospheres (atm). The design focused on very high reliability required for space applications where repairs would not be possible and featured only two moving parts, gas bearings to prevent any mechanical rubbing of parts, and a design lifetime of 60,000 hours. The engine was actually tested for 1,000 hours without any failures. As space electronics have become increasingly miniaturized and require less electric power, NASA-GRC has redirected their focus to Stirling engines that produce only tens of watts.

The parameters for the RSSPC were:

- input heat energy temperature.....1,050 K (777 °C);
- output heat energy temperature.....525 K (252 °C);
- electrical Output.....25.4 kilowatts (kW);
- heat to electric conversion efficiency 27%;
- dimensions .....several feet (ft) diameter and 5 ft long (cylindrical); and
- weight.....150 kilograms (kg)

MSE agrees with the conclusion of NASA-GRC that Stirling engines are too heavy for aircraft propulsion applications.

1.4.2 Thermophotovoltaic Technology

Thermophotovoltaic (TPV) technology is very similar to photovoltaic (PV) technology used to convert sunlight to electricity, except that it uses a fueled, man-made source of radiant energy placed approximately 1 inch from single crystal energy converter cells manufactured from a material such as gallium antimonide (GaSb) (Refs. 5 and 6). This material can convert infrared energy from a fuel-heated emitter into electrical energy and does not require a higher temperature heat source (e.g., the Sun).

This technology has been developed to where it is approximately 10% efficient; the theoretical upper limit is approximately 25% to 30%.

1.4.3 Electrochemical Processes

State-of-the-art energy conversion technology using electrochemical processes is more efficient and offers significantly higher power densities than heat-based processes. This approach (e.g., fuel cells) will be discussed in subsequent sections.

2. The Fuel Cell Energy Conversion Approach

2.1 Fuel Cells

At a high level, the major components of a fuel cell-based aircraft (P/P) system will be:

- fuel;
- fuel cells;
- electric motors; and
- propulsion fans.

2.1.1 Types of Fuel Cells (Lithium vs. Hydrogen)

In previous research, MSE investigated the possibility of using lithium fuel cells for aircraft propulsion but found two significant disadvantages.

1) The reactants include ***water*** as well as oxygen.

2) The amount of commercially available lithium is rather limited; therefore, any fuel cell for an emissionless aircraft application must use hydrogen fuel because:

   - hydrogen is the other element with a significantly high weight-based energy density;
   - reaction product water can be readily retained onboard until the completion of a flight mission; and
   - hydrogen fuel can be readily produced from abundantly available sources of hydrogen.

2.1.2 Types of Hydrogen Fuel Cells

There are five fuel cell types that can use hydrogen as the fuel (either oxygen or air would then be the oxidizer).

Selected characteristics of these five types are stated below.

1) Proton Exchange Membrane (PEM)

   - Electrolyte–hydrogen ion-conductive polymer (plastic) membrane
   - Operating Temperature–70 ºC to 90 ºC
   - Status–highly developed for vehicle applications with intense on-going further development
   - Typical Application–vehicles

2) Alkaline Fuel Cells (AFC)

   - Electrolyte–potassium hydroxide solution
   - Operating Temperature–<120 ºC to ~ 250 ºC

- Status–corrosive electrolyte; carbon dioxide in air would form potassium carbonate; uses asbestos matrix; developed by NASA for space use; currently being phased out
- Typical Applications–space vehicles

3) Phosphoric Acid Fuel Cell (PAFC)

- Electrolyte–100% phosphoric acid
- Operating Temperature–150 ºC to 220 ºC
- Status–acid retained in a silicon carbide matrix
- Typical Applications–utilities

4) Molten Carbonate Fuel Cell (MCFC)

- Electrolyte–mixture of molten alkali carbonates
- Operating Temperature–600 ºC to 700 ºC
- Status–ceramic matrix of lithium aluminate is used
- Typical Applications–utilities

5) Solid Oxide Fuel Cell (SOFC)

- Electrolyte–Solid zirconium oxide
- Operating Temperature–650 ºC to 1,000 ºC
- Status–tubular form undergoing life tests; planar form being developed
- Typical Applications–utilities, vehicles

2.1.3 Hydrogen Fuel Cells for Vehicular Applications

Of the above types of HFCs, the PEM and SOFC are the most suitable for vehicular applications.

2.1.3.1–Proton Exchange Membrane Fuel Cells Major automotive manufacturers and companies supporting PEM fuel cells are spending millions of dollars per year to develop these fuel cells for automobiles. A number of stacks of these fuel cells are powering cars and buses on an experimental basis.

2.1.3.2–Solid Oxide Fuel Cells Of the various types of fuel cells now known, the SOFC operates at a higher temperature than any other type of fuel cell and is better suited to operate with more widely available fuels. The state-of-the-art of SOFC consists of a 100-kW natural gas-fueled system manufactured by Siemens-Westinghouse in the United States and is currently being tested in the Netherlands. This system consists of 1,152 separate tubular cells connected in a series and parallel configuration to provide the required total output voltage.

The operating principle of the cells is that a proprietary catalyst causes oxygen molecules (from air) to split into oxygen ions and electrons. The 650 °C to 1,000 °C operating temperature allows the oxygen ions to diffuse through the zirconium oxide electrolyte to the exterior of the tube. The circuit is completed by the electrons, which go through wires to the electrical load and back to the other electrode of the cell.

2.1.3.3–Planar Solid Oxide Fuel Cells

The calculated ***size*** of the liquid-to-air heat exchanger required to remove heat generated in a PEM-type HFC is far too large to fit onboard the aircraft for this application. Therefore, NASA-LaRC/MSE have investigated the "planar solid oxide fuel cell" (PSOFC) and created a conceptual P/P system based on this technology. The results of this investigation (to date) are presented in Section 2.7.

Table 2 compares selected characteristics of PEM and PSOFC HFCs relevant to this application.

Table 2. PEM and PSOFC HFC characteristics.

Characteristic	PEM	PSOFC
Weight power density	1.24 kW/kg	2 kW/kg
Volume power density	1.75 kW/L	0.4–2.0 kW/L
Operating temperature	~ 80–90 °C	~ 650 – 1,000 °C
Electrochemical efficiency	~ 50%	~ 50%
Ionic current carrier	Protons	Oxygen
Coolant required	Yes	No
Catalyst	Platinum	None or inexpensive
Bottoming cycle	No	Yes

Physically, PEM HFCs consist of a platinum catalyst on a thin polymer membrane with carbon sheets on each side of the membrane to introduce hydrogen and air, remove liquid and vapor water, and collect the generated electricity. Approximately 50% of the fuel energy appears as heat, and coolant passages are required to remove this heat (to a liquid-to-air heat exchanger) so that the operating temperature will not exceed 90 °C.

Planar solid oxide HFCs consist of a thin sheet of ceramic (zirconium dioxide with proprietary additives) that carries the interelectrode ionic current (oxygen ions), as well as grooved metal electrodes, which introduce hydrogen and air, remove exhaust gases, and collect the generated electricity. Approximately 50% of the fuel energy appears as heat, but unlike PEM HFCs, ***no coolant is used***. In fact, PSOFCs are insulated to maintain a normal operating temperature that is approximately 650 °C to 1,000 °C. Heat is removed via the exhaust gas at a temperature of approximately 650 °C.

2.1.3.4–The Significance of Planar Solid Oxide Fuel Cells for the Emissionless Aircraft Concept Unlike PEM HFCs, the higher operating temperature of PSOFCs allows a ***bottoming cycle*** to be used, which significantly increases the percentage of useful energy available from the hydrogen fuel. Furthermore, the relatively higher operating temperature of PSOFCs means that no heavy and large liquid-to-air heat exchanger is required. Relatively smaller heat exchangers are required to cool the exhaust gases following the bottoming cycle because liquid water must be captured and retained onboard the aircraft as part of the emissionless aircraft concept. Current research is being directed toward lowering the PSOFC operating temperature, which consequently lowers stress on materials when temperatures change. The ***planar*** configuration of SOFCs is relatively compact and is the leading candidate for a fuel cell-based P/P system for the NASA-LaRC/MSE emissionless aircraft concept.

One company developing PSOFCs showed MSE circular stainless steel electrode plates, approximately 0.08 inch thick and 5 inches in diameter, from PSOFCs being tested as 1-kW "stacks." Every other plate has a thin layer of doped zirconium dioxide that is the (an) ionic conductor. The noncoated plates have spiral grooves machined into the surfaces in order to spread fuel (hydrogen) and oxidizer (air) uniformly over the plate surface. A unique feature of this design is that all the plate-to-plate gas seals are in the ***center***, which is claimed to solve the problem of maintaining a leak-free condition for a practical number of heatup/cooldown cycles.

The power output as a function of temperature (with 1.0 kW at 750 ºC as a basis) is claimed to be 0.5 kW at 700 ºC and 0.3 kW at 650 ºC. The primary research effort of this company is now to lower the operating temperature of their PSOFCs. Preliminary laboratory research indicates that operating temperatures less than 400 ºC may be achievable.

2.1.3.5–Advanced Fuel Cell Research—High Temperature NASA-LaRC Fuel Cell Membrane As described in Section 2.1.2, the PEM HFC uses a polymer (plastic) membrane as the internal ionic (proton) conductor. The upper temperature limit of this membrane material limits the operating temperature of the fuel cell to approximately 95 °C. If another ionic conducting membrane material could be developed that would allow the fuel cell to operate at a higher temperature, the advantages would be as given below.

1) Higher fuel cell electrochemical efficiency.

2) Less weight, volume, and cost for the heat exchanger required to transfer heat out of the fuel cell. (Because of the higher electrochemical efficiency, less heat would be generated per mass of fuel entering the fuel cell; furthermore, a greater difference between the fuel cell operating temperature and the ambient requires less heat exchanger size and weight).

3) Possibly, fuel cell exhaust heat could be recovered and converted to useful energy (as is potentially possible for PSOFCs, which operate at 650 °C to 1,000 °C).

NASA-LaRC researchers have stated they are developing a "liquid crystal" based polymer, suitable for fuel cells, which will have an operating temperature as high as 400 °C. One relatively well-known example of a "liquid crystal" polymer is "KEVLAR," known for its extreme strength-to-weight ratio. NASA-LaRC will soon be testing their new polymeric material in fuel cells to see if it performs as expected.

2.2 Hydrogen Storage

MSE examined several methods by which hydrogen fuel could be carried onboard an emissionless aircraft that would use this fuel for its fuel cells.

1) Liquid hydrogen (LH_2) carried in insulated tanks.

2) Ultrahigh-pressure gaseous hydrogen (GH_2) carried in lightweight, superstrong (e.g., carbon fiber composite) tanks. A typical initial pressure would be $\geq$ 5,000 pounds per square inch gauge (psig).

3) Hydrogen supplied chemically by reacting a small amount of onboard water with either lithium hydride (LiH) or calcium hydride. Water produced in the fuel cells would release additional hydrogen from the hydride in a cyclic process. The reaction product to be carried onboard the aircraft to the completion of the flight mission would be the respective metallic ***hydroxide***.

4) Hydrogen adsorbed on carbon nanotubes (CNTs).

2.2.1 Elimination of All Methods Except Liquid Hydrogen

Even though the U.S. Department of Transportation (DOT) has approved multilayer carbon fiber composite tanks for carrying GH_2 at 5,000 psig for ground-based vehicles, MSE (which is currently developing the means for ground-based testing of hypersonic aircraft using ultrahigh-pressure air) calculated that ***each cubic foot*** volume of hydrogen (or other gas) at 5,000-psig pressure contains a potential physical energy equivalent to approximately 1 lb of TNT explosive.

Even at a pressure of 5,000 psig, (hydrogen density at this pressure is 1.41 lb/ft^3) the takeoff weight of hydrogen fuel (20,000 to 40,000 lb) required for a typical flight mission would require many thousands of cubic feet of tank volume. Therefore, the failure of ultrahigh-pressure GH_2 tanks would probably be catastrophic, which eliminates this method of carrying hydrogen from further consideration.

The ***system*** energy density for carrying hydrogen via a reactive metal hydride was calculated by MSE and is eliminated from consideration because it is too low to be practical. This is essentially because the weight of the metal in the respective metallic hydride (e.g., lithium or calcium) must be carried throughout the flight.

MSE investigated claims that hydrogen could be adsorbed on CNTs (Section 2.5.1) and learned that:

- adsorption tests are not repeatable;
- some researchers had experimental errors due to moisture in their hydrogen;
- contaminants have been a problem;
- the net weight of adsorbed hydrogen in CNT systems is only 1.5% to 3.5%;
- there are significant problems with ***desorbing*** hydrogen from CNTs after it is adsorbed–a high (but unspecified) temperature is required to desorb hydrogen from CNTs;
- system pressure (though not ultrahigh) is far above ambient;
- the response time is slow;
- the cycle life is unknown; and
- CNT adsorption systems may not pass vehicle vibration tests.

Method one (LH_2) remains as the one viable choice, and furthermore (as will be explained in a subsequent section), the latent heat of vaporization of this fuel can have a valuable "byproduct" function of cooling the optimum electric motors (identified to date) that require LH_2 coolant.

2.2.2 Liquid Hydrogen Supplied in Preloaded Tanks

It might be possible to reduce the expected high cost of an LH_2 infrastructure at an airport by using trucks to transport ***preloaded*** tanks of LH_2 from the production facility to the airport. In this scenario, LH_2 would ***not*** be directly pumped into aircraft. No insulated LH_2 piping system or GH_2 recovery system would be required. There would need to be specialized equipment for positioning and connecting preloaded tanks into the aircraft as well as removing the empty tanks; however, these details have not yet been investigated.

MSE discussed the production, transportation, and economics of LH_2 with one of the major vendors. The information MSE learned from the vendor is given below.

1) Over-the-road tank trucks have a capacity of 13,000 gallons of LH_2, which weighs 7,100 lb (the consulted vendor does not ship LH_2 in rail cars).

2) The "boiloff" rate of LH_2 tank trucks is less than one-half of 1% per day.

3) The current selling price of LH_2 is $1.50 per lb at the production site (approximately 10 sites throughout the United States and Canada).

4) The transportation cost within 50 miles of the production plant is "free" (i.e., included).

5) The primary (and preferred) hydrogen production method used by the consulted vendor is the steam reforming of natural gas.

6) A "standard size" plant produces 30 tons of LH_2 per day. The "upfront" capital cost to build such a plant is approximately $1.4 to $1.5 million per ton, per day production capacity.

The vendor stated that at this conceptual level, the idea of trucking preloaded tanks of LH_2 from the production plant to the airport and then inserting entire full tanks of LH_2 onto future emissionless aircraft (while offloading empty tanks to take back to the LH_2 vendor to be refilled) is not only feasible but has a successful precedent. At one time, the company transported preloaded 11,000-gallon "superinsulated" tanks of LH_2 all the way to Guyana, where it was used to launch the Ariane satellite booster rocket. The hydrogen boiloff rate from these containers was said to be negligible.

2.3 Electric Motors

The most appropriate electric motor design yet identified for the NASA-LaRC/MSE emissionless aircraft project was built and tested in 1991 for the U.S. Air Force (USAF) by Larry Long of Long Electromagnetics, Inc. This device was built to be a generator but could readily function as a motor and will be so referred. [There is (typically) such a reciprocal relationship between generators and motors, and the mechanical-to-electrical power relationship is mathematically identical (but with a sign change)]. Some of the major design and operating parameters for this

motor built as a 1-megawatt (MW) prototype are presented in Table 3. Figure 1 is a photograph of this prototype.

Table 3. USAF 1-MW motor.

Parameter	Value
Power	1 MW (1,341hp)
Weight	220 lb
Diameter	18 in
Length	18 in
Coil material	High purity aluminum
Current density in aluminum wire	80,000 A per in^2
Stator cooling	LH_2 at 2 atm pressure
Rotor cooling	LH_2 (boiling) at 1 atm pressure
Voltage	4,000 V
Rotational speed	6,000 rpm
Frequency	400 Hz
Measured efficiency	99.48%

The high efficiency of this device results primarily from the very low (but not superconducting) electrical resistance of pure aluminum at the 1-atm pressure boiling temperature of LH_2 (20.4 K). The practical resistance of aluminum at this temperature is stated to be 1/500 of the electrical resistance of aluminum at room temperature.

Since the NASA-LaRC/MSE emissionless aircraft concept uses LH_2 as fuel and this substance must be vaporized and heated before it can be introduced to the fuel cells, it qualitatively meets the coolant requirement for this situation.

Mr. Long told MSE that the 1-MW machine was built as the "exciter" (i.e., the machine that generates electrical power to energize the magnetic fields) for a 40-MW generator. The 40-MW generator was designed to be a "flight-weight" component for a USAF missile defense system; however, it was never built. Both the 1-MW and 40-MW machines were designed to be shaft driven by one GTE fueled by LH_2 and liquid oxygen (LOX) (therefore, LH_2 was available to cool the aluminum windings to ~20 K in both machines).

2.3.1 Design for a 40-MW Motor

Table 4 shows some of the unique design parameters applicable for a 40-MW machine, which was designed but not built as the USAF contract was terminated for nontechnical reasons.

Table 4. USAF 40-MW motor.

Parameter	Value
Power	40 MW
Weight	2,640 lb
Diameter	40 in
Length	79 in
Rotational speed	6,000 rpm

Figure 1. A 1-MW cryogenic motor successfully built and tested for aerospace applications (1991).

Mr. Long stated that weight vs. power is proportional at 0.03 kg/kW in the 5- to 40-MW power range (for a single LH_2 cooled machine) and furthermore, that efficiencies could "probably" reach 99.8% at the upper end of this power range. These exceptionally high motor power densities and efficiencies are highly beneficial for the NASA-LaRC/MSE emissionless aircraft concept.

2.3.2 Motor Controller Strategy

Mr. Long stated that (in his opinion) the best strategy to control large motors operating from a direct current (dc) power supply (i.e., fuel cells) would be to use an electronic dc to alternating current (ac) converter with a 3-phase output for which the expected efficiency would be approximately 98%.

2.3.3 Inapplicability of Superconducting Technology

Mr. Long and his associates formerly worked on both large superconducting and non-superconducting cryogenic motors and generators. Contrary to promotional claims, Mr. Long believes that high temperature superconductivity (HTSC) requires much more development before it is suitable for this type of rotating equipment. This is primarily due to the fact that this superconducting material is extremely brittle. Furthermore, a machine using this material would be heavier rather than lighter compared to what Mr. Long achieved with LH_2 cooling. Additionally, it is weight-effective to use the LH_2 that is already part of the aircraft system as a coolant rather than carry liquid nitrogen (LN_2) onboard to maintain HTSC material in the superconducting state.

2.4 Advanced Aerodynamics

Whether an aircraft is conventional or emissionless, improved aerodynamics will increase range per weight of onboard fuel at takeoff (all other factors being considered the same). NASA-LaRC believes there are a number of methods that could be implemented to improve aerodynamics (increase the lift-to-drag [L/D] ratio), thereby increasing total range miles per pound of fuel. These include:

- strut-braced wings (SBWs) with high wing span and high aspect ratio;
- riblet film to reduce fuselage drag;
- fuselage skin heating;
- winglets at wingtips that are aerodynamically equivalent to longer wings; and
- laminar flow control (LFC).

Some aircraft manufacturers currently use winglets, and some airlines are beginning to experiment with riblet film on parts of the fuselage in order to reduce fuel consumption. However, various other aerodynamic improvements have not yet been used on a commercial basis.

For state-of-the-art commercial transport aircraft, the average L/D ratio for the cruise phase of a flight mission is approximately 17. For this emissionless aircraft project, NASA-LaRC uses assumptions for their performance calculations that cause the calculated L/D to be approximately 23 to 28 for the cruise phase of a flight mission. (Of course, this number varies as a function of weight change, altitude change, and other stated assumptions during the cruise phase).

The following sections describe some advanced aerodynamic technologies in more detail.

2.4.1 Strut-Braced Wings

One aeronautical concept that could increase L/D is the use of SBWs. (This concept has been used for many years in designs of small general aviation aircraft.) According to Mr. Mark Guynn of the NASA-LaRC Systems Analysis Branch, the benefits of SBWs include:

- the wings can be thinner for the same strength and weight;
- the wing span can be increased with less weight increase;
- a thinner wing can have less wing sweep without increasing wave drag; and
- unsweeping the wing increases the laminar flow over the wing by reducing cross-flow instabilities, which promote transition to turbulent flow.

Mr. Guynn also referred to a presentation by Virginia Polytechnic Institute and State University given at NASA-LaRC on May 12, 1999, that stated possible L/D numbers that could be achieved by modifying aircraft aerodynamic characteristics based on the objectives given below.

- Optimize to minimize takeoff gross weight (TOGW) to complete the design mission, L/D approximately 25 (23 of the 25 were factors ***other*** than SBWs).

- Optimize to minimize fuel consumption, L/D approximately 29 (26 of the 29 were factors other than SBWs). Mr. Guynn points out the wingspan for this latter configuration is 80 meters (m) [which is a limit imposed by the Federal Aviation Administration (FAA)].

A 1996 paper by Mr. Dennis Bushnell of NASA-LaRC provided the insight that an important new metric for transport aircraft design will be ***cost*** and that aircraft designers should be thinking of the ***synergies*** between propulsion, aerodynamics, and structural systems (Ref. 7). Mr. Bushnell pointed out that Pfenninger advocated SBWs in 1977, and the calculated L/D values were in the 40s (more than twice current levels). However, such wings would have had a span greater than 80 m and therefore would not have met FAA regulations. Mr. Bushnell also advocates that aircraft designers reconsider other ideas for increasing L/D such as the use of a double fuselage, the "biplane" concept, the "ring" wing, and blended wing-body configurations (as deployed in the B-2 bomber).

2.4.2 Riblets for Fuselage Drag Reduction and Increased Heat Transfer

2.4.2.1–Heat Transfer It has been experimentally shown that microscopic "V" shaped ribs or grooves referred to as "riblets" on a solid surface immersed in a moving fluid will decrease skin friction and increase heat transfer from that surface compared to a surface without such a

microscopic structure. Decreased skin friction and increased heat transfer would each enhance the performance (increase the range) of the baseline emissionless transport aircraft being considered by this study. NASA-LaRC referred to one of its papers on this subject that describes experimental research on heat transfer from surfaces with microgeometries (Ref. 8). Drag was also measured in these experiments. The article stated "the riblet surfaces, which produced the highest heat transfer, are documented drag reducing surfaces (absolute drag levels reduced below the flat plate)." The concluding sentence of the article stated, "basically, this research would suggest decreases of the order of +20% in heat exchanger volume, cost, and weight for designs with extensive planar surfaces."

2.4.2.2–Drag Reduction NASA-LaRC also stated that fuselage skin friction can be reduced by 6% by using riblets. An article sent by NASA-LaRC to MSE describes an experiment by Cathay Pacific Airlines in which 30% of the surface area of one of their Airbus Industrie A340-300 aircraft was covered with a thin adhesive-backed plastic film containing riblets on the exterior surface for the purpose of reducing drag and thereby saving fuel (Ref. 9). Riblet film was applied to the upper surface of the wings, the upper fuselage, both sides of the vertical stabilizer, and the tailplane. This aircraft flies "long haul" routes such as Hong Kong to Toronto or Hong Kong to Rome. At the time the article was written, it was expected that fuel savings would be approximately 1% to 2% compared to using a painted "flat" surface, all other operating conditions being the same. Riblet film has approximately the same weight per area as paint; consequently, there is no aircraft weight penalty. It was not considered practical to place riblet film on the underside of the aircraft where it could get "sandblasted off" from ground dirt associated with takeoffs and landings.

2.4.3 Fuselage Skin Heating

This analysis addresses whether there is a significant conceptual benefit (i.e., greater maximum aircraft range) to be gained by using waste heat from the HFCs to heat the boundary layer of air passing over the fuselage of the aircraft.

2.4.3.1–Calculated Aircraft Drag Reduction Due to Fuselage Skin Heating NASA-LaRC located a reference that presented curves of drag reduction vs. temperature ratio for a computational analysis of a fuselage-shaped body (Ref. 10). From these, a 90 °C skin temperature vs. a minus 57 °C (cruise altitude) atmospheric temperature gives a drag reduction of 15% (for the area of the fuselage skin).

2.4.3.2–Increase in Aircraft Range Caused by Heated Fuselage Skin Drag Reduction Inserting the fuselage drag reduction caused by fuselage skin heating into the NASA-LaRC Flight Optimization System (FLOPS) code (Section 2.6), the calculated increase in the maximum range of the aircraft was approximately 7%. The 90 °C temperature was assumed as the temperature of liquid water leaving PEM HFCs (being considered at the time of the calculation). It should be noted that such a heat distribution would be very difficult to accomplish.

2.4.4 Winglets

Winglets are aircraft wingtip extensions at some angle with respect to the main part of the wings. The function of winglets is to limit the formation of air vortices that would otherwise form at each wingtip. Therefore, by limiting these vortices, drag is reduced, and the fuel efficiency of the aircraft is increased. Winglets are currently in commercial use on some aircraft. The tradeoff to drag reduction is a slight increase in aircraft weight.

NASA-LaRC used the characteristics of the winglets offered as an option on the Boeing 737-800 as a basis for estimating the drag reduction and weight penalty associated with adding winglets to the NASA-LaRC/MSE emissionless aircraft. The Boeing 737-800 winglet size was scaled up proportional to wing area, and the weight penalty (winglet weight + increase in the weight of the wing structure to accommodate the winglet) was assumed to be proportional to winglet size. The resulting estimated weight penalty for applying winglets to the emissionless aircraft was 1,756 lb. Based on data from Aviation Partners, Inc., which designed the winglets for the Boeing 737-800, a drag reduction of 6% has been assumed.

2.4.5 Laminar Flow Control

Aerodynamic technologies, which increase the (L/D) ratio, will result in corresponding performance increases for an aircraft, whether it is emissionless or conventional.

NASA-LaRC has provided an overview report on LFC from which the information in this section has been selected (Ref. 11).

As stated in the referenced report, skin friction drag can amount to approximately 45% to 75% of the total drag for an aircraft. When the airflow over (part of) an aircraft is laminar, the skin friction can be as much as 90% less than when that airflow is turbulent. At and near the leading edge where an aircraft component encounters moving (subsonic) air, the flow is laminar but has a natural tendency to convert to turbulent flow (with much higher friction drag) in the direction towards the trailing edge.

Laminar flow control is defined as "an active boundary-layer flow control (usually suction) technique employed to maintain the laminar state" (for flow conditions that would otherwise be turbulent in the absence of that control). "Suction" refers to sucking ambient air through perforations or pores in the external skin of an aircraft component. Laminar flow control can also be provided by other means such as cooling the external skin.

Representative range increases (for conventional aircraft) are approximately 20% to 25% when LFC is used. The downside of using LFC is carrying the weight of the air suction system. An estimated weight (presented in the cited reference) is 8,500 lb for a 745,000-lb TOGW conventional (but supersonic) aircraft. This is an approximate weight penalty ratio of 1.1%.

Even though many LFC experiments have been performed for more that 60 years, commercial aircraft manufacturers are reluctant to use this technology because its long-term technical and

economic viability has not yet been demonstrated; and LFC benefits are intimately tied to aircraft fuel prices, and these have fluctuated considerably over the course of many years.

For the purpose of the NASA-LaRC/MSE emissionless aircraft maximum range calculations, it is assumed that LFC could be employed in the long term to obtain (for the cruise phase of a flight mission) 50% laminar flow on the wings, tail, and fan nacelles.

2.5 Structural Weight Reduction

As stated previously, an emissionless aircraft must carry the added weight of reaction product (water) until a flight mission is complete. Therefore, weight reduction is more important for an emissionless aircraft than it is for a conventional design. MSE has been monitoring technology based upon CNTs as these nanometer (nm)-diameter carbon tubes have the highest strength-to-weight ratio of any known material (approximately 600 times that of steel). NASA personnel have stated that composite materials based upon CNTs offer a potential conservative strength-to-weight increase of at least a factor of two relative to conventional materials. Thus, if other factors such as temperature limitations were favorable, a state-of-the-art aircraft or aircraft system component presently fabricated from aluminum alloy weighing 100 lb could instead be fabricated from CNT composite material, have equal strength, and weigh 50 lb. Even though the technology is relatively young, in recent years CNT researchers have learned how to scale up pilot production of CNTs by orders of magnitude. A subsequent section (2.7) of this report will numerically illustrate to what extent component weight reduction can increase the calculated maximum range of an emissionless aircraft.

Another revolutionary material that has a potential high strength-to-weight ratio is foamed metals. MSE has performed a preliminary investigation of this technology and learned that it could also offer a weight reduction factor (WRF) of approximately two.

2.5.1 Carbon Nanotubes

In 1991, a Japanese researcher named Iijima first recognized in micrographs a cylindrical form of a large carbon molecule, which became known as a CNT.

The geometric structure of a CNT can be easily visualized in the following manner.

1) Start with a single layer sheet of carbon atoms combined as they are in graphite. This looks exactly like familiar "chicken wire," with its well-known hexagonal grid pattern. Every carbon atom is linked to three other carbon atoms.

2) Align the graphite "chicken wire" so that two of the opposite sides of the hexagons are placed "horizontal" (so to speak).

3) Roll the graphite sheet "top to bottom" and connect top to bottom, and the result is a CNT that is an excellent metallic conductor.

4) Roll the graphite sheet at any other (skewed) angle, and the result is a CNT that is not metallic but is a semiconductor.

Carbon nanotubes form in either a "single-wall" or "multiwall" version. Multiwall nanotubes consist of concentric, coaxial tubes within tubes and can be up to 100 nm in diameter. The smallest single-wall nanotube would be 0.6 nm in diameter. Typical nanotubes are only microns long, and to date, none have been produced longer than 100 microns (approximately 0.004 inch).

To date, researchers have announced several methods for producing nanotubes; all of which have been developed empirically.

1) Laser beams are fired into the end of a specially prepared metal-doped graphite rod in an oven of flowing argon. The oven temperature is 2,000 °F. The laser energy vaporizes graphite, which immediately condenses into nanotubes.

2) An electric arc is established between graphite electrodes (also specially prepared and metal-doped but differently than for the laser method) in a flowing helium atmosphere.

3) Carbon monoxide, at high pressure, and iron carbonyl [$Fe(CO)_5$] catalyst are reacted at 1,000 °C in a special chamber that recirculates both unreacted carbon monoxide and heat.

4) Either benzene or acetylene are carefully combusted in oxygen with catalytic compounds.

Methods 1 and 2 are capable of producing approximately 1 gram (g) of CNTs per day, which is sold at $1,000 per gram. Method 3, referred to as the "HIPCO" (high-pressure carbon monoxide) process, is being developed at Rice University in Houston, Texas, in conjunction with NASA-Johnson Space Center (NASA-JSC) personnel, in a process designed to produce 100 g of CNTs per day.

2.5.2 Other Reduced Weight Materials

2.5.2.1–Foam Metals Researchers have fabricated foam metals with a highly uniform pore size. Such foam metals are claimed to offer a strength-to-weight ratio of approximately 2 vs. the same metal without pores.

2.5.2.2–GLARE GLARE (glass fiber-reinforced aluminum) is the name given to alternate layers of aluminum and fiberglass bonded together. In June 2001, Airbus, Inc. announced it will use this material (offering a 15% to 20% weight reduction vs. aluminum) in some fuselage parts of the A380 aircraft (Ref. 12).

2.5.2.3–Moldite In October 2001, Moldite Technologies announced a resin-composite material with a proprietary core that it claims can reduce product weight up to 90% (Ref. 13).

2.6 The NASA-LaRC Flight Optimization System Code

NASA-LaRC has developed an extensive code used to analyze the following (and many additional) parameters of commercial transport aircraft:

- weights;
- efficiencies;
- fuel consumption; and
- aerodynamic factors.

Quoting from the introduction of the FLOPS users manual:

"The Flight Optimization System (FLOPS) is a multidisciplinary system of computer programs for conceptual and preliminary design and evaluation of advanced aircraft concepts. It consists of nine primary modules: 1) weights, 2) aerodynamics, 3) engine cycle analysis, 4) propulsion data scaling and interpolation, 5) mission performance, 6) takeoff and landing, 7) noise footprint, 8) cost analysis, and 9) program control."

Modules 3, 6, 7, and 8 were not used for this analysis. When parameters are entered into the code in an iterable form (i.e., as a mathematical function of other parameters), the code can be used to optimize on a given parameter (e.g., it can minimize onboard fuel weight at takeoff).

2.6.1 Input and Output Parameters

The use of the NASA-LaRC FLOPS code is best illustrated in the next section. Significant inputs include energy conversion efficiencies and component weights. The output parameter of interest is maximum calculated range.

2.7 System Results

2.7.1 Emissionless Aircraft P/P Systems Based on Planar Solid Oxide Fuel Cells

Based on what has been learned to date, the "best" P/P system would use:

- LH_2 fuel;
- PSOFCs for electricity generation;
- a bottoming cycle using turbines coupled to generators to convert PSOFC exhaust heat to additional electric power;
- LH_2-cooled electric motors; and
- propulsion fans driven by the motors.

The propulsion fans would essentially be state of the art, but each engine "core" would be an LH_2-cooled "cryomotor" rather than a GTE.

Figure 2 is a schematic diagram depicting the parameters of the power production side of such a P/P system operating during the cruise phase of a flight mission. The masses in the figure are based upon each kilogram of ambient air that enters the system as a reactant. Temperatures, pressures, and Mach number result from:

- ambient atmospheric conditions at cruise altitude;
- aircraft velocity;
- compressor and turbine characteristics calculated according to standard codes;
- stated PSOFC operating conditions;
- using air properties for PSOFC exhaust; and
- selecting a final system exhaust temperature at which (in theory) 99.5% of the water in the exhaust gas will condense.

2.7.2 Component Weight Summary

Table 5 presents the weights (near-term conditions and conventional materials) of the major components of the PSOFC-based P/P system on a per megawatt basis. All items are sized for the "climb" power level ***except*** items 7 and 8 (exhaust heat exchangers), which are sized for the cruise power level. The reason for this difference is given below.

1) Until more is known about the practical operating characteristics of electric aircraft P/P system components, NASA-LaRC and MSE are assuming these components may not be operated at more than a 100% power level. Thus, they are sized for climb conditions where the total P/P generated power is calculated to be approximately 85 MW. (This climb power level was for "near-term" conditions with no weight reduction from using lighter material. However, the climb power level was not significantly less even for cases where more advanced technology was assumed because landing weight is the same and therefore, the power required to climb out of a missed landing approach is the same).

2) The altitude above which water vapor emission has potential adverse effects has been stated to be 25,000 ft by Dr. Patrick Minnis of NASA-LaRC. Therefore, NASA-LaRC and MSE envision that it would be permissible for an HFC-powered aircraft to bypass (or partially bypass) exhaust cooling for the purpose of water capture during the ***climb*** phase of the flight mission. From takeoff up to 25,000 ft, water emission would not be detrimental, and the remainder of the climb phase from 25,000 ft to 42,000 ft would require approximately 10 minutes. Such a procedure reduces the combined heat exchanger weight (which can thereby be sized for cruise power conditions) by approximately 22,000 lb and also reduces the retained water weight (which is otherwise carried to the landing phase of the flight mission) by up to approximately 34,000 lb.

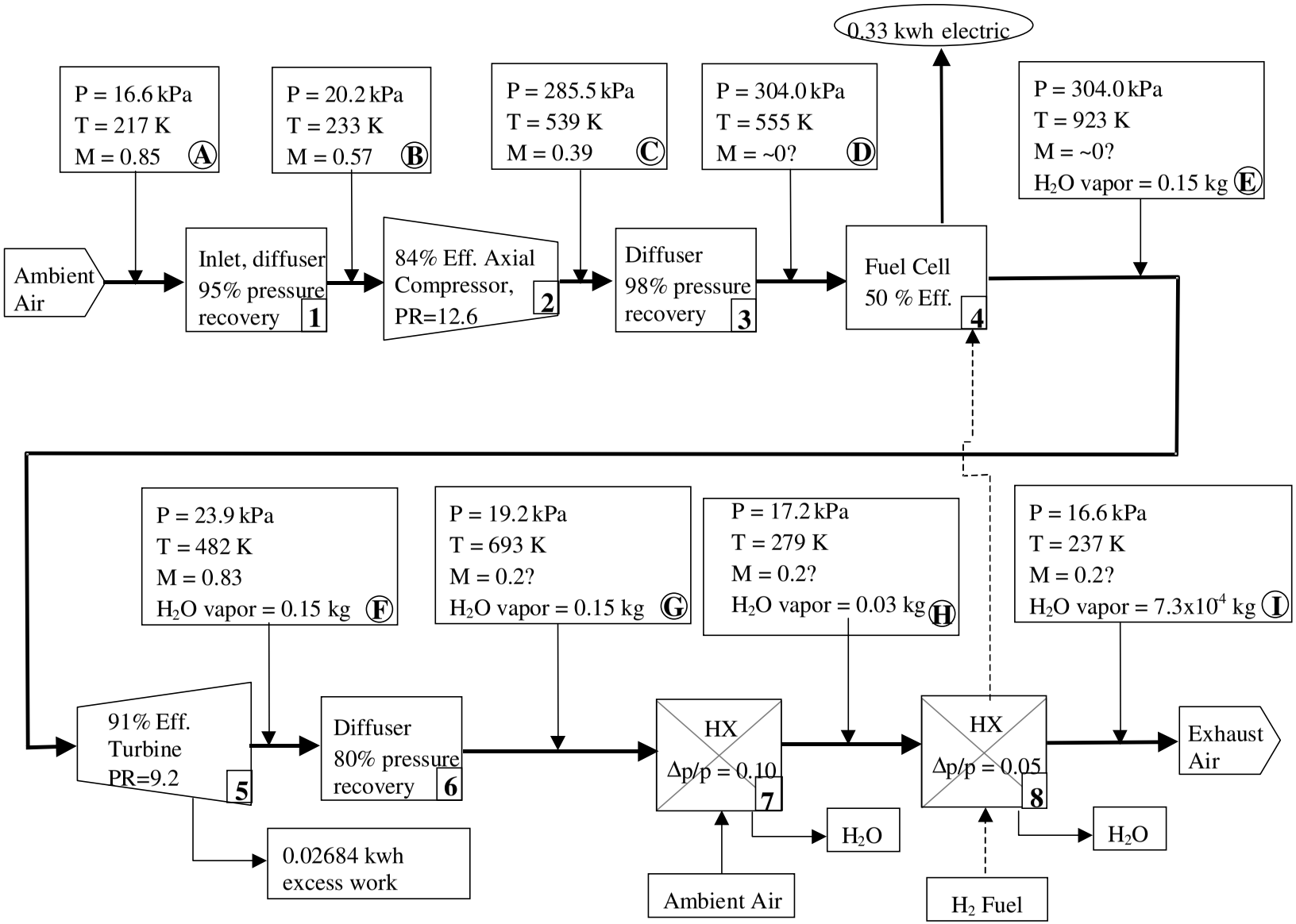

Figure 2. PSOFC P/P system.

Table 5. PSOFC P/P system near-term component weights (per MW, no weight reduction).

Component	Weight per MW PSOFC Output (Max.)
1) Inlet diffuser	Part of nacelle weight
2) Axial compressors	12.9 lb/MW
3) Pressure recovery diffuser	Relatively small
4) PSOFCs	1,102 lb/MW
5) Bottoming turbine	25.8 lb/MW
6) Pressure recovery diffuser	Relatively small
7) Exhaust-to-air heat exchanger	116 lb/MW
8) Exhaust-to-GH_2 heat exchanger	16.9 lb/MW
9) Bottoming generators	22.9 lb/MW
10) Propulsion motors	66 lb/MW[1]
11) Compressor motors	17.8 lb/MW
Total	1,385 lb/MW
[1]Based on propulsion motor output.	

2.7.3 Typical FLOPS Code Calculations for the Emissionless Aircraft Concept

The following parameters are used by NASA-LaRC and MSE in the FLOPS code calculations of emissionless aircraft performance. These are for both a near-term scenario using aerodynamic parameters and P/P system efficiencies that are essentially current state of the art and a long-term scenario using more aggressive aerodynamic and P/P system assumptions. Respective assumptions for Table 6 (near term) and Table 7 (long term) are as given below.

- PSOFC electrochemical efficiency:
  near-term: 50% cruise, 60% descent
  long-term: 60% cruise, 70% descent

- PSOFC power density (weight basis):
  near-term: 1,102 lb/MW
  long-term: 100 lb/MW

- Propulsion fan efficiency:
  near-term: 85%
  long-term: 87%

- Percentage laminar flow:
  near-term: 20%, on the wing only
  long-term: 50%, on the wing, tail, and fan nacelles

For both tables, another input parameter was WRF. Where applicable, a component or system of the aircraft (which would presently be fabricated from aircraft-grade aluminum alloy) could potentially be fabricated from lighter weight materials of equal strength (e.g., foamed metals or composite material based upon CNTs). Both types of lightweight materials are currently under development. Assumptions used that are common to both near- and long-term conditions are stated below.

Table 6. Results with near-term scenario assumptions.

Item #	Parameter	Units	WRF=1.0	WRF=1.5	WRF=2.0	WRF=2.5	WRF=3.0
1	Fuel cell air inlet/diffuser	lb	0	0	0	0	0
2	Axial compressor	lb	1,007	679	504	403	336
3	Compressor motor	lb	1,390	1,404	1,390	1,390	1,390
4	Diffuser	lb	0	0	0	0	0
5	PSOFC	lb	86,139	87,042	86,132	86,132	86,172
6	Power turbine	lb	2,015	2,036	2,015	2,015	2,016
7	Power generator	lb	1,789	1,808	1,789	1,789	1,790
8	Diffuser	lb	0	0	0	0	0
9	Exhaust-to-air HX	lb	9,032	9,127	9,032	9,032	9,036
10	Exhaust-to-hydrogen HX	lb	1,320	889	660	528	440
11	Cooling air inlet/diffuser	lb	0	0	0	0	0
12	Propulsion motors	lb	5,489	5,547	5,489	5,489	5,491
13	Product water tank	lb	5,759	5,435	4,779	4,155	3,653
14	LH_2 tank	lb	4,403	3,884	3,052	2,601	2,255
15	LH_2 insulation	lb	2,108	2,789	3,191	3,429	3,594
16	Propulsion fan and nacelle	lb	11,603	7,817	5,801	4,641	3,869
17	Structure	lb	201,246	139,893	105,830	85,281	70,773
18	Systems, equipment	lb	65,608	55,495	49,981	46,765	44,856
19	Passenger service	lb	6,266	6,266	6,266	6,266	6,266
20	Cargo containers	lb	2,450	1,634	1,225	980	808
21	Passengers	lb	49,500	49,500	49,500	49,500	49,500
22	Baggage	lb	13,200	13,200	13,200	13,200	13,200
23	Crew and baggage	lb	2,090	2,090	2,090	2,090	2,090
24	Takeoff wt.	lb	499,100	431,842	392,315	369,083	353,025
25	Landing wt.	lb	608,818	600,818	595,818	592,657	590,394
26	Max. water wt.	lb	180,543	255,559	299,651	325,604	343,537
27	Takeoff fuel wt.	lb	24,017	31,777	36,350	39,061	40,940
28	Maximum landing wt.	lb	655,626	655,626	655,626	655,626	655,626
29	Initial cruise altitude	ft	43,995	45,000	45,000	45,000	45,000
30	Final cruise altitude	ft	41,145	41,578	41,541	41,613	41,715
31	Cruise power (end of cruise)	MW	31.46	31.38	30.94	30.82	30.77
32	Climb power	MW	84.04	84.92	84.03	84.03	84.07
33	Unconsumed fuel at landing	%	24.5	21.7	20.7	20.3	20.1
34	Fuel energy density	Btu/lb	61,100	61,100	61,100	61,100	61,100
35	Electrochemical eff. (cruise)	%	50	50	50	50	50
36	Electrochemical eff. (descent)	%	60	60	60	60	60
37	Motor efficiency	%	99	99	99	99	99
38	Fan efficiency (at cruise)	%	85	85	85	85	85
39	WGF (lb increase/lb fuel)	---	7.94	7.94	7.94	7.94	7.94
40	L/D ratio (cruise)	---	25.0-25.5	24.1-25.2	23.6-25.3	23.2-25.3	22.7-25.2
41	Climb range	nmi	129	99	85	77	72
42	Cruise range	nmi	2,216	3,626	4,578	5,148	5,549
43	Descent range	nmi	223	222	224	224	224
44	**Total range**	**nmi**	**2,568**	**3,947**	**4,886**	**5,448**	**5,844**
45	Number of passengers	---	300	300	300	300	300
46	Cost per lb LH_2	$	1.5	1.5	1.5	1.5	1.5
47	LH_2 cost per seat-mile	cents	3.541	3.159	2.955	2.862	2.805
48	Wing area	ft^2	5,132	5,130	4,977	4,968	4,973
49	Wing span (including winglets)	ft	262.5	262.5	262.5	262.5	262.5
50	Wing aspect ratio	---	13.4	13.4	13.8	13.9	13.9
51	Percentage laminar flow	%	20	20	20	20	20
52	% fuselage drag reduction	%	3	3	3	3	3
53	% drag reduction due to winglets	%	6	6	6	6	6

Table 7. Results with long-term scenario assumptions.

Item #	Parameter	Units	WRF=1.0	WRF=1.5	WRF=2.0	WRF=2.5	WRF=3.0
1	Fuel cell air inlet/diffuser	lb	0	0	0	0	0
2	Axial compressor	lb	858	567	425	340	283
3	Compressor motor	lb	1,180	1,170	1,170	1,170	1,170
4	Diffuser	lb	0	0	0	0	0
5	PSOFC	lb	7,975	7,908	7,908	7,908	7,908
6	Power turbine	lb	1,712	1,697	1,698	1,698	1,697
7	Power generator	lb	1,521	1,508	1,508	1,508	1,508
8	Diffuser	lb	0	0	0	0	0
9	Exhaust-to-air HX	lb	7,681	7,616	7,616	7,616	7,616
10	Exhaust-to-hydrogen HX	lb	1,124	743	557	446	371
11	Cooling air inlet/diffuser	lb	0	0	0	0	0
12	Propulsion motors	lb	5,536	5,490	5,490	5,490	5,490
13	Product water tank	lb	7,903	7,046	5,974	5,119	4,458
14	LH_2 tank	lb	5,543	4,341	3,592	3,033	2,605
15	LH_2 insulation	lb	2,654	3,434	3,838	4,089	4,259
16	Propulsion fan and nacelle	lb	11,696	7,732	5,799	4,639	3,866
17	Structure	lb	209,029	142,285	107,984	87,003	72,858
18	Systems, equipment	lb	66,619	55,753	50,418	47,174	45,040
19	Passenger service	lb	6,266	6,266	6,266	6,266	6,266
20	Cargo containers	lb	2,450	1,634	1,225	980	816
21	Passengers	lb	49,500	49,500	49,500	49,500	49,500
22	Baggage	lb	13,200	13,200	13,200	13,200	13,200
23	Crew and baggage	lb	2,090	2,090	2,090	2,090	2,090
24	Takeoff wt.	lb	438,133	363,435	324,838	301,025	284,907
25	Landing wt.	lb	609,467	599,728	594,102	590,483	587,996
26	Max. water wt.	lb	247,727	331,307	374,514	401,183	419,232
27	Takeoff fuel wt.	lb	30,237	39,113	43,725	46,580	48,515
28	Maximum landing wt.	lb	655,626	655,626	655,626	655,626	655,626
29	Initial cruise altitude	ft	45,000	45,000	45,000	45,000	45,000
30	Final cruise altitude	ft	40,016	40,079	40,243	40,391	40,518
31	Cruise power (end of cruise)	MW	27.59	27.16	27.04	26.95	26.90
32	Climb power	MW	84.74	84.03	84.04	84.04	84.03
33	Unconsumed fuel at landing	%	19.2	18.0	17.7	17.6	17.6
34	Fuel energy density	Btu/lb	61,100	61,100	61,100	61,100	61,100
35	Electrochemical eff. (cruise)	%	60	60	60	60	60
36	Electrochemical eff. (descent)	%	70	70	70	70	70
37	Motor efficiency	%	99	99	99	99	99
38	Fan efficiency (at cruise)	%	87	87	87	87	87
39	WGF (lb increase/lb fuel)	---	7.94	7.94	7.94	7.94	7.94
40	L/D ratio (cruise)	---	27.6-28.4.	26.7-28.4	25.4-28.3	24.2-28.2	23.2-28.1
41	Climb range	nmi	98	74	62	56	52
42	Cruise range	nmi	4,989	7,491	8,894	9,798	10,416
43	Descent range	nmi	247	248	247	247	247
44	**Total range**	**nmi**	**5,334**	**7,813**	**9,204**	**10,101**	**10,715**
45	Number of passengers	---	300	300	300	300	300
46	Cost per lb LH_2	$	1.5	1.5	1.5	1.5	1.5
47	LH_2 cost per seat-mile	cents	2.294	2.056	1.957	1.902	1.869
48	Wing area	ft^2	5,129	4,968	4,968	4,968	4,968
49	Wing span (including winglet)	ft	262.5	262.5	262.5	262.5	262.5
50	Wing aspect ratio	---	13.4	13.9	13.9	13.9	13.9
51	Percentage laminar flow	%	50	50	50	50	50
52	% fuselage drag reduction	%	3	3	3	3	3
53	% drag reduction due to winglets	%	6	6	6	6	6

1) It is assumed that the total P/P system actually consists of four independent equal-size systems. This aids component placement and adds a redundancy safety factor.

2) The maximum designed landing weight of the emissionless aircraft will never exceed the maximum designed takeoff weight of its counterpart hydrocarbon fueled aircraft (655,626 lb).

3) Product water will not be recovered and retained onboard the aircraft during the climb phase of a flight mission. This allows for a significant reduction in the weight and volume of:

   - heat exchangers, which are required to condense and recover water from the HFC exhaust gas;
   - reaction-product water holding tanks; and
   - weight of the nonretained water.

4) If required, it will be permissible to increase the aircraft fuselage diameter and/or length. The FLOPS code will automatically calculate the resulting increase in friction drag.

5) Wing span will be restricted to the 262.5 ft (80 m) as required by the FAA.

6) Regulated aircraft flight requirements (already included in the FLOPS code) must be satisfied. For example, if one of the four P/P systems has failed, the other three must be able to allow the aircraft to sustain a specified angle-of-climb and reexecute a missed landing approach.

7) At this time, it will not be considered possible for any P/P system component to operate at greater than 100% of its maximum-rated power level. (In the future, NASA-LaRC and MSE may determine that some power overrating is permissible, and this will allow the design weights of [selected] P/P system components to be reduced).

8) The P/P system to be used will be based on PSOFCs with a bottoming cycle designed according to aircraft GTE guidelines.

9) NASA-LaRC limited cruise altitudes (Items 29 and 30 in Tables 6 and 7) to a ceiling of 45,000 ft. For those situations using a WRF high enough to allow the aircraft to be somewhat "light" at the beginning of the cruise phase, the aerodynamics may favor the aircraft flying higher than 45,000 ft. However, thinner air at that altitude will require more energy to compress air for the PSOFCs; this energy would not be available for propulsion. Since this and other altitude effects on propulsion are not being modeled for this current level of analysis, the true optimum cruise altitude cannot be determined at this time.

10) WGF (item 39 in Tables 6 and 7) is the weight growth factor, which is the pounds increase in emissionless aircraft weight for each pound of LH_2 consumed.

2.7.4 Power/Propulsion System Component Placement

The concept for an emissionless transport aircraft is innovative; therefore, the P/P system uses components and component placements onboard the aircraft that are nonconventional compared to current commercial aircraft. Based on what has been learned to date, the important component placement requirements are given below.

1) Due to the required insulation thickness, LH_2 fuel is more efficiently carried in the aircraft fuselage rather than in the wings (Ref. 14).

2) The exhaust-to-air heat exchangers must be placed so that atmospheric air can flow through them.

3) Liquid hydrogen tanks and product water tanks must be located such that the center of gravity of the aircraft will not significantly change during a flight mission.

Table 8 presents the calculated dimensions of P/P system components. As mentioned above, most "components" are actually four equal-sized items (except for the two LH_2 tanks).

Table 8. PSOFC P/P system component dimensions and total weight.

Component	Dimensions (Each)	Total Weight	WRF
1) Inlet diffusers		-----	X
2) Axial compressors	25-in dia. x 27-in length	1,007 lb	X
3) Pressure recovery diffusers		-----	X
4) PSOFCs	5.9 ft x 5.9 ft x 11.4 ft	86,139 lb	
5) Bottoming turbines	25-in dia. x 34-in length	2,015 lb	
6) Pressure recovery diffusers		-----	
7) Exhause-to-air heat exchangers	6.25 ft x 5.9 ft x 1 ft	9,032 lb	
8) Exhaust-to-GH_2 heat exchangers	5.9 ft x 1.1 ft x 2 ft	1,320 lb	X
9) Bottoming generators	~ 2-ft dia. x ~ 5-ft length	1,789 lb	
10) Propulsion motors	3.3-ft dia. x 6.2-ft length	5,489 lb	
11) Compressor motors	~ 2-ft dia. x ~ 4-ft length	1,390 lb	
12) Product water tanks	5,503 ft^3 (for WRF=3)	5,759 lb	X
13) LH_2 tanks	11,584 ft^3 (for WRF=3)	4,403 lb	X
14) LH_2 insulation		2,108 lb	
15) Propulsion fans and nacelles	7.5-ft dia.	11,603 lb	X

The following notes apply to Table 8.

1) Propulsion fans and the motors driving them are hung from the aircraft wings. Some of the product water is stored in the wings. All other components are located in the fuselage.

2) Equipment is sized for near-term assumptions with no weight reduction (WRF = 1.0, except as noted in table).

3) With the present scheme, it was not possible to locate air compressors for the PSOFCs in the proximity of the bottoming cycle turbines; therefore, separate electric motors must be used to drive the air compressors.

4) The weight and size of product water tanks, LH_2 tanks, and LH_2 insulation is based on the amount of LH_2 that may be carried onboard (as calculated by the FLOPS code). All other weights and sizes of P/P components (except heat exchangers, as explained previously) are based on required climb power using near-term assumptions.

5) It is assumed that the propulsion motors will fit as "cores" within the propulsion fans.

6) An "X" in the right column of Table 8 indicates the potential of replacing aircraft aluminum alloy with a lighter material with the same strength (e.g., CNT–resin composite).

Figures 3 and 4 illustrate a conceptual design or placement of P/P and other components for the NASA-LaRC/MSE emissionless aircraft.

2.7.5 Particular Features of this Conceptual Design

- It was necessary to increase the fuselage diameter from 20 ft to 25 ft. This allows for all 300 passengers to be placed in a "double-deck" arrangement, as well as the LH_2 tanks to be placed in the fuselage as explained previously.

- Liquid hydrogen fuel is carried in two tanks (front end and back end of the fuselage) so that the aircraft center of gravity can be controlled.

- NASA-LaRC considers it probable that a feasible fuselage diameter could be less than 25 ft (though larger than the 20-ft-diameter fuselage of the baseline aircraft); however, at the presently known level of detail, NASA-LaRC and MSE consider that the extra effort required to design a conceptual component placement using a fuselage diameter intermediate between the 20 and 25 ft values is not justified.

- Planar solid oxide fuel cell stacks and their associated air compressors, turbines, and heat exchangers have been conceptually placed at the bottom of the fuselage where reaction and cooling air can be "scooped in," and cooled exhaust air (with water extracted and retained onboard) can exit out the back.

2.7.6 Tradeoff: Fraction of Retained Water vs. Aircraft Weight

The final exhaust temperature of 237 K in Figure 2 resulted from design calculations and tradeoffs involving inlet HFC air pressure, inlet turbine temperature, heat exchanger weight, and atmospheric airflow required for cooling the exhaust-to-air heat exchanger.

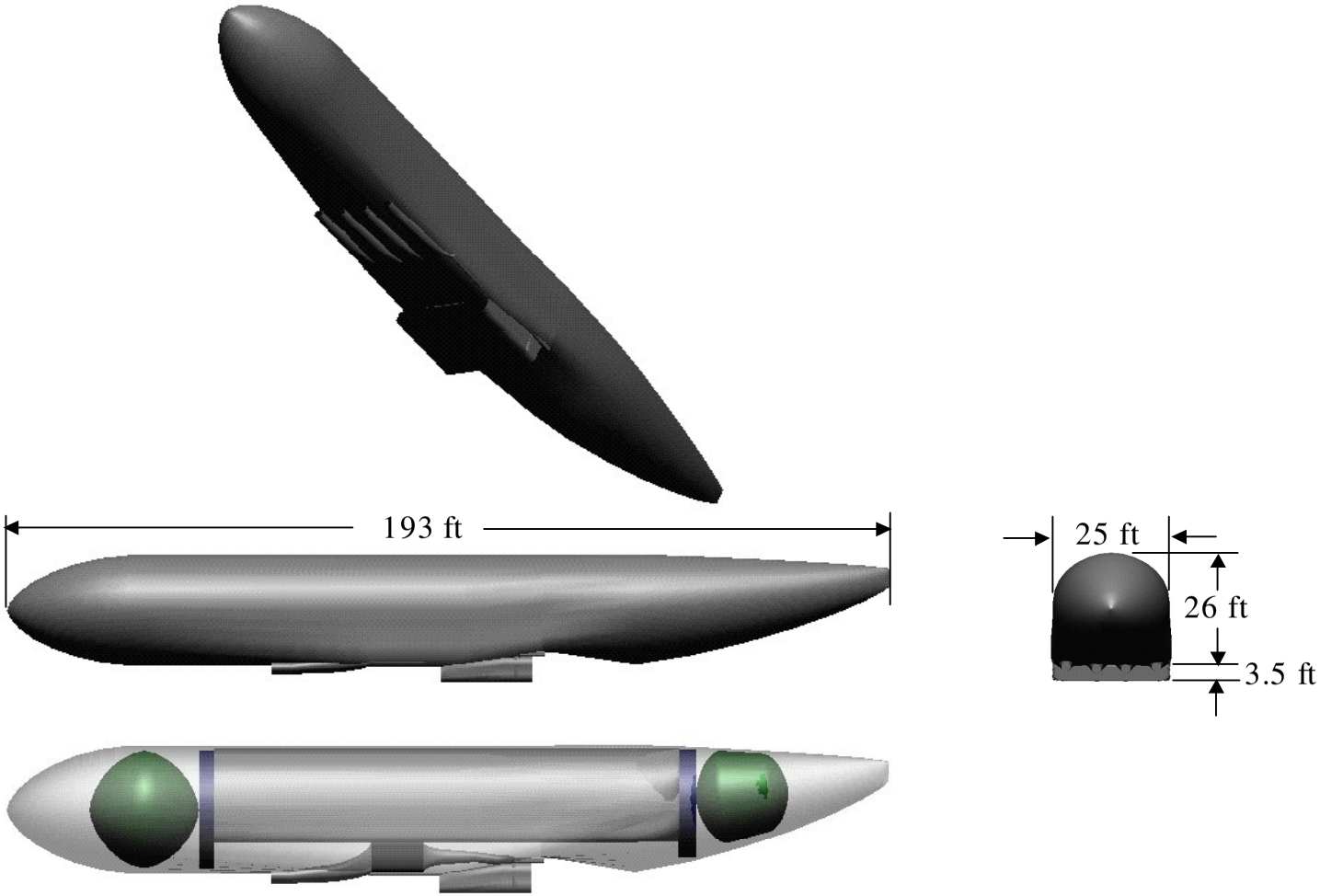

Figure 3. Fuselage arrangement.

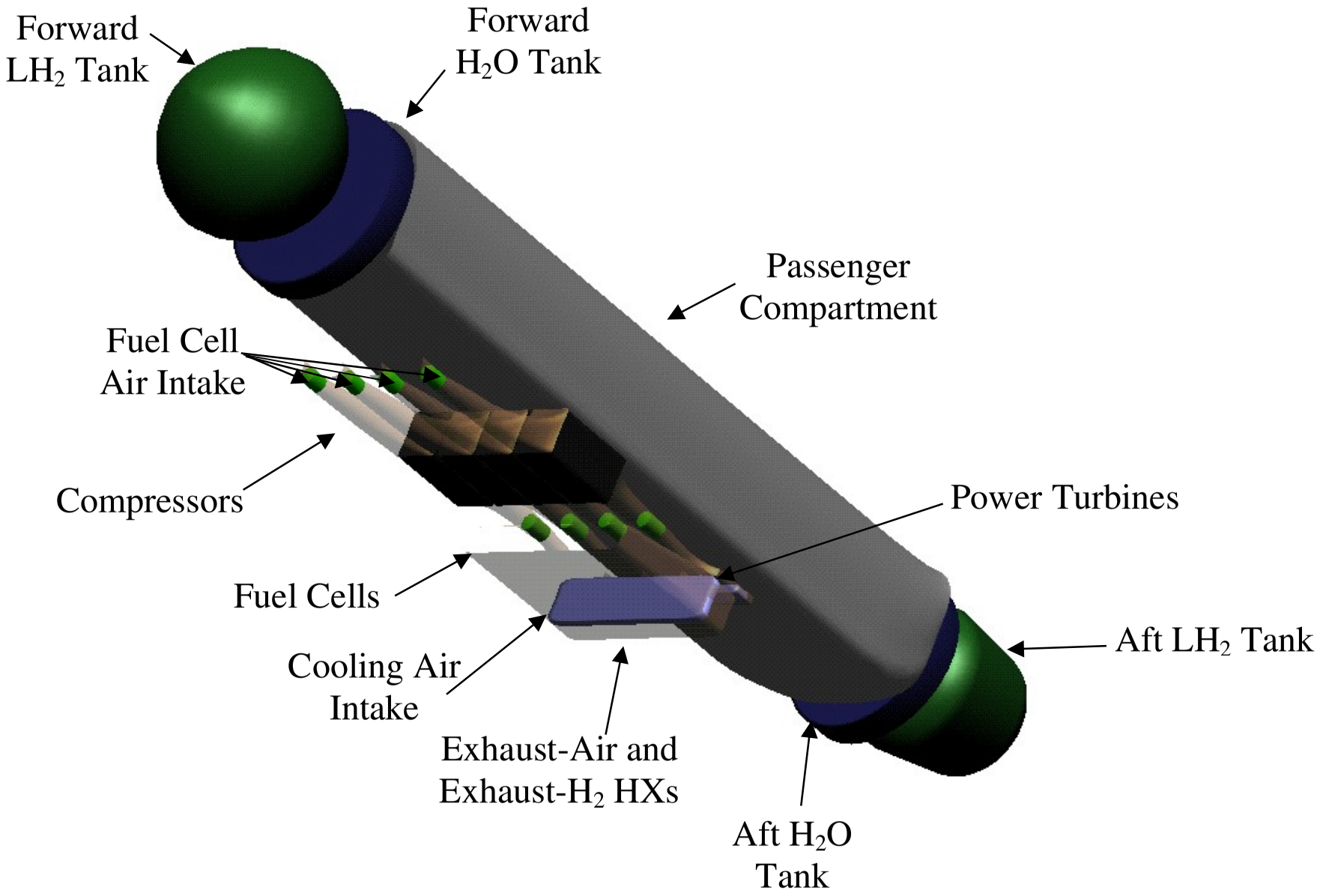

Figure 4. Internal fuselage arrangement.

At this temperature, approximately 99.5% of the water in the exhaust gas will theoretically condense. The fraction of "captured" water could be increased slightly but only with a severe onboard weight penalty, as the inherent mechanism of heat transfer would require the weight of the exhaust-to-air heat exchanger to increase exponentially to reduce the exhaust temperature a few more degrees in an attempt to condense slightly more water. It is believed that 99.5% water capture (and zero emission of all other chemical reaction products) is sufficiently "emissionless" for a transport aircraft with a practical range vs. a much heavier aircraft (with theoretical water capture closer to 100%) that may indeed be too heavy to fly or possess a maximum range too short to be practical.

2.7.7 Discussion of Selected Emissionless Aircraft Components

Comments on some of these components are given below.

1) The future prospects for significantly reducing the volume (and weight) of PSOFCs are excellent. This is because the technology is relatively immature (but progressing rapidly at this time).

2) The following are potential approaches by which the weight and size of P/P heat exchangers can be reduced:

    a) Greater PSOFC electrochemical efficiency allows fuel cell and power generating equipment to be sized inversely proportionately smaller (e.g., when electrochemical efficiency is increased from 50% to 60%, compressors and fuel cells can be reduced to five-sixths of their original weight and size to deliver the same level of power).

    b) When PSOFC manufacturers learn how to use an air-to-fuel ratio less than 1.75 (conservatively used by MSE) and closer to 1.00, there will be a decreased mass flow of exhaust gas that will also allow heat exchanger sizes and weights to be reduced.

    c) Additionally, calculations may show that the replacement of standard types of heat exchangers with technology based upon "Supertubes" (Section 3.2.2), may significantly decrease heat exchanger sizes and weights. At this time, MSE estimates that a total weight reduction of one-half (compared to the state of the art) is potentially possible by using Supertubes (Section 3.2.3) and riblet technology on heat exchanger heat transfer surfaces (Section 2.4.2.1) and is using these estimated weight reductions for calculations in this report.

    d) The exhaust entering the exhaust-to-air heat exchanger would be approximately 544 K (271 °C). Therefore, NASA-LaRC/MSE have not conceptually applied a WRF to this heat exchanger (as is done for the downstream exhaust-to-hydrogen heat exchanger in which the exhaust gas is considerably cooler) because the resin of a potential CNT composite material could probably not withstand such a temperature. However, if foam metals could be fabricated into heat exchanger internal parts, the WRF could be applied.

e) Heat exchanger weight and size are ***somewhat*** arbitrary (i.e., adding more heat exchanger weight and surface area will cool the fuel cell exhaust gas to a lower temperature and theoretically condense a higher fraction of water to liquid). The design presented in this report will theoretically achieve a 99.5% liquid water retention factor (during the cruise phase of a flight mission). However, if 99% liquid water retention was considered acceptable for the cruise phase of a flight mission, the required amount of cooling and resulting size and weight of heat exchangers would automatically be reduced.

3) By far, the highest volume component in the fuselage is LH_2 fuel; LH_2 by its very nature is a very low density fuel. Figures 3 and 4 are drawn to scale and illustrate the volume required for LH_2 fuel for near-term assumptions with a WRF of 3. Nearly 41,000 lb of LH_2 at takeoff requires a 24-ft-diameter spherical forward tank ***and*** a 21.5-ft-long tapered cylindrical tank at the aft end of the fuselage (with a combined volume of 11,584 ft^3) for its containment. As other emissionless aircraft technologies advance, the calculated maximum range of such an aircraft will also increase. When the calculated maximum aircraft range equals the highest range that is commercially viable, further technological advances will allow the volume and weight of onboard LH_2 to be decreased.

4) Two fans, each driven by an LH_2-cooled core electric motor, would be hung from each wing. The outside visual appearance of these fans would probably be similar to current gas turbine-based engines.

5) Reaction product water (up to 200,000 lb) is stored in the wings during a flight mission. The remainder of the reaction product water is stored in fore and aft cylindrical tanks (blue disks shown in Figures 3 and 4).

2.7.8 FLOPS Calculation Maximum Range Results

Calculated maximum emissionless aircraft ranges for respective near-term and long-term conditions are presented in Figure 5. A discussion of selected results follows.

1) Using near-term assumptions and ***no weight reduction***, an emissionless transport 300-passenger aircraft of the size under consideration would have a maximum calculated range of 2,568 nmi. This is enough to service many coast-to-coast U.S. flights and (***in principle***) could be done with near-term technology.

2) Near-term assumptions coupled with WRFs up to 3 for applicable components would increase the calculated maximum range to 5,844 nmi. This is 27% of the distance around the world and would service a majority of airline flights.

3) Using long-term assumptions, the calculated maximum range for no weight reduction would be 5,334 nmi, and for a WRF of 3, the calculated maximum range would be 10,715 nmi, which is 50% of the distance around the world. Note that the maximum range of the conventional baseline aircraft used in this study is 7,500 nmi.

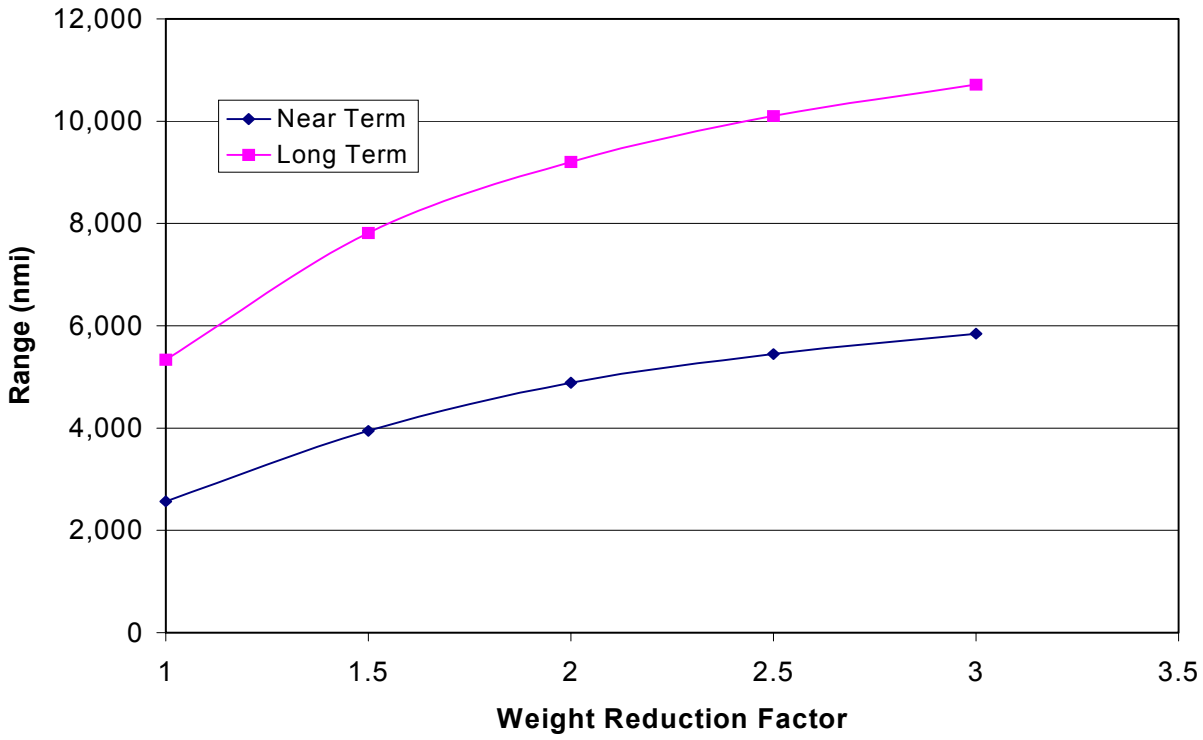

Figure 5. Emissionless aircraft ranges.

2.7.9 FLOPS Calculation Maximum Range Results—if Liquid Water is Expelled—The "Weinstein Approach"

It should be pointed out that it is very misleading to compare the performance characteristics of an emissionless aircraft with an aircraft that exhausts all of its reaction products to the atmosphere. Specifically, the cost for an aircraft to be emissionless (achieved by retaining liquid water reaction product onboard for the duration of a flight mission) is a dramatic reduction in maximum range.

Dr. Leonard Weinstein of the Advanced Measurement and Diagnostics Branch of NASA-LaRC suggested that the problem of water vapor emission into the upper atmosphere could potentially be solved (without a high weight penalty) by ejecting water formed in HFCs as soon as it is cooled. This water could be ejected as either widely dispersed liquid drops or finely powdered ice. Weinstein believes neither form of water would significantly reevaporate while falling from a typical cruise altitude of 42,000 ft to the "critical altitude" of 25,000 ft identified by Dr. Patrick Minnis of NASA-LaRC, or be a danger if it impacted the ground (i.e., did not reevaporate at a lower altitude).

In the opinion of NASA-LaRC and MSE, the Weinstein approach could be made to work and would achieve the project goal (no water vapor to the upper atmosphere) sooner than any other approach. However, modeling followed by experiments would need to be performed to verify

that the liquid water (or finely powdered ice) could be expelled in such a form that it could not increase in size and cause damage on the ground if very humid atmospheric conditions are encountered at lower altitudes during some flights.

To illustrate the significance of this approach, NASA-LaRC repeated the (near-term assumptions, WRF=1) FLOPS code calculation of maximum range for the emissionless aircraft (2,568 nmi), but for this specific calculation assumed that all the reaction product water would be condensed to liquid (and/or frozen to ice) and expelled after exhausting the bottoming cycle turbines, and therefore heat exchangers would be required, but water tanks and retained water would not be onboard.

The resulting calculated maximum range (for a maximum takeoff weight of 655,626 lb equal to that of the baseline hydrocarbon-fueled aircraft) is 15,018 nmi (70% of the way around the world). This means the Weinstein approach would increase maximum calculated aircraft range for the assumed conditions by 585% compared to the water retention approach.

However, NASA-LaRC/MSE believe that an advanced method of producing energy that produces no water is preferable in the long term.

2.8 Other Organizations Developing Fuel Cells for Aviation Applications

2.8.1 FASTec Electric Plane

The Foundation for Advancing Science and Technology Education (FASTec) is designing and building a fuel cell-powered electric plane (e-plane). The leader of the project team is Mr. James Dunn. MSE recently observed the e-plane that is located at the Worcester, Massachusetts, airport, and discussed technical details of this project with Mr. Dunn.

2.8.1.1–Background Mr. Dunn's approach for the e-plane was to first locate a general aviation aircraft possessing low drag and light weight, replace the internal combustion engine and its auxiliary systems with an electric motor and advanced rechargeable batteries, and conduct test flights of up to a range of 100 miles. The ultimate plan for the project is to replace most of the rechargeable batteries with HFCs (75-kW total power rating) and fly the aircraft for a distance of 500 miles. For fuel cell flight, the onboard hydrogen fuel (stored as pressurized gas in tanks) would weigh 3 to 5 kg. For either battery or fuel cell-powered flight, maximum takeoff power is rated at 53 kW, and maximum continuous cruise power is rated at 32 kW. The MGTOW of the e-plane is designed to be 1,100 lb. The airplane that is being modified is an all-carbon composite French-built "DynAero Lafayette III," donated by American Ghiles Aircraft of Dijon, France.

2.8.1.2–Project Status As of late 2002, the project team had mounted the batteries, controller, electric motor, and propeller on a test stand for extensive testing. MSE observed the motor and propeller revolving at 1,000 revolutions per minute (rpm) (limited to that value by local regulations, as the construction and ground testing is occurring indoors).

The electric motor is a brushless, neodymium-boron-iron (Nd-B-Fe) magnet, 3-phase design and is rated at 75-kW peak power. An onboard electronic controller converts dc power from the

batteries (or fuel cells) to 3-phase controlled-width pulses. (Pulse width is proportional to electric power sent to the motor).

During the battery phase of testing, approximately 100 batteries (cells) must be connected in series in order to provide the voltage range required for the motor [200 to 400 volts (V)]. A formidable problem being solved by the project team is to place a "monitor-controller" electronics package on ***each*** individual battery to eliminate (i.e., bypass) from the series connection any individual battery that becomes overheated or defective during either charging or discharging.

2.8.1.3–Supporting Calculations Personnel at the NASA Glenn Research Center (NASA-GRC) have performed calculations that support the calculations and design work of the FASTec team.

2.8.2 Boeing Fuel Cell Auxiliary Power Unit

In late 2001, the Commercial Airplanes division of Boeing Corporation announced a joint effort with the Boeing Research and Technology Center in Madrid, Spain, to replace the engine of a small single-engine propeller aircraft with fuel cells and an electric motor (Ref. 15). Boeing's goal is to replace the auxiliary power unit of a large commercial aircraft with fuel cells having an approximate power range of 300 to 400 horsepower (hp) (225 to 300 kW). The strategy is to use a fuel cell-powered motor-glider in the approximate power range of 35 to 50 hp to determine how efficiently fuel cells function at various altitudes. Flight tests are scheduled to begin in early 2004.

3. Midterm Energetics and Advanced Technology Alternative Approaches

3.1 Advanced Energetics

In order to overcome the limitations of chemical reaction-based energy producing systems for aircraft propulsion applications, MSE has been investigating advanced research currently being conducted at a number of locations. The goal of the advanced research is to produce a significantly higher energy density on a weight basis. This section describes some of this research.

3.1.1 High Energy Density Material Fuels

NASA-LaRC requested that MSE investigate the state-of-the-art of high energy density material (HEDM) fuels and fuel-oxidizer systems. In general, HEDM fuels, in contrast with more normal fuels, can be characterized as significantly more:

- energy dense;
- difficult to produce;
- difficult to store; and
- difficult to control.

The present goal of HEDM fuel research is to increase rocket propulsion specific impulse (I_{sp}), and as a result, HEDM fuel performance (or potential performance) is generally quoted in I_{sp} units, which are "seconds" (s). As explained by Mr. Gloyd Simmons of MSE, there is no direct relationship between the energy density of a fuel system and the I_{sp} of rocket propulsion using those fuels unless all the major parameters inside the rocket engine as well as atmospheric pressure outside the engine are known. Nevertheless, a baseline reference is the Space Shuttle main engine (SSME), which combusts LH_2 with LOX and produces an I_{sp} of approximately 450 s.

The following summaries are what MSE has learned about HEDM fuels (Refs. 16 and 17).

3.1.1.1–Atomic Boron NASA-GRC is freezing separate boron atoms in solid hydrogen snow in liquid helium (LHe); this was accomplished on a microscope slide. The microscope slide was heated, and everything on it flashed. The expected I_{sp} is 500 to 750 s. A propellant such as this would have to be moved out of the fuel tank faster than the detonation wave, or the fuel tank would explode.

3.1.1.2–Strained Ring Hydrocarbons Hydrocarbon molecules with abnormal geometric shapes carry extra energy within their strained chemical bonds that is released when these compounds combust. Such compounds could increase I_{sp} by approximately 10% higher than that for conventional hydrocarbons. One example of such an exotic hydrocarbon is cubane (C_8H_8). The molecular structure of cubane can be visualized as a cube of eight carbon atoms with one hydrogen atom bonded to each carbon atom.

3.1.1.3–Metallic Hydrogen Researchers at Lawrence Livermore National Laboratory produced a small amount of metallic hydrogen by firing a projectile containing hydrogen into a concrete wall at 7 kilometers per second (km/s). The material lasted 50 nanoseconds which was long enough for a conductivity measurement to show they had obtained the metallic state of hydrogen. If stable metallic hydrogen could be made in enough quantity, it would have a I_{sp} of 1,100 s.

3.1.1.4–Metastable Helium Helium atoms each have two electrons with their "spins" in opposite directions. Metastable helium would have the two electron spins in each atom aligned in the same direction and would release significant energy when converted back to normal helium with its opposed spins. According to Mr. John Cole of the NASA Marshall Space Flight Center (NASA-MSFC), "metastable helium is probably a myth."

3.1.1.5–Fluorine Reactions Mr. John Cole also stated that NASA discontinued fluorine experiments approximately 20 years ago when they had (an unspecified) "bad incident."

3.1.1.6–Polynitrogen Normal nitrogen is a two-atom molecule (N_2). The Air Force Research Laboratory at Edwards Air Force Base is currently attempting experiments with "polynitrogen" (unstable molecules such as N_5). The status of these experiments has not been reported, other than that they are preliminary.

3.1.1.7–Liquid Ozone Ozone (O_3) is unstable and could therefore release more energy as compared to oxygen when oxidizing fuels. When liquefied, ozone forms an azeotropic mixture of two imiscible liquid phases. Unfortunately, one of these phases will explode spontaneously, and this property inhibits the use of this material.

3.1.1.8–Summary of High Energy Density Materials In summary, the high reaction energy of these materials is directly related to and inseparable from their extreme instability. For that reason, MSE recommends that HEDM fuels should not be seriously considered for the emissionless aircraft project unless such a fuel is found that possesses a significantly higher stability in addition to a high energy density.

3.1.2 High Energy Hydrogen Atom Systems

Blacklight Power, Inc. (BLP) is promoting a technology that it claims produces a significant amount of energy from novel reactions of hydrogen atoms in the plasma state (Ref. 18).

BLP claims to have achieved (in laboratory plasma reaction tubes) a resonant transfer of energy from atomic hydrogen (caused by the presence of catalyst atoms, typically alkali metals) such that the electron of the hydrogen atom goes to a stable orbit, significantly lower in energy than the normal ground state.

It is standard chemistry for a chemically reacting atom to decrease its energy level 1 or 2 electron volts (eV) when it forms a chemical bond; the BLP claims are for electron orbit energy changes of tens of electron volts with the formation of previously unobserved and unusual chemical compounds featuring correspondingly high bond energies.

BLP has stated that these claimed extraordinarily high electron energy shifts imply that a given mass of hydrogen could yield on the order of 100 times as much energy as that of hydrogen reacted with oxygen.

From an objective viewpoint, such claims are scientifically possible, but because they are quantitatively extraordinary, they must be supported with independent experimental measurements in order to be credible. MSE visited the BLP laboratories on two separate occasions but was not shown data for a material/energy balance of the plasma reactor tubes.

BLP cites unusual peaks in nuclear magnetic resonance (NMR) spectra of compounds made in its plasma reactors as evidence of extra strong hydrogen chemical bonds. However, samples of two of these compounds provided by BLP were sent by MSE to an ***independent*** NMR testing laboratory (selected by MSE), and these samples did ***not*** exhibit the unusual spectral peaks claimed by BLP.

MSE's position on this is that BLP claims are potentially possible, but not credible until supported by independent measurements and replication.

3.1.3 Nuclear Isomers for Energy Storage

Nuclear isomers are excited states of nuclei that can typically decay to release orders of magnitude more energy per atom than is associated with standard chemical reactions. The energy storage cycle using nuclear isomers would have the following steps.

1) Selected nuclei (atoms) would be separated (i.e., purified).

2) The selected nuclei would be energized to the high energy (storage) state.

3) The high energy states of these nuclei are selectively triggered to release this energy when it is needed.

4) The released energy, in the form of gamma rays containing energy levels of approximately 1 million electron volts [i.e., megaelectron volts (MeV)] must then be converted to a useful form of energy (e.g., capable of propelling an aircraft).

A 1999 paper published in Physical Review Letters by C. Collins and 12 other researchers claims that the 2.5-MeV excited-state level of the Hafnium 178 nucleus has its rate of decay increased by approximately 4% when it is stimulated by 40-kiloelectron volt (keV) x-rays (Ref. 19). (These researchers produced such x-rays with a standard dental x-ray unit.)

As correctly pointed out in the Collins paper, 40 keV stimulating an energy release of 2.5 MeV is an energy gain of approximately 60 times. However, a 4% change in the rate of decay is very small and might not be significant compared to the statistical error limit.

Two of the notable gamma ray transition energies in this research were 426 keV and 495 keV. All other gamma ray transitions up to the total energy of the 2.5-MeV excited state were smaller.

If the release of gamma rays at these energy levels could be perfectly controlled, then the next problem, as stated above, is to convert that form of energy to a form that is more useful. Gamma rays at these energy levels cannot be completely absorbed (or shielded).

Calculations by MSE according to standard methods show that to absorb 99.9% of 0.5-MeV gamma rays would require one of the following (Ref. 20):

- concrete–61 centimeters (cm);
- aluminum–47 cm;
- iron (Fe)–15 cm; or
- lead–8 cm.

Attempting to absorb gamma rays with a photoluminescent material (and then converting the resulting visible light to electricity with PV solar cells) would not be viable as the high energy level in the gamma rays would quickly destroy the crystal structure of the photoluminescent material.

The bottom line for this concept is that even though there has been one experiment that suggested the rate of decay of nuclear isomers can be slightly modified, there is no known way to effectively control or shield this process to a significant degree or to convert gamma ray emissions at these high energy levels into usable forms of energy.

Note that if the gamma ray emission is not entirely shielded, the aircraft is not "emissionless."

With sufficient shielding material, gamma rays could be converted entirely to heat, but then the energy conversion system is similar to and no better than a nuclear reactor coupled with a heat cycle, which would not be a politically acceptable method of providing the energy source for an emissionless aircraft.

3.1.4 Inertial Electrostatic Confinement Fusion as a Potential Power/Propulsion Source

3.1.4.1–History of Inertial Electrostatic Confinement Fusion The basic concept of inertial electrostatic confinement (IEC) fusion was discovered by Mr. Philo T. Farnsworth (inventor of the electronic television) in the 1930s. In the 1960s, Farnsworth and his associates obtained four U.S. patents on this technology, built and operated prototype IEC fusion devices (referred to as fusors), and produced approximately 10^{12} neutrons/s (from deuterium-deuterium and deuterium-tritium fusion reactions). A small IEC fusion device is currently manufactured commercially by Chrysler-Daimler Corporation and sold as a neutron source (10^{7} neutrons/s) intended for material analyses.

In the 1990s, Dr. Robert W. Bussard (author of the book *Nuclear Rocket Propulsion* published in 1958), presented several American Institute of Aeronautics and Astronautics (AIAA) Joint Propulsion Conference papers that described how interplanetary space travel could potentially be reduced in cost by several orders of magnitude by taking advantage of IEC fusion as a power source for rockets designed as both low Earth orbit (LEO) launchers and interplanetary vehicles

(Refs. 21 and 22). Dr. Bussard also argued that interplanetary travel times would also be dramatically decreased if IEC fusion were used.

3.1.4.2–System Description The basic concept of IEC fusion uses a spherical geometry ion accelerator to cause positive ions to collide with sufficient energy so that they will undergo a nuclear fusion reaction. The simplest version of such a device (which has been successfully built and operated) consists of an inner spherical wire grid approximately 2 inches in diameter concentric with an outer spherical wire grid approximately 10 inches in diameter. Each grid consists of six circles of small-diameter wire spot-welded to each other in a pattern similar to the Earth's longitudinal circles. Insulated lead-in wires are used to place an electrostatic potential between the inner and outer grids. The inner grid is negative, and the outer grid is positive. The potential difference between the grids is approximately 10,000 V for a smaller device up to approximately 1 million V for a larger machine designed to generate significant levels of fusion power. The concentric spherical grids are contained in an outer (spherical) metal shell, which enables the device to operate at an internal gas pressure of approximately 10^{-5} atm.

3.1.4.3–Operating Principle Positive ions injected into an IEC fusion device accelerate to the negative spherical grid but then pass through the other side of the inner grid and accelerate back to the center. Therefore, the central core of such a device consists of positive ions passing through, reversing direction, and then reconverging to the center until ion collisions result in nuclear fusion reactions. Although the positive ions are oscillating in a radial direction, the electrostatic potential between the inner and outer grids confines them to the central core. (The name of the device is derived from this mode of operation). It is important to understand that nuclear fusion results from relative ion kinetic energy between colliding ions. This technology uses ***ion kinetic energy derived from electric field voltage*** (as opposed to temperature) to achieve sufficient impact momentum between ions to cause fusion.

3.1.4.4–Appropriate Fusion Reaction The reaction proposed by Dr. Bussard is that which uses protons [ordinary hydrogen (H^1)] and the most common isotope of boron with atomic weight 11 (B^{11}).

$$H^1 + B^{11} \rightarrow 3\,He^4 + 8.7 \text{ million electron volts (MeV) (kinetic energy of } He^4 \text{ ions)}$$

The advantages of this reaction for producing fusion power are:

it does not produce neutrons (secondary reactions between protons and some of the helium product nuclei could produce a small number of neutrons; this requires further investigation);
no gamma rays are produced;
the three helium nuclei (alpha particles) are charged, allowing ***direct conversion from nuclear energy to electrical power***;
the helium reaction product is totally safe; and
boron is a plentiful element; 80% of natural boron is B^{11}.

3.1.4.5–Energy Density of the H^1, B^{11} Reaction and Resulting Weight Saving The (mass basis) energy density ratio for the $H^1 + B^{11}$ nuclear reaction compared to that for the hydrogen-

oxygen chemical reaction is 4.36×10^6. In order to put this ratio into perspective, it should be noted that the calculated LH_2 weight at takeoff for the conceptual NASA-LaRC/MSE emissionless aircraft is approximately 30,000 lb, and the corresponding water landing weight would be as high as 270,000 lb (if all the LH_2 were reacted). Potentially, 0.06 lb of hydrogen and B^{11} reactants could replace this requirement and thereby eliminate the need to retain 270,000 lb of water onboard until the completion of a flight mission. Additionally, the elimination of equipment such as fuel cells, power turbines, air compressors, tanks, and heat exchangers needed for the hydrogen/oxygen electrochemical P/P system (see Sections 2.7.2 and 2.7.3) raises the total weight saving of the conceptual emissionless aircraft P/P system to approximately 420,000 lb. Approximately 17,000 ft^3 of tank volume (mostly for LH_2) are also not required.

3.1.4.6–Direct Energy Conversion Almost all of the energy released in the $H^1 + B^{11}$ fusion reaction appears as kinetic energy of the ions (helium nuclei).

The most appropriate method yet identified by MSE to convert the relatively high kinetic energy of helium nuclei exiting the IEC fusion reactor into electric power at voltages compatible with electric motors would potentially use a device known as a "traveling wave tube" (Ref. 23). MSE will be investigating this concept further. High energy ions traveling through such a device generate radio waves that are reduced in voltage in a radio frequency transformer. The low voltage output from the transformer could then be rectified to dc or electronically matched in frequency to that required for the propulsion motors. It is believed that the weights of such equipment would be relatively light.

3.1.4.7–Inertial Electrostatic Confinement Fusion Propulsion System Component Weights and Sizes Recognizing that the following values are ***very preliminary***, the major equipment components (required for the conceptual IEC fusion power generator to produce high-voltage dc power) have estimated weights as shown in Table 9. A conceptual diagram of such a power generator is shown in Figure 6.

Table 9. IEC fusion power generator—major components.[1]

Item	Comments	Weight in lb
Spherical containment shell	Radius = 1 m, 0.10 inch steel wall[2]	560
Ion accelerators	For H and B ions	2,000
Inner and outer sherical wire grids	Made from thin wire	~0
High-voltage source to initiate potential between grids	Potential self-sustained after reaction initiates	1,000
Hydrogen and boron compound systems	Provide ions for acceleration	1,000
Vacuum pump	Sustains near vacuum[3]	3,770
Other	Controls, wiring, contingency	1,000
TOTAL	**Listed items**	**9,330**

Notes:
1. Two complete systems would be used for reliability.
2. Wall thickness calculated per American Society of Mechanical Engineers Boiler and Pressure Code, Sec. VIII, (safety factor = 4); 1-m radius, based on Bussard's 1995 paper, for approximately 100-MW net electric power output.
3. Weight extrapolated from laboratory-size pump, lighter pump expected to be available.

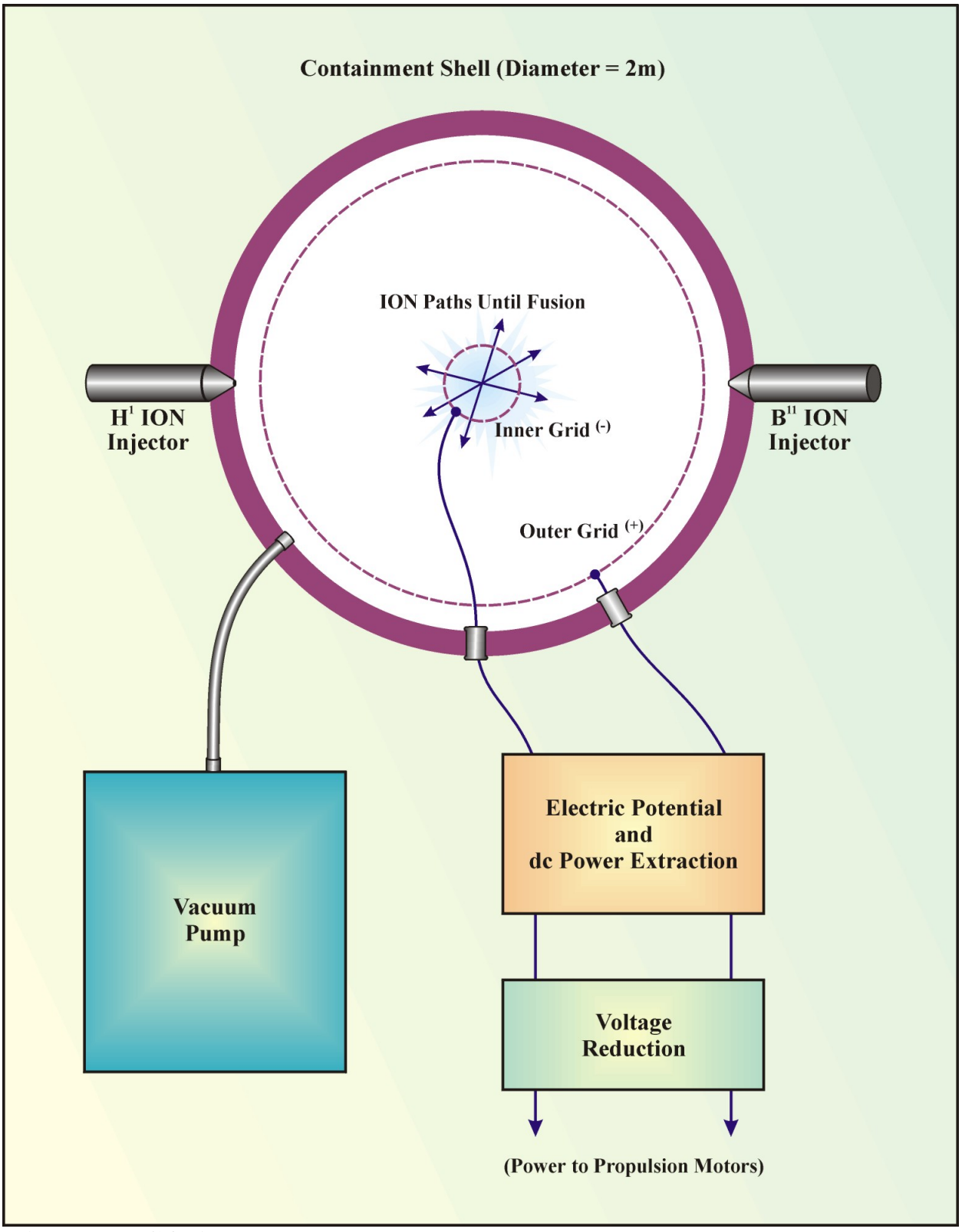

Figure 6. IEC fusion power generator concept.

3.1.4.8–Radiation Hazard Considerations The radiation hazards associated with any conventional nuclear reaction-based vehicle propulsion system are significant. Fission reactors emit lethal amounts of neutrons and gamma radiation (which requires massive shielding to protect personnel) and contain extremely hazardous amounts of short- and long-lived radioisotopes after being operated for any appreciable time. The structural materials of proposed (hypothetical) high temperature (thermonuclear) plasma fusion reactors would also be highly radioactive (from neutron activation) after being operated for extended periods.

However, the $H^1 + B^{11}$ fusion reaction would not produce external radiation, radioisotopes, or fission products. This reaction produces moving helium nuclei (alpha particles), and these could be very easily shielded. (As explained in Section 3.1.4.4, there could be a small number of neutrons produced, but this is not yet quantified). Information acquired to date indicates there are no radiation concerns related to either the initial materials or the system materials after the reaction is stopped. Additionally, any bremsstrahlung radiation (similar to x-rays) produced during system operation could be readily shielded.

In the event of a catastrophic event (crash) severe enough to cause the spherical containment shell to leak, air would fill the near-vacuum within the shell, and the nuclear reactions would stop. In contrast to a chemical fuel powered aircraft, there would be no spilled LH_2 or hydrocarbon fuel and the resulting fire.

3.1.5 Low Energy Nuclear Reactions

3.1.5.1–Electrochemically Induced Deuterium Fusion in Palladium The first-discovered form of solid-state fusion was that achieved by electrochemically splitting heavy water in order to cause the deuterium to absorb into pieces of palladium metal. When this experiment is conducted according to procedures that have resulted from the work of many researchers since 1989, it is reproducible.

The evidence that a nuclear process is occurring is that excess energy in the form of heat (greater than what could be produced by any possible chemical reaction in the system) and helium 4 (He^4) (in quantities exceeding any possible contamination) occur. The primary nuclear reaction is:

$$_1D^2 + {}_1D^2 \rightarrow {}_2He^4 + \text{heat}$$

Unlike plasma-phase fusion reactions, the very low production of neutrons and gamma rays (for the amount of excess energy produced) is very noteworthy. Even though the heat originates in palladium metal, the process produces warm liquid electrolyte at temperatures significantly less than the normal boiling point of water. Because the fraction of heat that can be converted into electrical or mechanical energy at this relatively low temperature is small, aircraft propulsion using such an aqueous-phase system is probably not practical. (Pressurization, to achieve a "steam" cycle with the associated steam condenser, would be heavy).

3.1.5.2–Deuterium Gas and Palladium Some low energy nuclear reaction (LENR) researchers ***claim*** that an "off-the-shelf" palladium-based catalyst (used to accelerate chemical reactions) is capable of causing deuterium gas to fuse to He^4 and release significant heat (with the operating temperature not limited to an aqueous boiling temperature). It is the view of MSE that the deuterium gas/ catalytic palladium fusion reaction requires further validation before it is fully credible.

3.1.5.3–Proton Power Cells Proton Power Cells (PPCs) are being developed by Dr. George Miley and his associates at the University of Illinois (U of I) at Champaign-Urbana, Illinois, and at Lattice Energy Corporation (LEC) (Refs. 24 and 25). MSE visited Dr. Miley's laboratories in September 2000 to directly observe this technology.

These devices also use an electrochemical process to saturate nano-thickness metallic layers with hydrogen, which result in a temperature rise in the aqueous electrolyte (but it is significant that the hydrogen is normal, not deuterium). The active metals can include nickel and titanium (which both absorb hydrogen); the much more expensive palladium can be used but is not required.

U of I experiments use thin (~300 angstroms) films of nickel, palladium, or titanium in an electrochemical system with 0.5 to 1.0 molar lithium sulfate in normal water as the electrolyte. It is claimed that a power production of 100 to 200 watts per cubic centimeter (W/cm^3) has been measured in the metal films, and that measured excess heat is reported to be on the order of 20% to 100% times the electrical input. Measurements of nuclear isotopes produced in these films suggest a nuclear origin for this excess heat.

The thin films are sputtered in order to obtain better control and consistency in the crystalline structure. The advantage of these thin films is that their flexibility provides a release for internal and external stress (preventing microcracks that could cause deloading), and thin films can be loaded with hydrogen within minutes rather than weeks as required by thick electrodes. Great care was taken to ensure that "new" elements produced in 3- to 4-week cell runs are distinguished from possible impurities including:

- use of high-purity components;
- analysis of all components before and after a test; and
- performing "reference" experiments with metals that do ***not*** load hydrogen, where no "new" elements are found.

The reported characteristics of the reaction processes that formed the "new" elements are given below.

1) The reaction products that occurred in quantities exceeding their amounts prior to electrolysis by an order-of-magnitude or more have atomic mass numbers lying well above and below the atomic mass number of the original metal film and showed isotopic ratios different than what that element typically possesses.

2) Reaction rates are as high as 10^{16} atoms/s/cm^3 for high-yield elements.

3) The highest yield elements fall into mass bands around A ~22-23, 50-80, 103-120, and 200-210.

4) The "high-yield" bands are similar for the various metals films (nickel, palladium, and titanium); however, the relative yields in each band depend on the initial metal.

5) Reactions and products release little high energy radiation but do emit lower energy (≤20 keV) x-ray and/or beta emission (measured on electrodes removed after a test). Present experiments use thin film cathodes sputtered onto a small glass plate the size of a microscope slide. The anode can also be sputtered onto a separate region of the slide, or a separate wire may be used. Methods were developed to enhance film bonding to the glass to achieve good film lifetime. It is claimed that tests with such cells consistently produce excess power (defined as total thermal power produced in the cell minus thermal power caused by electrical resistance heating in the thin films). On the other hand, reference experiments performed with cells whose metal films were selected to be incapable of absorbing hydrogen produce no excess heat.

From a future applications viewpoint, it is very significant that these heat-producing reactions do ***not*** produce particles or radiation capable of penetrating from the inside to the outside of the electrolytic cells.

A step-by-step explanation hypothesized by Dr. Miley and his colleagues to explain what they claim to observe is stated below.

1) Two thin films of metal are required with one deposited on another and with the bottom layer deposited on a smooth (glass) substrate (a standard microscope slide). Thinness prevents the films from cracking and delaminating and allows for rapid hydrogen absorption. The metal layers need to be thin for better electron coherence but not so thin as to jeopardize structural integrity. The ideal layer thickness is stated to be approximately 300 angstroms.

2) The two metals must have different fermi levels such that there is a high density of electrons at the interface between the metals.

3) One or both metals must be able to absorb enough hydrogen in order that the ratio of hydrogen atoms to metal atoms is at least 0.85. U of I researchers are developing a method using x-rays to measure the hydrogen-to-metal loading fraction in real time.

4) If the "bottom" metal is the hydrogen absorber, then the "top" metal must allow hydrogen to diffuse through to reach the bottom metal. Present experiments use nickel and either titanium or palladium as the two metals.

5) The metals at the interface must be definitely bonded to each other (from the sputtering process that deposits them) but must not be fused together.

6) When the hydrogen density in one or both of these films is raised to the critical ratio of 0.85 (by being the cathode in an electrolytic cell), it is hypothesized that a "coherent multielectron structure" (over a volume of several cubic angstroms) enables a number of protons and metal atoms to fuse into one atom of a superheavy element.

   An example of a hypothesized reaction is:

$$20\ P^{1} + 5\ Ni^{58} \rightarrow X^{310}$$

7) By nuclear standards, these superheavy elements are relatively stable (lasting from milliseconds to 30 s) but then decay by a fission process to a multitude of "new" elements not present in the metal films:

$$X^{310} \rightarrow \text{Stable Fission Products + Heat in the Metal Film,}$$
$$\text{immediately transferred to the aqueous electrolyte}$$
$$\text{(but no penetrating radiation)}$$

8) The available binding energy in the nucleus of the superheavy element allows only a "gentle" approximately 20-MeV fission vs. the 200-MeV fission exhibited by elements such as uranium.

9) The excess heat matches (within error limits of measurements) the amount of energy released by calculating nuclear binding energy differences between metals in the initial films and the final transmutation products. The hypothesis proposed by U of I researchers is based upon "back calculating" from the known reaction products (using plausible fission pathways) to deduce the existence of the metastable superheavy elements that produced these products.

Proton power cell researchers know that the metal films in these reactions must reach a relatively high operating temperature in order to convert an appreciable fraction of thermal energy to electrical (or mechanical) energy (this is due to the Carnot limitation, Section 1.4.1.1). Dr. Miley mentioned several possibilities that he believes would enable the metal film to attain a temperature far above the boiling point of (aqueous) electrolyte.

1) Electrical fields could be used to induce a hydrogen pressure in metal films exposed to an ambient hydrogen atmosphere.

2) The metal could be immersed in a molten hydride (e.g., LiH or a mixture of metal hydrides that would have a melting point lower than that of any one pure component). For molten hydride electrochemistry (as opposed to aqueous electrochemistry), the cell polarity is reversed since the hydride ion is negative.

3) A recent claim by the U of I research team is the invention of a new concept of providing hydrogen from a solid-state hydride layer (such as those developed by Ovonics Corporation for batteries) and then switching the flow of hydrogen (protons) on or off by means of a solid-state proton "switching layer" placed between the hydride layer and the

active metals. The U of I team considers the switching layer composition to be proprietary, but it is very similar to state-of-the-art fuel cell components. This type of multilayer concept should allow the nuclear reactions to be controlled via an electric field in the thin film structure. The operating temperature of the hydride layer is stated to be 500 ºC, and this then becomes the system operating temperature. According to the U of I team, each layer in this proposed system has been tested; however, no testing of the combined system has been accomplished.

Both the U of I and LEC claim the aqueous version of PPCs is totally reproducible. They also claim that the all-solid-state version of PPCs would have the following typical parameters (Table 10).

Table 10. Significant features of PPCs.

Item	Typical Parameter
Geometry	Flat plate
Backing plate	Provides mechanical support
Hydrogen source	Single reversible metal hydride layer
Typical active metals	Nickel and titanium
Heat-producing metal, "sandwich"	Layer of nickel on layer of titanium with total thickness = 1,000 angstroms; (each metal = 50% of volume)
Number of stacked heat-producing "sandwiches"	1,000
Operating temperature	500 °C (presently limited by reversible metal hydride identified to date)
Thermal power production	2 W/cm^2 (area basis)
Useful conversion fraction (nickel)	75%
Calculated lifetime (nickel basis)	2.7 x 10^6 s; (32 days)

3.1.6 Nanofusion

3.1.6.1–Background Dr. Brian Ahern, whose background is physics and materials science, claims his nanofusion concept will take advantage of the demonstrated fact that nanosize particles (containing approximately 1,000 to 3,000 atoms) have different chemical and physical properties than bulk-size pieces of the same material. One reason Dr. Ahern gives for this is explained as given below.

1) When a particle of a substance consists of 1,000 to 3,000 atoms in a cluster, there is a higher fraction of surface atoms than for atoms in a bulk piece of the same material.

2) Military research (suggested by the nuclear physicist Enrico Fermi), which had been classified in 1954, but was later declassified, demonstrated that if a cluster of atoms in the 1,000 to 3,000 size range was given an impulse of energy (e.g., as heat) and if a significant number of these atoms have a nonlinear coupling to the rest (e.g., the coupling of surface atoms to interior atoms), the energy will not be shared uniformly among all the atoms in the cluster but will localize on a very small number of these atoms.

3) Thus, a few atoms in the cluster will rapidly acquire a vibrational energy far above what they would have if they were in thermal equilibrium with their neighboring atoms.

4) This "energy localization" explains why clusters in this size range are particularly good catalysts for accelerating chemical reactions.

5) If the cluster is palladium saturated with deuterium, Dr. Ahern claims the localized energy effect will enable a significant number of the deuterons to undergo a nuclear fusion reaction, thereby releasing a high amount of energy.

3.1.6.2–Experimental Evidence Supporting Nanofusion Plausibility Other reasons Dr. Ahern presents to support the plausibility of his concept for producing nanofusion relate to electric discharge phenomena.

1) Experiments conducted at the National Institute of Standards and Technology (NIST) have demonstrated that electric discharges through liquids containing suspended particles will self-focus on these particles. This is known as inverse capillary discharge.

2) Explosive electric discharges (from capacitor banks) through deuterated filaments produce a significant number of neutrons, indicating that nuclear fusion reactions are occurring. The neutron emission is directional, indicating the fusion process is shock wave-induced rather than a thermal process.

3.1.6.3–Dr. Ahern's Proposed Steps of the Nanofusion Process Dr. Ahern summarizes his proposed nanofusion process as given below.

1) Electric arc discharges between palladium electrodes (in heavy water) will remove small "nanoclusters" of palladium approximately 20 to100 nm in diameter (which are referred to as nanodots) and suspend these in the heavy water, forming a colloid. The colloid is inherently stable because water molecules cluster around the nanodots and keep them suspended.

2) These same discharges ionize the heavy water producing deuterium and oxygen.

3) The deuterium is highly soluble in palladium and readily saturates the palladium nanodots.

4) Subsequent electric discharges (which are continually occurring) are focused by the deuterated nanodots.

5) The energy localization described in Section 3.1.6.1 gives an extremely high energy to a significant fraction of deuterium atoms, which causes them to undergo nuclear fusion reactions and release significant energy.

6) The nuclear fusion reaction energy can be removed from the process as electricity by a conventional Rankine Cycle (as used in utility power plants).

7) If the apparatus is placed within a 1-tesla magnetic field, Dr. Ahern claims there is supporting evidence to show that the nuclear reactions can be "steered" to produce neutrons rather than protons and tritium.

8) According to Dr. Ahern, if the apparatus is designed asymmetrically, neutrons emitted from the nuclear reactions will be absorbed in one direction but they readily penetrate out of the reaction system in the opposite direction and could therefore be used directly for spacecraft propulsion.

9) A fuel cell can be used to recombine the (unfused) deuterium and oxygen and produce additional electricity by a hybrid process in which nuclear energy provides the fuels (because nuclear reactions are causing ionization of the heavy water in addition to the ionization caused by the electric discharges).

10) Obviously, if containment and shielding issues could be solved, the fuel cell electricity could be used for electric aircraft propulsion (or other uses). When the fusion system is intended to produce energy rather than a propulsive thrust, the reaction would not be steered towards the neutron production mode.

Dr. Ahern stressed that even though his proposed process uses deuterium dissolved in palladium, it is ***not*** the same as the type of LENR that has become known as cold fusion.

3.1.6.4–Current Status of Dr. Ahern's Nanofusion Concept The current status of Dr. Ahern's nanofusion project to date is:

- an experiment team has been selected;
- much of the (proof-of-concept) experimental apparatus has been acquired or located;
- a considerable number of references have been located to support the plausibility of the concept; and
- proposals have been submitted to various agencies of the U. S. Government seeking funding to test the process.

3.1.7 Radiation Hazard Considerations

As explained in Section 3.1.4.8, radiation hazards associated with any conventional nuclear reaction-based vehicle propulsion system are highly significant. By contrast, most of the nuclear reactions discussed in this report are of a fundamentally different type, which produce radiation levels that are orders of magnitude less (for an equivalent release of energy) as compared to traditional types of nuclear reactions.

Deuterium-based solid-state nuclear reactions emit low levels of neutrons and gamma rays; however, an aqueous-based system is unlikely to be developed into part of an aircraft P/P system because the operating temperature is not high enough.

Based on claims from the U of I research team, if PPCs (Section 3.1.5.3) could be developed into a power source for an aircraft P/P system, they would provide absolutely no hazard to operations/ maintenance personnel or passengers because:

- the initial fuel and matrix materials are not radioactive;
- no neutrons or gamma rays are produced by the hypothesized fusion/fission reaction; and
- alpha particles (He^4 nuclei), Beta particles (electrons), and recoil fission products (newly created elements) are of low enough energies to be easily shielded.

In the event of a catastrophic event (crash) severe enough to shatter the PPC containers, residual radiation emitted by the nickel/titanium matrix (and resulting new reaction product elements, which had been created until that time) would be so low that it would not be a problem. The U of I team claims that the residual (Beta) radiation is at such an extremely low intensity that substrates from PPCs (that had been operating until the time of measurement) must be wrapped in ultrahigh-speed photographic film for several weeks in order to cause noticeable fogging of that film.

The alternative tradeoff for a crash scenario for an aircraft propelled by these new types of nuclear reactions should be noted. In contrast to a chemical fuel powered aircraft, there would be no spilled LH_2 or hydrocarbon fuel and the resulting fire.

3.2 Energy Conversion

Some of the energy produced by any energy producing system will be in the form of heat. This section presents the results of current research into advanced methods of converting a higher fraction of heat to electric power than may be accomplished with current technology. The electric power may then be used in an aircraft P/P system to provide propulsion.

Additionally, a newly discovered method of transferring relatively large amounts of heat (without a temperature gradient) is described. This technology allows heat exchanger weights and volumes to be reduced and reliability to be significantly increased and is suitable for a very wide range of technical applications.

3.2.1 The Thermal Diode

3.2.1.1–Background If the claims made for it can be verified, the "Thermal Diode" technology recently announced by ENECO Inc., located in Salt Lake City, Utah, may be the first practical and efficient way to convert low-grade or waste heat to useful electricity (Ref. 26).

As shown in Section 2.7 the addition of a "bottoming cycle" consisting of an expander (turbine) that uses heat generated by PSOFCs to generate a net excess of power (greater than the power required to compress air for the fuel cells) can significantly raise the overall system efficiency. However, for most energy conversion systems, it generally has not been practical to introduce the low temperature heat exhausted from the second-stage energy conversion process into a third-stage energy conversion process in an attempt to extract additional useful energy. The Thermal Diode may change that.

3.2.1.2–Thermal Diode Concept The Thermal Diode uses concepts from two previously well-established and historic energy conversion technologies, namely "thermionic" technology and "thermoelectric" technology.

Thermionic technology was discovered by Thomas Edison in 1883. An incandescent metal in a vacuum "boils off" some of its electrons, which may then be used as an electric current. Thermionic energy converters using this principle have found niche applications as energy converters on space vehicles (where the heat is provided by radioisotopes). The major disadvantage of thermionic energy conversion is that the electron-emitting surface must have a temperature of at least 1,000 °C.

In 1826, Seebeck discovered that if two different conductors are joined at two separate junctions "A" and "B," electric current will flow in the circuit from A to B and then back to A if there is a temperature difference between the junctions. State-of-the-art thermoelectric generators use specialized semiconductors that enhance this effect; nevertheless, the conversion efficiency from heat energy to electricity is only approximately 8% at best. Thus, thermoelectric conversion is also limited to niche applications such as remote terrestrial sites, as well as some space missions.

As a result of a fundamental investigation of converting heat to electricity, ENECO obtained a breakthrough by replacing the vacuum of a state-of-the-art thermionic converter with a solid-state semiconductor layer such as would have been used in a thermoelectric converter. ENECO then referred to this new technology as a "Thermal Diode." The important characteristics of the Thermal Diode are:

- typical operating temperatures need only be a few hundred degrees Celsius; and
- the percentage energy conversion to electricity is typically approximately three times that of state-of-the-art thermoelectric technology, resulting in a remarkably high efficiency for such a relatively low temperature.

3.2.1.3–Present Status ENECO is now providing laboratory demonstrations of "proof-of-concept" prototype Thermal Diodes at its Salt Lake City, Utah, laboratories and has submitted articles describing the principle to physics journals (Ref. 27). Additionally, ENECO is currently applying for patents in several countries.

3.2.1.4–Characteristics In its present form, prototype Thermal Diodes consist of a "sandwich" structure of three layers of differently doped semiconductors that have the typical parameters as shown in Table 11.

Table 11. Typical Thermal Diode parameters.

Parameter	Value
Typical materials	Silicon, indium antimonide, mercury cadmium telluride, cadmium arsenide
Dimensions	1 mm x 1 mm x ½ mm thick
Current	10-100 A per device
Voltage	mV per device
Current density	15 W/cm^2 typical
Power density	20 kW/kg
Efficiency	Approximately ½ x e_c

It is worth noting that:

1) The power output consists of relatively low voltage and relatively high current per device. Therefore, many Thermal Diodes would be connected in series (electrically) to achieve useful voltages.

2) The claimed power density (weight basis) exceeds state-of-the-art fuel cells by a factor of 10, but since they use "waste" heat, these devices are (essentially) "fuel-less."

3) Energy efficiency is limited by the same relationship (that of Carnot) that applies to heat engines. For example, if the "hot" and "cold" sides of a Thermal Diode were 300 C and 20 °C (573 K and 293 K), respectively, then the maximum Carnot efficiency (e_c) would be:

$$e_c = \frac{T_1 - T_2}{T_1} = \frac{573 - 293}{573} = \frac{280}{573} = 0.489$$

The Thermal Diode efficiency (e_{TD}) is claimed to be approximately one-half of the Carnot value, therefore:

$$e_{TD} \cong 1/2 \text{ x } e_c \cong 1/2 \text{ x } 0.489 \cong 0.25$$

3.2.1.5–Incorporation of the Thermal Diode into the P/P System of the NASA-LaRC/MSE Emissionless Aircraft Concept—with Bottoming Cycle Turbine The basis of the energy conversions and energy flows in the PSOFC P/P energy system block diagram (Section 2.7) is per kilogram of ambient air entering the system at cruise altitude conditions. The parameters or assumptions given below are used for this analysis.

1) If Thermal Diodes could be incorporated into the structure of the exhaust-to-air heat exchanger (equipment item "7" in Figure 2), then:

$$T_1 = 693 \text{ K and } T_2 = 279 \text{ K}$$

2) Assume there are no other energy inputs or losses.

The system efficiency calculation proceeds as given below.

1) The available chemical energy (in hydrogen fuel) would be 0.66 kilowatt hour (kWh).

2) The 50% efficient PSOFC then provides 0.33 kWh electric energy.

3) Air compressor work (required for the PSOFC) requires 0.0886 kWh.

4) Excess work or energy (turbine minus compressor) = 0.02684 kWh.

5) The remaining energy at point "G" (entering equipment item "7" in Figure 2) is 0.303 kWh of heat (0.66 kWh minus 0.33 kWh minus 0.02684 kWh) in the exhaust gas at approximately 693 K.

6) The potential conversion of this heat to electricity by the Thermal Diodes (E_{TD}) is:

$$E_{TD} = \frac{1}{2} x \frac{693-279}{693} x\ 0.303\ kWh = 0.091\ kWh$$

7) The overall system efficiency (e_s) is then:

$$e_s = \frac{0.33kWh + 0.02684\ kWh + 0.091\ kWh}{0.66\ kWh} = \frac{0.447\ kWh}{0.66\ kWh} = 67.8\%$$

Without Thermal Diodes, the e_s is 54.1%.

3.2.1.6–Incorporation of the Thermal Diode into the Power/Propulsion System of the NASA-LaRC/MSE Emissionless Aircraft Concept—without Bottoming Cycle Turbine For this analysis, the following must be assumed.

1) Temperatures and efficiencies are the same as previously stated, up to condition "E."

2) Thermal Diodes could be incorporated into the structure of the air-to-exhaust heat exchanger but ***without*** a turbine energy conversion stage, which lowers exhaust temperature. Therefore, $T_1 = 923$ K and $T_2 = 279$ K. (ENECO does not claim operating temperatures higher than 500 °C; however, the trend with PSOFCs is to ***lower*** operating temperatures; so more than likely, there will not be a temperature mismatch in the future).

3) There are no other energy inputs or losses.

By a very similar procedure as was performed in the preceding section, the ***system*** energy efficiency is calculated to be 58.7%.

These calculated system efficiencies are summarized in Table 12.

Table 12. System efficiencies using Thermal Diodes.

System Description	Efficiency
(Case 1) PSOFC + turbine	54.1%
(Case 2) PSOFC + turbine + Thermal Diodes	67.8%
(Case 3) PSOFC + Thermal Diodes	58.7%

3.2.2 Supertube Enhancement of Heat Exchanger Technology

Supertubes are potentially important for aerospace applications because they can offer significant decreases in the weight of heat exchangers, such as will be required for the NASA-LaRC/MSE emissionless aircraft concept. The potential advantages of Supertubes were revealed by demonstrations of this technology observed on two occasions by MSE and are explained in the following sections.

3.2.2.1–Background Information Dr. Yuzhi Qu has developed and patented what he claims to be a different type of heat transfer technology used by devices he refers to as "Supertubes" (Ref. 28).

Supertubes have been manufactured up to 75 ft in length and 6 inches in diameter. The tube itself can apparently be any material capable of being hermetically sealed and that will not leak. The heat transfer is accomplished by an extremely thin layer (approximately 2 parts per million of internal tube volume) of a complex mixture of chemicals described in the patent. The heat transfer capabilities of these devices have been rigorously tested by the Stanford Research Institute (SRI). MSE has obtained copies of the SRI reports.

These devices are claimed to transport heat internally without a temperature gradient and could therefore be classified as a "heat superconductor." MSE witnessed demonstrations in January 2001 and June 2001 where evidence for this claim was presented by Dr. Qu's associates.

3.2.2.2–Description of the Demonstrations Performed at MSE

3.2.2.2.1–Two Pot Demonstration Figures 7a and 7b show the experimental apparatus that consisted of a stainless steel Supertube approximately 1-1/4 inch in diameter and 4 ft long that was penetrating diametrically opposite sides of two stainless steel pots. The volume of each pot was approximately 1 quart. The tube was welded to the pot sides in such a way that no water could leak from the pots at the penetrations. A 1-kW electric heater and "source" thermocouple (T_s) were located at the "right" end (as viewed). A "distant" thermocouple (T_d) was located at the left end of the tube. The pots were located at approximate positions of 1 and 3 ft from (either) end. Thermocouple leads were periodically switched between two temperature readout instruments to demonstrate that there was no instrumentation bias. The following steps were performed with the results as noted.

1) The heater was turned on (with no water in the pots) and within a few minutes, the T_s measured 125 °C, and the T_d measured 130 °C. (This would be difficult to explain by any standard means of heat transfer).

2) One cup of water was poured into the right (source-side) pot and immediately began to boil. The source temperature rapidly decreased to approximately 80 °C, but the distant temperature decreased very slowly.

3) Water was placed in both pots (and after the respective-end temperatures achieved the nearest they would get to being equal—with the distant temperature measured as 85 °C whereas the source temperature measured 80 °C), several cups of ice cubes were placed into the distant pot. The distant temperature dropped slowly (a few tenths of a degree), but the source temperature dropped rapidly to approximately 60 °C. Again, what was observed was ***not*** what would be expected.

3.2.2.2.2–Two Tube Demonstration Two transparent, colorless, visually empty, sealed pyrex tubes approximately 18 inches in length and 3/8 of an inch in diameter (these can be seen in the left side of Figure 7a) were held vertically by clamps and immersed in the same beaker of hot

7a

7b

Figure 7a and 7b. Supertube heat transfer demonstrations at MSE.

(approximately 80 °C) water. The tube containing no internal coating was felt (by one's fingers) to be at ambient temperature throughout its vertical length except for the approximately ½-inch distance above the hot water where the pyrex felt hot. However, the other tube, which had a barely visible interior coating of the so-called Supertube heat transfer powder, felt equally hot throughout its length. There was no discernable gradient along the entire length of the tube.

3.2.2.2.3–Flame Demonstration A metal Supertube approximately 3/16 inch in diameter and 8 inches long was hand held at one end while the other end was placed within a small butane (lighter) flame for approximately 10 s. The flame was removed, and the end that had been in the flame was immediately grasped by one's fingers and felt only slightly warm. There was no discernable temperature gradient along the entire length of the tube.

3.2.2.2.4–Stirring Rod Demonstration The same Supertube used in the "flame" demonstration was felt to be rapidly hot on the end held by one's hand when the other end was stirred in hot water with a temperature of approximately 80 °C. Then, this Supertube was felt to be rapidly cold on one end when the other end was stirred in ice water. By contrast, a metal spoon transmitted comparable temperature differences significantly more slowly.

3.2.2.3–Present Supertube Applications Personnel from Dr. Qu's companies claim that Supertubes are being readily accepted into Chinese industry (current annual production is approximately 1 million) because their extremely high heat transfer rate allows otherwise wasted heat from industrial processes or utility power plants to be "recycled" into incoming air streams (e.g., combustion air) in these processes. Overall, process efficiency is said to be increased by approximately 5% to 10% (depending on its former state of efficiency). The payback time for Supertubes in these applications is said to be less than 1 year.

3.2.2.4–Planned Supertube Applications For a wide variety of personal, commercial, industrial, government, and military technological applications, it is necessary to transfer heat either into or out of various processes, devices, or equipment. Cost effectiveness must be determined on a case-by-case basis, but Supertube applications could potentially be very large. Some Supertube applications that have been identified are:

- saving industrial heat (as in the preceding section, claims of 5% to 10% energy savings were presented);
- using underground heat to keep ground surfaces (e.g., airport runways) ice-free (a photograph of an ice-free area surrounded by an ice-covered area was shown);
- using ground heat to heat houses without requiring fuel (not yet tested);
- cooling electric motors (not yet tested); and
- cooling computer chips (not yet tested).

3.2.2.5–Temperature Range for Supertube Application The Supertubes patent describes this heat transfer effect operating at elevated temperatures (in a suitable tube), as well as applications involving LN_2. Regarding possible operating temperatures, Dr. Qu's applications engineers have stated that:

- five different coating compounds were formulated for different temperature bands, which cover ambient temperatures up to 1,700 °C; and
- Supertubes have not yet been tested at cryogenic temperatures.

3.2.2.6–Potential Aerospace Supertube Applications Supertubes could potentially be of great value to the aerospace industry and in particular the NASA-LaRC/MSE emissionless aircraft because they combine an extremely high heat transfer rate with a very simple lightweight package.

Standard heat exchangers typically have alternating layers of hot and cold fluids separated by metal plates, and a leak between the fluids can have catastrophic results. A heat exchanger designed with Supertubes would consist of a bundle of such tubes (there could be hundreds or more) with one end of these tubes in a plenum/chamber containing one fluid and the other end of the tubes in a plenum/chamber of the other fluid. A partition penetrated by the tubes separates the plenum/chambers. In this design, a leaking Supertube would not present a serious problem.

If Supertubes are operable at LH_2 temperatures, it might be possible to construct hollow aircraft wing sections or other components using an internal coating of Supertube powder and thereby equally distribute temperatures to provide LFC (Section 2.4.5). This concept was presented by NASA-LaRC.

3.2.2.7–Discussion of the Supertube Heat Transfer Mechanism Dr. Qu is currently writing a book to explain the physics he discovered, which provides the mechanism by which Supertubes transfer heat. At this time, MSE points out that gradientless energy transfer (in general) is an old concept. Two examples are:

- electrical superconductors - relatively high electrical currents are transferred from one end to the other with zero voltage gradient; and
- lasers - light is reflected by way of mirrors from end to end in a device or tube until it penetrates a "weaker" mirror at one end.

Supertubes may appear to be less "mysterious" if one considers they may be incorporating principles used in electrical superconductors and lasers.

3.2.3 Potential Heat Exchanger Weight Reduction using Supertubes

Initially, the conceptual design of the NASA-LaRC/MSE emissionless aircraft was based on PEM-type HFCs (the design now features PSOFCs, which allow additional energy to be extracted from the HFC exhaust heat).

Then, the heat exchanger (similar to an automobile radiator) required to transfer heat from the PEM HFC to high altitude (cruise phase of flight mission) air weighed 1,815 lb/MW. Hydrogen fuel cell electrical efficiency was assumed to be 50%.

Dr. Qu's engineers performed a preliminary design calculation for a heat exchanger based on parallel aluminum Supertubes with an outside diameter (OD) of 1 inch and wall thickness of 1.0 millimeter (mm) (Figure 8). Parallel aluminum ring fins 5 mm apart having an OD of 2 inches would be used on the "air end" of the Supertubes to enhance heat transfer from the Supertubes to the airstream. (No fins were to be used on the "liquid" end of the Supertubes as the liquid-to-metal heat transfer coefficient is significantly greater than the coefficient for gas to metal.) The resulting weight basis power density of the Supertube heat exchanger was 997 lb/MW, approximately one-half of the standard design value.

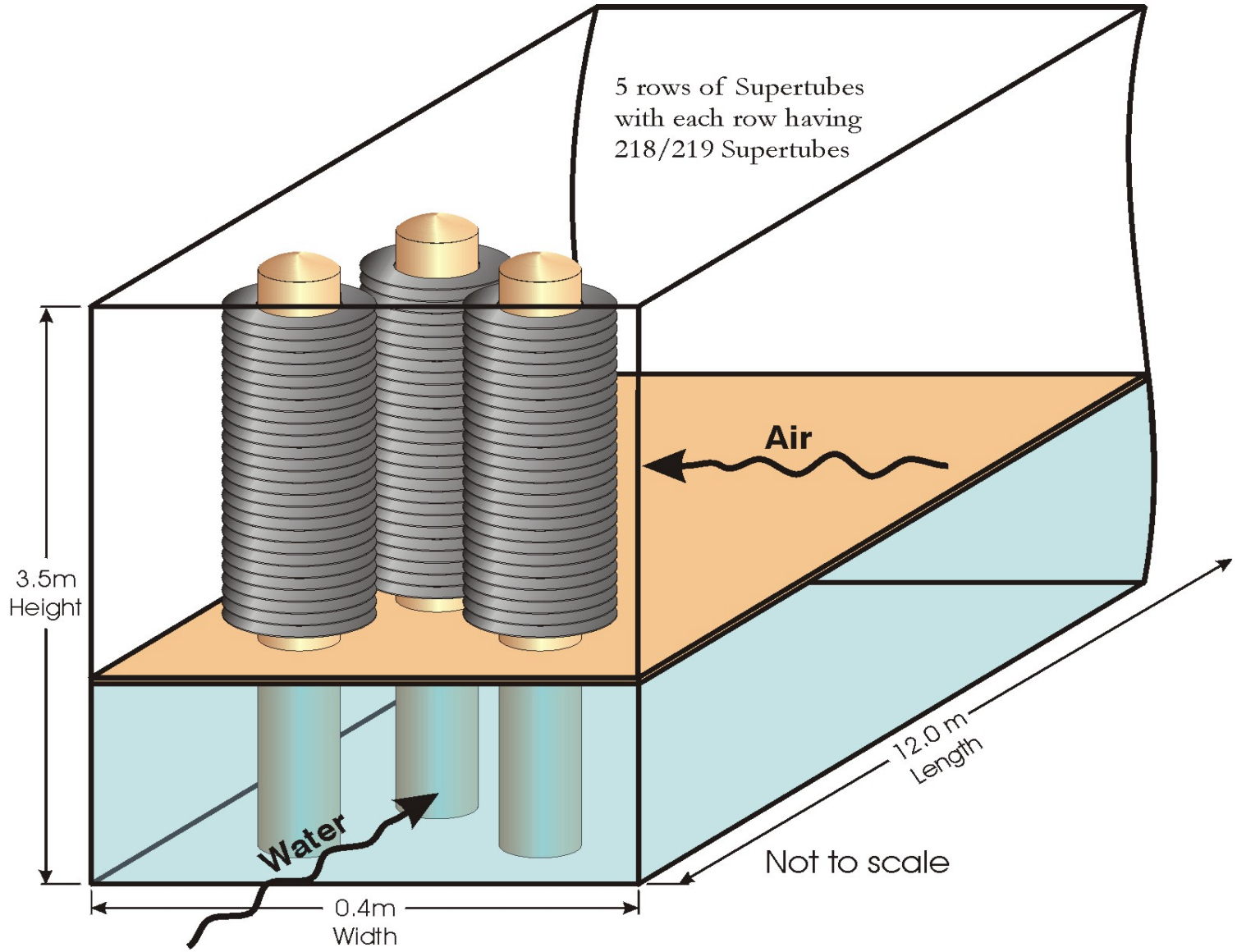

Figure 8. Conceptual Supertube-based emissionless aircraft fuel cell heat exchanger.

MSE calculations then estimated that slight improvements to the above design (e.g., riblet film on fins and slightly thinner metal for the Supertube walls) would significantly reduce the weight required to transfer a given amount of heat. It is potentially possible that the use of more exotic and stronger metals (e.g., titanium alloys) could provide an additional weight reduction.

Dr. Qu's U.S. companies are reorganizing and not able to perform heat exchanger design calculations at this time. However, MSE estimates that based upon weight reductions that have already been calculated, a weight reduction of one-half (compared to the state of the art) is potentially possible by using Supertubes and riblet film (Section 2.4.2.1).

3.2.4 Reliability: Supertube Heat Exchanger vs. State of the Art

Perhaps even more important than the significant potential weight reduction is the much greater reliability inherent in the Supertube heat exchanger design as compared to the state-of-the-art design. A Supertube-based heat exchanger consists of all the Supertubes transferring all the heat in ***parallel***. If any one Supertube develops a leak and fails, then that one Supertube will no longer transfer heat, and the entire device will be only slightly less effective. More than likely, this relatively miniscule reduction would not cause a noticeable reduction in aircraft performance.

3.3 Energy Storage

The form of energy required to propel an aircraft is inherently dynamic and therefore difficult to store in a fixed location. Nevertheless, research is being conducted in a number of facilities in order to learn how to store a higher density of energy per system weight than is now possible with current technologies. Stored energy consumed during a flight could be replenished at a destination airport prior to the next flight. The three types of advanced energy storage described in this section are:

- mechanical–in a rotating mass;
- electrical–in a charged capacitor; and
- magnetic–in an energized coil.

3.3.1 Flywheels

The basic concept of flywheel energy storage is very simple; a rotating mass contains stored energy due to the rotation. However, the technology of storing, maintaining, and using energy from state-of-the-art flywheel systems is rather complex.

The most useful information on this technology came from NASA-GRC, which is developing flywheel energy storage systems for space applications.

The state-of-the-art ***system*** energy storage density is 31 watt hours per kilogram (Wh/kg). This is equivalent to 48 Btu/lb. (The rotor itself stores 90 Wh/kg, but the relevant parameter is energy density for the entire system.)

The flywheel system components include:

- rotor;
- motor/generator;
- support structure;
- magnetic bearings;
- bearing control system; and
- vacuum housing.

Geometrical and operational parameters are as follows:

- rotor outside diameter: 13.5 inches
- rotor inside diameter: 5 inches
- rotor length: 19 inches
- rpm maximum: 53,000
- rpm minimum: 20,000
- rotor material: graphite fiber
- operating temperature range: 80 °F to 180 °F
- design life: 60 years

Additional details on some of the system components are described in the following paragraphs.

The energy stored in the spinning rotor creates considerable stress in that rotor. Stress increases toward the outer surface where the rotational speed is highest. Therefore, the rotor is built in a multi-ring configuration with the inner layers constructed from graphite fibers with a tensile strength rating of 700,000 pounds per square inch (psi) and the outer layers constructed from "T1000" graphite fibers, which are rated at 1 million-psi tensile strength. The upper rotational speed of 53,000 rpm represents a significant derating from what is mechanically possible to ensure safety (i.e., so the rotor will not explode from rotation-induced stress). At this speed, the design life is a very conservative 60 years.

The magnetic bearings prevent any mechanical contact between the rotor and the housing. The bearings are based on permanent magnets providing a constant bias coupled with an electromagnet whose field strength is constantly adjusted (increased or decreased) in real time so that the spinning rotor is always levitated and makes no mechanical contact with any material. If the magnetic bearing system should fail for any reason, there is a backup "touchdown" (ball) bearing system designed to take the rotor from maximum rpm to a complete stop without damage. Magnetic bearings and a vacuum-tight housing (the latter is not required when operating in space) are what allow rotational energy to be stored with minimal dissipation.

To increase stored energy, it would be advantageous to considerably increase the maximum rotational speed. NASA is attempting to push flywheel state of the art to significantly higher rpm and stored energy densities, as well as using a test fixture capable of spinning a relatively small test flywheel at speeds up to 200,000 rpm. At these speeds, the mechanical design will include no shaft, and the magnetic bearing components will be embedded ***inside*** the rotor to provide strength. However, the "weak link" in the system technology is the magnetic materials

as used in magnetic bearings (not graphite fiber or other materials) from which rotors are fabricated. At higher rpm than those currently used, energy losses from standard magnetic bearing materials become significant, and the strength of these magnetic materials is inadequate, thus preventing effective energy storage at the higher rpm.

Nevertheless, CNTs are the strongest material presently known, and MSE has requested that NASA-GRC estimate the upper limit of energy per mass that may potentially be stored in flywheels based upon CNTs (provided that the present magnetic bearing limitation can be overcome) (Section 2.5.1). NASA-GRC estimates this value would be 330 Wh/kg (510 Btu/lb). This value is based upon the assumptions given below.

1) Carbon nanotubes that are as strong as theoretically possible (i.e., 40 times stronger than graphite fibers) will be developed.

2) It will be possible to spin CNTs into fibers, and these fibers will then be used to fabricate flywheel rotors.

3) It will be possible to use CNT fibers to strengthen magnetic bearing materials.

4) Shear strength as well as tensile strength can be increased.

To put the potential ultimate specific energy storage capability of flywheels in perspective, the above-quoted value is approximately an order of magnitude ***greater*** than lead acid batteries but also approximately an order of magnitude ***smaller*** than the energy density of LH_2 fuel (61,100 Btu/lb), ***allowing for the weight increase when that hydrogen reacts with oxygen to produce water***, which is carried onboard the aircraft to the completion of a flight mission.

Unless a breakthrough far more dramatic than that of CNTs is discovered and can be applied to flywheel energy storage systems, it appears that although these systems will have many useful applications, storing the relatively large amount of energy required for aircraft propulsion will not be feasible.

3.3.2 Supercapacitors

As an order-of-magnitude value of their electrical charge capacity, typical standard capacitors used in the fabrication of electronic circuits seldom have capacitances greater than hundreds of ***microfarads***. However, carbon-based supercapacitors can have capacitance values of 1, 10, 100, or even more ***farads*** for sizes and weights comparable to their standard counterparts.

The operational principle of supercapacitors was discovered by Helmholtz in 1887. The interface between a conductor and liquid electrolyte, known as the electrical double layer or EDL, is capable of storing electrical charge. This is an ***area*** effect; therefore, activated carbon, which has a very high surface area per mass, is typically used as the conducting solid. Mechanically, the packaged supercapacitors consist of the following five components in sequence:

- metal current collector;
- activated carbon/electrolyte mixture;
- central membrane;
- activated carbon/electrolyte mixture; and
- metal current collector.

If an aqueous electrolyte (potassium hydroxide solution or sulfuric acid) is used, the operating voltage is limited to the order of 1 V. However, if an organic electrolyte (propylene carbonate) is used, the voltage limitation is then on the order of 5 V. This results in a higher energy storage density. However, the higher internal resistance with an organic electrolyte will limit the application range. The ***power*** density (***not energy density***) of supercapacitors is at least an order-of-magnitude higher than that of batteries.

An improved method for building supercapacitors consists of mixing carbon fibers, stainless steel fibers, and cellulose fibers to form a type of "paper" from this mixture of interlocked fibers. The mixture is then heat treated in a high temperature hydrogen atmosphere to convert the cellulose into additional carbon fibers. The stainless steel fibers increase power density by increasing electrical conductivity.

Supercapacitors are much less energy dense than batteries; however the power density is orders of magnitude better. Supercapacitors are used for memory backup and as short-term backup power supplies. The carbon/electrolyte mixture in supercapacitors can be up to several millimeters thick. Carbon in the form of "carbon black" is used in these devices because it has a surface area as high as 2,000 m^2/g.

Supercapacitors with carbon black alone are called "supercapacitors" and have an energy density storage of the order of 1 kilojoule (kJ)/kg (0.43 Btu/lb). When metals are combined with the carbon black, the energy storage capability is of the order of 10 kJ/kg (4.3 Btu/lb–similar to conventional batteries), and such devices are called "ultracapacitors."

3.3.3 Superconducting Magnetic Energy Storage

This section presents the current state of the art of superconducting coils used for the purpose of storing electric energy in their magnetic field. The next section (3.3.4) will examine the possibility of increasing the stored energy per mass of a superconducting magnetic energy storage (SMES) system.

3.3.3.1–Commercial Superconducting Magnetic Energy Storage Technology The relatively high magnetic fields associated with a coil strongly inhibit superconduction in the "high temperature superconductor" (HTS) materials; therefore, only the "low temperature superconductors" (LTS) are available for coil applications. The material used commercially is niobium-titanium alloy within a copper matrix, which is then extruded into wire (Ref. 29). Coils wound with this material must be maintained within LHe at its normal boiling point (approximately 4 K). The highly thermally insulated housing containing the SMES coil is a "cryostat." Because of the limitations of thermodynamics at these temperatures approaching absolute zero, mechanical heat pumps consuming approximately ***12 kW*** are required to remove

the 1 W of heat flow that leaks into the cryostat from the ambient. Typical characteristics and operating parameters for a commercially available SMES system are summarized in the following table (Table 13).[1]

Table 13. Commercial SMES characteristics and parameters.

Item	Characteristic Or Parameter
Superconducting material	Niobium-titanium alloy in copper matrix
Refrigerant	LHe
Weight of superconducting wire in coil	800 lb
Coil form material	Fiberglass
Coil form weight	300 lb
Total coil weight	1,100 lb
Electric current	1,050 A
Stored energy	3 MJ
Coil shape	Cylindrical solenoid
Pressure when energized	23,000-24,000 psi
Total weight of cyrostat	5,000 lb
Calculated energy storage (weight basis)	0.57 Btu/lb

The ***energy storage*** (weight basis) of such a system is obviously poor. The commercial value (to electric utility companies) is high; however, because the energy stored in the magnetic field of a coil may be delivered (as electric current) at an extremely high rate, thereby allowing momentary imbalances in high capacity electric power systems to be corrected in real time (for durations up to 2 s).

3.3.4 Possible Enhanced Superconducting Magnetic Energy Storage

Both NASA-LaRC and NASA-MSFC have discussed the possibility of enhancing the density of stored energy in SMES systems by applying the concepts given below.[2]

1) Wind a superconducting coil in such a way that the self-induced magnetic field produces no force, thus eliminating potential problems related to the strength of materials.

2) Use the claimed high electrical conductivity properties (and strength properties) of CNTs to replace the copper matrix metal of commercial LTS wire, thereby extending operating currents and stored energy to significantly higher levels than that of the current technology.

3) Use CNTs to directly replace LTS wire, based on (not conclusively proven) claims that CNTs exhibit some characteristics of electrical superconductivity.

These concepts and their potential applications are discussed in the following sections.

[1] Phone call from Tom Abel at American Superconductor to MSE, 6/12/02.
[2] E-mail from John Cole, NASA-MSFC, to MSE, 7/01/02.

3.3.4.1–The Force-Free Coil Concept A research paper provided by NASA-MSFC explains how a magnetic coil can be wound in such a way that it produces zero mechanical force due to its magnetic field (Ref. 30). The two design criteria that allow the coil to be "force-free" are:

- there can be no hollow cavity within the coil, which is acceptable if the coil is designed to store energy; and
- each layer of wire in the coil is wound at an "offset" angle from the layer beneath it. In this manner, the force in a given layer is automatically counteracting against or neutralizing the force in the other layers.

(The article explains that zero force could only be achieved (in theory) if the coil wire has no thickness. In practice, physical wire has a finite thickness; therefore, the residual force can be greatly minimized but not totally eliminated.)

If the SMES solenoidal coil in Section 3.3.3.1 were wound in a force-free configuration, the 300-lb fiberglass form would not be required. For the same amount of stored energy, this would reduce the solenoid weight by 27% or the weight of the 5,000-lb cryostat by 6%. It is also noted that a force-free (or nearly force-free) coil configuration would make the high strength-to-weight ratio of CNTs much less relevant.

3.3.4.2–Carbon Nanotubes used as a Superconducting Magnetic Energy Storage Quench Prevention Matrix

3.3.4.2.1–State-of-the-Art Quench Prevention The superconducting state in state-of-the-art superconductors exists within an operating envelope, which is limited by the maximum values of:

- temperature;
- magnetic field strength; and
- current density within the superconducting filaments.

The metallic matrix (typically copper) of state-of-the-art SMES coil wire not only provides mechanical support for the superconductor filaments but helps prevent a potentially catastrophic "quench" from the superconducting state to the normal state.

If a small region of superconducting filament in an energized SMES coil should begin to "go normal," it would generate I^2R heat (as the resistance is no longer zero), which would start a potentially catastrophic heating and energy-releasing chain reaction throughout the coil. (Heat generated by electric current in a conductor equals the current squared multiplied times the resistance.)

The copper matrix prevents a quench by a two-fold action.

1) The thermal conductivity of the copper removes I^2R heat from the small region of superconducting filament and transfers that heat into the SMES LHe refrigerant.

2) The copper simultaneously provides an electric conducting path parallel to that of the small region of superconducting filament undergoing the resistance transient until that small region can "recover" and go back to the superconducting (zero resistance) state. That stops the generation of I^2R heat, because R is again equal to zero.

Therefore, the copper matrix allows the superconducting filaments to operate closer to the edge of the (temperature-magnetic field-current density) envelope, and the SMES coil can thereby store more energy in its magnetic field.

3.3.4.2.2–Quench Prevention Using Carbon Nanotubes If CNTs were to provide the quench prevention role with state-of-the-art superconducting filaments, the following parameters would be important:

- CNT thermal conductivity;
- CNT electrical conductivity;
- the means to provide a continuous thermal conducting path from the superconducting filament to the CNT and from the other end of the CNT to the LHe refrigerant;
- the means to provide a continuous electrical conducting path from the superconducting filament into the CNT, as well as from the CNT back to the superconducting filament (the length of this bypass path needs to be determined); and
- the requirement that the windings of a SMES coil are rigid (i.e., there is no relative motion between coil turns).

These parameters are discussed below.

3.3.4.2.3–Carbon Nanotube Thermal Conductivity According to Dr. Paul McEuen of the Cornell University Physics Department, one of his graduate students succeeded in measuring the thermal conductivity of a CNT and found it to be ~ 3,000 W/mK at room temperature, but it decreased to ~ 1 W/mK at approximately the temperature of LHe.[3] These thermal conductivity values at these respective temperatures are very similar to the values at the same corresponding temperatures for copper. The CNT thermal conductivity was measured on "multiwall" CNTs and is assumed to be the same (or similar) for "single-wall" CNTs, which are mechanically stronger.

3.3.4.2.4–Carbon Nanotube Electrical Conductivity Dr. McEuen stated that the electrical conductivity of (single-wall) CNTs is in the range of one to ten times that of an equal cross section of copper at room temperature and approximately the same at LHe temperature. He specifically stated that this conductivity was ***not*** as large as 100 times that of an equal cross-section of copper as others have claimed.

3.3.4.2.5–Carbon Nanotube Thermal Conducting Path Based on information that has been reported to date, it would be extremely difficult to construct a heat-conducting path (using CNTs) from the surface of state-of-the-art superconducting filaments leading into the LHe refrigerant. A report by LyTec LLC discusses experimental attempts to connect CNTs to

[3] Phone call to MSE, 6/28/02.

electrodes or leads (Ref. 31). In addition to differences in chemical properties between metallic alloys and carbon, there is a considerable size difference between state-of-the-art superconducting filaments (tens of microns diameter) and CNTs (a few nanometers diameter). This is a size ratio of approximately 10,000.

3.3.4.2.6–Carbon Nanotube Electrical Conducting Path For the same reasons presented in the preceding section, the creation of a continuous electrical conducting path using CNTs in parallel with the superconducting filaments is challenging. CNTs are essentially one-dimensional conductors. According to the LyTec Report, "sideways" conduction from one CNT to an adjacent parallel neighbor is minimal. Quoting from page 16 of the LyTec report, "The currently understood characteristic of the tubes are that they do not conduct well to adjacent tubes. Thus, electrical connections have to be made to each tube and the tube must be continuous without breaks to function as a satisfactory conductor." Therefore, CNTs would need to be individually connected to the superconducting filaments (although many could be connected simultaneously if the means to accomplish this were known).

3.3.4.2.7–SMES Rigidity Requirement The relative motion of an electrical conductor within a magnetic field induces an electrical current within that conductor. For a winding within a magnetized SMES coil, this additional transient current could cause the total current to exceed the current density limitation and lead to heating, as well as a coil "quench" to the normal conducting state and possible catastrophic failure of an energized coil. Therefore, in order to prevent any relative internal motion, state-of-the-art SMES (and other types of superconducting) coils have the windings embedded in a special (low temperature) epoxy during manufacture. If all the other requirements could be met to allow CNTs to replace the copper matrix surrounding state-of-the-art superconducting filaments, there would also need to be a way to fill all voids with epoxy during the manufacturing process.

3.3.4.3–Carbon Nanotubes as Superconducting Filaments in a Superconducting Magnetic Energy Storage Coil Regarding the issue of whether CNTs could be used as superconducting filaments that would constitute the windings of a SMES coil, there are a number of questions that need to be answered.

1) Can it be ***conclusively*** proven that CNTs (or modified—perhaps doped CNTs) are in fact superconductors?

2) If CNTs are in fact superconductors, what combination of maximum values of temperature, magnetic field strength, and current density will define the "operating envelope?"

3) Can CNTs provide their own "quench path," or do they need an auxiliary matrix material as do state-of-the-art superconducting filaments?

4) Can ***continuous*** lengths of CNTs, which are literally thousands of feet long (required for coil winding), be developed, or can short lengths of CNTs be connected into what is effectively one continuous strand?

5) What is the effect on the physical properties caused by the deformation of CNTs as they are bent into the round shape of a coil turn?

6) How can all the CNT filaments be immobilized such that there is no relative motion anywhere in the SMES coil?

These questions are discussed below.

3.3.4.3.1–Conclusive Proof of Superconductivity in Carbon Nanotubes Page 9 of the LyTec report refers to the following information that has been claimed regarding the issue of superconductivity in CNTs:

- "superconducting correlations;"
- "transition to a low resistance state;"
- resistances which showed a "sharp drop at a temperature of order 0.3 K" and actual superconductivity up to 15 K "in a matrix of individual" (single-wall) CNTs, "having very small diameters of 0.4 nm, embedded in a zeolite;" and
- "reports of possible superconductivity at temperatures as high as 400 K."

The MSE interpretation of the above information is that CNT superconductivity is possible but not at all conclusively proven in the material presented to date.

3.3.4.3.2–Carbon Nanotube Superconductivity Operating Envelope If experimenters report conclusive evidence that superconductivity exists in CNTs, it is expected that they will also report on the relevant experimental conditions including the respective maximum values of temperature, magnetic field strength in the region of the CNTs, and the electrical current density in the CNTs whose properties are being measured. These parameters will define the superconductivity operating envelope, as well as the type of refrigeration system required to maintain the superconductivity state.

3.3.4.3.3–Carbon Nanotube Inherent or Auxiliary Quench Path If CNTs are conclusively shown to be superconducting, experimental data will be needed to determine if they are inherently self-quenching or require an auxiliary quench path (as do state-of-the-art superconductors).

3.3.4.3.4–Carbon Nanotube Maximum Producible Lengths As of June 2002, Dr. Rodney Ruoff of Northwestern University (who has briefed NASA-MSFC regarding CNTs and also contributed to the LyTec report) told MSE that he has reviewed a Chinese claim of the production of a "bundle" of CNTs, which is 20 cm long; however, the length of individual CNTs in the bundle is unknown.[4] Many researchers are currently attempting to maximize the length of individual CNTs, as this will make these materials more suitable for a wide variety of mechanical and electrical applications (whether or not they are in fact superconducting).

[4] Phone call from Dr. Rodney Ruoff of Northwestern University to MSE, 6/6/02.

Bonding CNTs into composites does not solve the length problem. According to Ms. Mia Siochi of NASA-LaRC, dispersing CNTs into a polymer material only produces a very slight increase in the electrical conductivity of the polymer; however, it remains essentially an electrical insulator.[5] Ms. Siochi had not yet measured the changes in thermal conductivity characteristics of the polymer caused by incorporating CNTs. The key is that CNTs must be effectively connected end to end as they are "locked" into the polymer as it hardens.

3.3.4.3.5–Changes in Carbon Nanotube Properties Caused by Bending Since the diameter of a typical (single-wall) CNT is only equivalent to a few carbon rings, bending such a structure could cause more of a change in properties (e.g., for conduction electrons and chemical bonds) than would be the case for a much greater diameter metallic filament. This is another area of research that requires experimental investigation.

3.3.4.3.6–Carbon Nanotube Immobilization in a Superconducting Magnetic Energy Storage Coil If CNTs are conclusively shown to be superconducting and can be wound into a SMES coil, it is expected that the CNT filaments must be immobilized (as is the case for state-of-the-art superconductors).

3.3.4.4–Conclusions Relevant to the NASA-LaRC/NASA-MSFC Concepts Based upon the information available to date, the following can be concluded.

1) If experimental results agree with theoretical calculations, then it should be possible to construct a SMES coil that possesses no self-induced magnetic force. Such a coil would not require the extra mass of material(s) required to provide strength, nor would it require a form on which to be wound.

2) If a method can be developed to bond CNTs to state-of-the-art superconducting filaments in such a way that the junction is thermally and electrically loss-free, if the CNTs are of a continuous length capable of carrying heat from a transient "normal" region into the LHe refrigerant (as effectively as copper), and the CNTs are capable of carrying electric current around the transient "normal" region (as effectively as copper), then CNTs could replace the copper matrix metal of state-of-the-art superconductors and would therefore increase the energy density of an SMES coil because carbon is less dense than copper.

3) If it can be conclusively and reproducibly proven that CNTs are superconductors, if the superconducting properties are at least equivalent to that of state-of-the-art superconductor filaments, if none of the superconducting properties are adversely affected by bending the CNTs into the curved shape required for winding a coil, if no auxiliary quench protection is required, and if CNT superconductor filaments can be produced in continuous lengths of at least thousands of feet, then (if all the other parameters were equal to that of a state-of-the-art SMES coil) the energy density would be increased as compared to the state of the art because carbon is less dense than state-of-the-art materials.

[5] Phone call from Mia Siochi of NASA-LaRC to MSE, 6/12/02.

4) If a SMES ***coil*** can be produced with a higher energy density than that of the state of the art, then it should be noted that the ***refrigeration system and cryostat*** of a state of the art SMES ***system*** are far more massive than the SMES ***coil*** itself.

5) The overall conclusion is that according to the information available to date, analysis, and caveats of this report, it might be possible to enhance the energy density of SMES coils by using a force-free coil design and incorporating CNTs. The magnitude of such an enhancement (if it is achieved) would need to be determined experimentally.

4. Longer Term Advanced Concepts

4.1 Breakthrough Propulsion Technologies

State-of-the-art aerospace vehicles are propelled by moving mass in the direction opposite to the direction the vehicle is moving. A number of researchers believe that it may be possible to propel aerospace vehicles by revolutionary methods.

It is not commonly known that Newton's classic laws of motion do ***not*** extend to derivatives higher than the second order. The functioning of the Thornson propulsion system described in this report could possibly be explained through the extension of the principles of motion as they are commonly understood.

Many experimenters throughout the world are flying lightweight model "aircraft" using a few watts of electric power that is applied at a voltage of tens of thousands of volts. At this time, the explanation of how this occurs is not conclusively known. Others have claimed to achieve a small-scale propulsive thrust in a vacuum, a result (which if further replicated) requires a more thorough understanding of the physics involved.

The reason these advanced propulsion technologies are important is that they potentially offer the possibility (if proven) of propelling aerospace vehicles (aircraft and space vehicles) with much greater efficiency than is currently possible.

4.1.1 The Thornson Propulsion Device

The Thornson Propulsion Device is a rotating mechanism powered by a standard electric motor run by a battery (all totally enclosed within a wooden box) with nothing protruding from, entering, or leaving that box; yet, it is claimed to produce a net unidirectional force. Tom Valone, the president of Integrity Research Institute, has described holding the box in his hands and clearly feeling a net force pushing in one direction when the device is operating.

A booklet published by Valone is a partial mathematical analysis of the device's rotating mechanism (Ref. 32). An additional description of Thornson's invention may be found in his U.S. Patent (Ref. 33). A simplified description of the device's mechanism and operation follows.

1) A small "sun" gear is centrally placed upon a larger disk.

2) This sun gear and disk are rotated conventionally by a standard battery-driven electric motor.

3) A second "planetary" gear, identical with the sun gear, has its rotation axis located one "gear diameter" from the center of the sun gear (or the center of the disk) and meshes with the sun gear.

4) The planetary gear has a small lead weight fastened to one position on its circumference.

5) When the disk and sun gear rotate, the "wheel within a wheel" rotation of the planetary gear causes the lead weight to trace an "epicycloid" path that looks like the classic heart shape.

6) A key feature is that once per revolution of the large disk and sun gear, the lead weight on the planetary gear impacts upon the central shaft of that large disk and sun gear and transfers a linear impulse that is derived from a rotational motion.

7) Steps 1 through 6 are exactly and synchronously duplicated with an identical mechanism, but in mirror image geometry, in order to nullify unwanted vibration.

Some high-level tentative ideas about the functioning of this device are as given below.

1) From Valone: "Forces that are equal and opposite in one frame are not necessarily so in another frame. They remain equal and opposite only if their points of application have equal velocities."

2) From Thornson: He has learned how to "rectify vibration." This is no more mysterious than rectifying ac electricity to dc. Thornson also says he is using ***internal*** reaction forces rather than ***external*** reaction forces.

3) Articles written by Dr. William O. Davis, former Assistant to the Director of Laboratories, Wright Air Development Center, describe USAF research findings from the 1950s that motion involving the third derivative and higher does ***not*** agree with Newton's law that force equals mass times acceleration (Ref. 34). A point on a rotating disk experiences acceleration (second derivative motion), but a point tracing an epicycloidal path seems to involve higher derivatives of motion and, if so, we are describing a realm where Newton's force/mass equation does not apply. (This is not a precedent, standard equations of motion also do not apply at velocities approaching the speed of light.)

Thornson claims that physicist Hal Puthoff who heads the Institute for Advanced Studies at Austin, Boeing Aircraft, and the manufacturer of "Seadoo" recreational water vehicles have all expressed significant interest in his invention.

4.1.2 High-Voltage Propulsion in Air

It is possible to demonstrate that a high-voltage dc potential (approximately tens of thousands of volts) applied to a specially designed device in ambient air will cause that device to experience a net force in a specific direction. The theoretical explanation for this phenomenon is not presently understood; MSE is primarily reporting what has been previously demonstrated and observed. This force/propulsion effect was observed by MSE on three separate occasions in the laboratory of Transdimensional Technologies, Inc. (TDT) of Huntsville, Alabama, as well as at the August 2002 Institute of New Energy (INE) Symposium in Salt Lake City, Utah.

TDT claims that these devices require:

- high-voltage electricity flowing through a "leaky dielectric," which means a material with electrical conduction properties ***between*** those of a metallic conductor and a dielectric insulator; and
- an asymmetric electric field between the positive and negative polarity parts of the device.

4.1.2.1–Smaller TDT Device The geometric configuration of the smaller TDT "thruster" consists of a thin circular metal disk approximately 1 inch in diameter separated by two different dielectrics from a 2-inch long piece of copper tubing, also approximately 1 inch in diameter. One thruster is mounted on each end of a plastic arm approximately 1 ft long; the assembly rotates in a horizontal plane with the central axis where the arms join. Wires carry high voltage from a small Van de Graaff voltage source to upper and lower metallic pivots that are also connected by other wires to the two thrusters at each end of the rotating arm. TDT estimated (this was ***not*** measured) that the voltage at the thruster was 80,000 V, and the current was 1 microampere (μA) (the threshold voltage for thrust production was stated to be 35,000 V above the ground state). Small metal tips at the leading edge of the circular disks were used to allow a corona emission to occur to prevent major arcing. As the device rotated at 90 rpm, one could definitely feel the "ion wind" emitted from the tips ***in the direction of rotation***. TDT believes this is proof that the thrusters are ***not*** pushing forward in response to a "back-pushing" ion wind. The front facing disks are charged positive, and the copper tube is negative.

4.1.2.2–Larger TDT Device MSE witnessed two identical thrusters at opposite ends of a 4-ft-long rotor, with the thrust directions additive such that the rotor would begin to rotate and then accelerate up to a maximum rpm (limited by frictional forces, mainly air drag) when the thrusters were supplied with the maximum electric power available from a high-voltage dc electric power supply.

The rotor's central shaft was held at the top and bottom by simple "cone and cup" metal bearings, which also served to introduce high-voltage dc electricity provided by a (nominal) 70,000 V (70 kV) dc power supply via wires to the two thrusters.

Figure 9 shows the thruster geometry. Each thruster is actually a capacitor. An electric capacitor consists of a dielectric (insulator) physically located between two metals (conductors).

Geometric shapes of thruster components can be varied to some extent; however, (according to TDT) the four basic components of these thrusters are (in sequence from front to back) (Table 14):

Table 14. Thruster components.

Component	Composition
Forward conductor	Copper wire, 0.007-in diameter x 17.5 in long
"Leaky" dielectric	Air
Non-leaky dielectric	Lucite plastic sheet
Rear conductor	Aluminum sheet, 15.5 in x 3.5 in x 0.0625 in thick

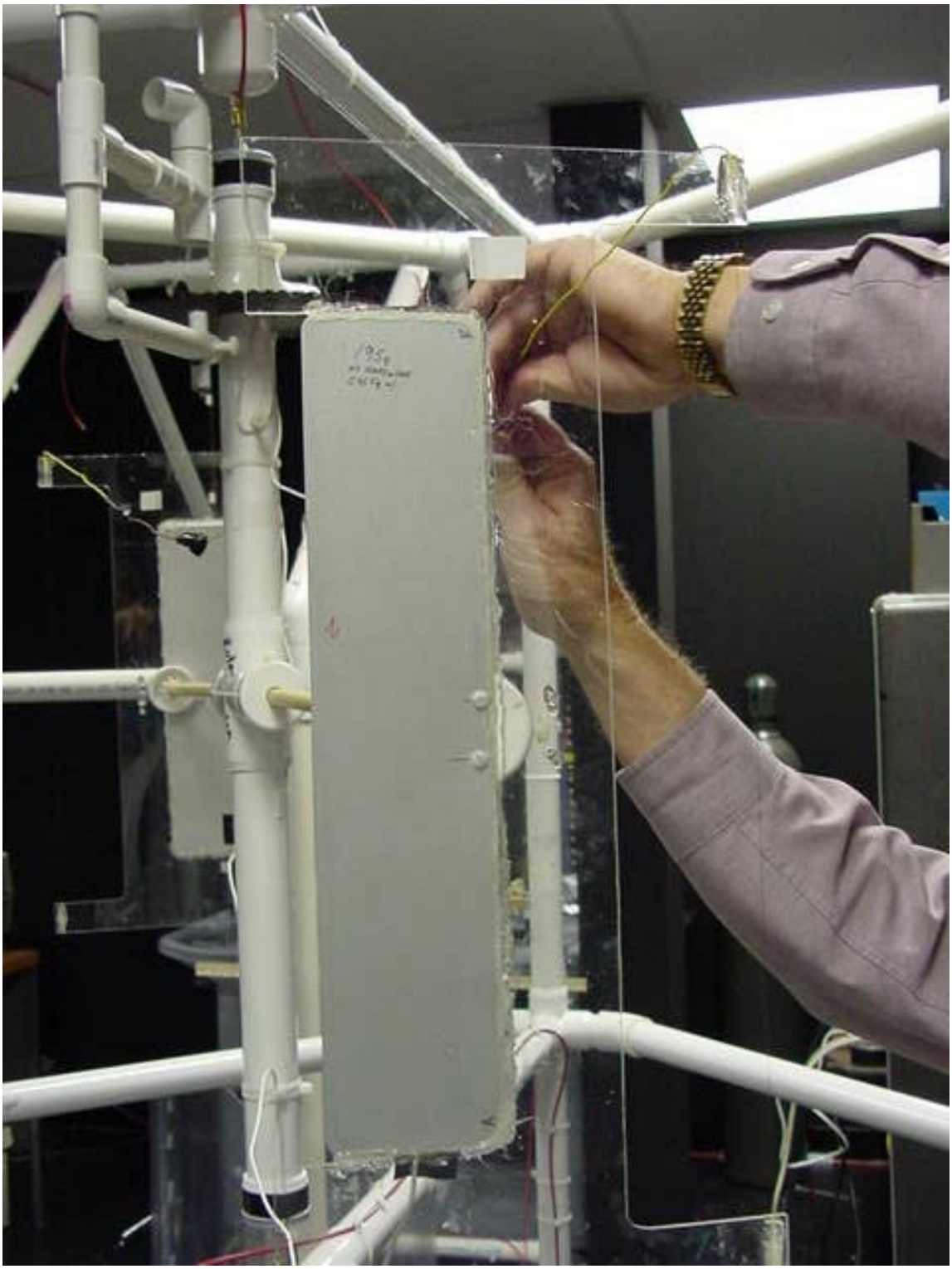

Figure 9. Closeup view of a TDT thruster on the end of the rotor arm.

The thruster geometry is asymmetric in two ways: 1) the forward conductor is geometrically smaller (in two dimensions) than the rear conductor and 2) the electric field distribution of the dielectric regions between the two conductors is asymmetric.

The forward conductor copper wire (just to the right of the man's wristwatch) is barely discernable in the photograph extending vertically from top to bottom.

A rotor test of the larger device consisted of the voltage across the thruster capacitors being gradually increased, while rotor rpm was monitored via an electronic circuit counting pulses produced with a laser beam that was interrupted by a notched disk mounted on the rotor. The rotor would typically begin to move at 26 kV (the typical voltage at which the front conducting wire emits corona discharge – which makes a hissing sound) and reached approximately 63 rpm when the maximum 71 kV (which resulted in a current of 584 μA) was applied. This is a power level of 41.5 W. The forward conductor was positive, and the rear conductor was negative. TDT calculated that approximately 90% of the input power creates the corona discharge surrounding the forward conductor and therefore does not directly contribute to the thrust. TDT also claimed that voltages and currents as read from the power supply were each accurate within ± 10%.

4.1.2.3–Pendulum Tests In the view of those who investigate advanced propulsion technologies, a device when hung like a pendulum passes the "pendulum test" when ***it is placed in a sealed container and can maintain a steady-state position that is not vertical*** (when energized). The TDT thrusters passed this test. A single thruster, which was identical to those on the rotor arms, was wrapped in a completely enclosing box consisting of plastic and transparent plastic film; this entire assembly was then hung as a pendulum away from objects that might have influenced the thruster's electric fields. Thin wires to carry high-voltage dc to the thruster components did, of course, penetrate the enclosure. A measuring scale was placed behind the device in order to measure deflection, and this deflection was measured from approximately 10 ft away via a video camera and TV screen. This distance prevented observers from being close enough to distort the thruster electric fields or get shocked. Table 15 shows the typical test parameters.

Table 15. TDT pendulum test parameters.

Parameter	Value	MKS Value
Pendulum length	59.75 in	1.52 m
Pendulum mass	670 g	0.67 kg
Pendulum deflection	1/8 in	3.2×10^{-3} m
Applied voltage	71 kV	71 kV
Applied current	180 μA	180 μA
Applied power	12.8 W	12.8 W

When the deflection angle is relatively small, as it is in this case, the following equation allows the force causing the deflection to be calculated:

$$F = MgD/L$$

where:

F = force in newtons (N)
M = mass in kg
g = gravitational acceleration constant in meter-kilogram-second (mks) system units
D = deflection in meters
L = pendulum length in meters

Using the parameters observed by MSE:

M = 0.67 kg
D = 3.2 x 10^{-3} m
L = 1.52 m

The force causing the deflection is calculated to be 1.4 x 10^{-2} N.

TDT calculated that the force that ***could*** be produced by ion wind is approximately 6.4 x 10^{-6} N, which is more than three orders of magnitude smaller. Nevertheless, the enclosing box eliminates all such arguments that ion wind may be producing the observed force.

4.1.2.4–High-Voltage Propulsion in Air Demonstrated by Others—Lifters On one occasion, MSE observed (at the TDT laboratory) a triangular-shaped high-voltage model flying device, referred to as a "Lifter" because it would lift off of a table top and levitate (while provided high-voltage dc electric power via a small diameter metallic wire).

The operation of a very similar device (Figures 10a and 10b) was also observed by MSE at the INE Symposium in Salt Lake City, Utah, in August 2002.

The characteristics of the demonstrated device are given in Table 16 and are as follows:

Table 16. High-voltage propulsion device demonstrated at INE 2002 Symposium.

Item	Description
Shape	Triangular, equal sides
Dimensions	Each edge–3 ft; height–4 inches
Materials	Balsa wood, aluminum foil, wire
Weight	35 g
Power supply (offboard)	35,000 V dc, 1 mA, 35 W
Electrical polarity	Thin positively charged wire parallel to and 2 inches above a 2-inch-high continuous piece of negatively charged aluminum foil, perimeter of triangular frame
Weight/power ratio	~ 1 g/W (***claimed*** to increase with size)
Power connection to power supply	~ 0.002-inch stainless steel wire
Flight controls	Insulated tethers
Operating principle	Presently unknown

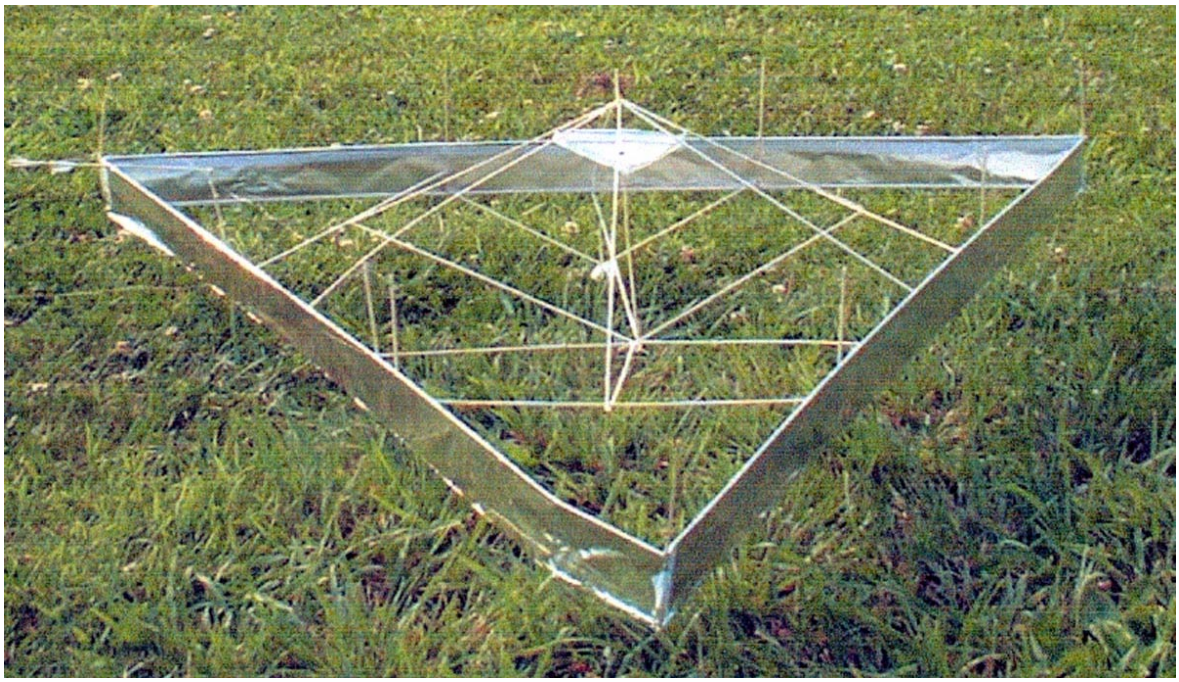

10a

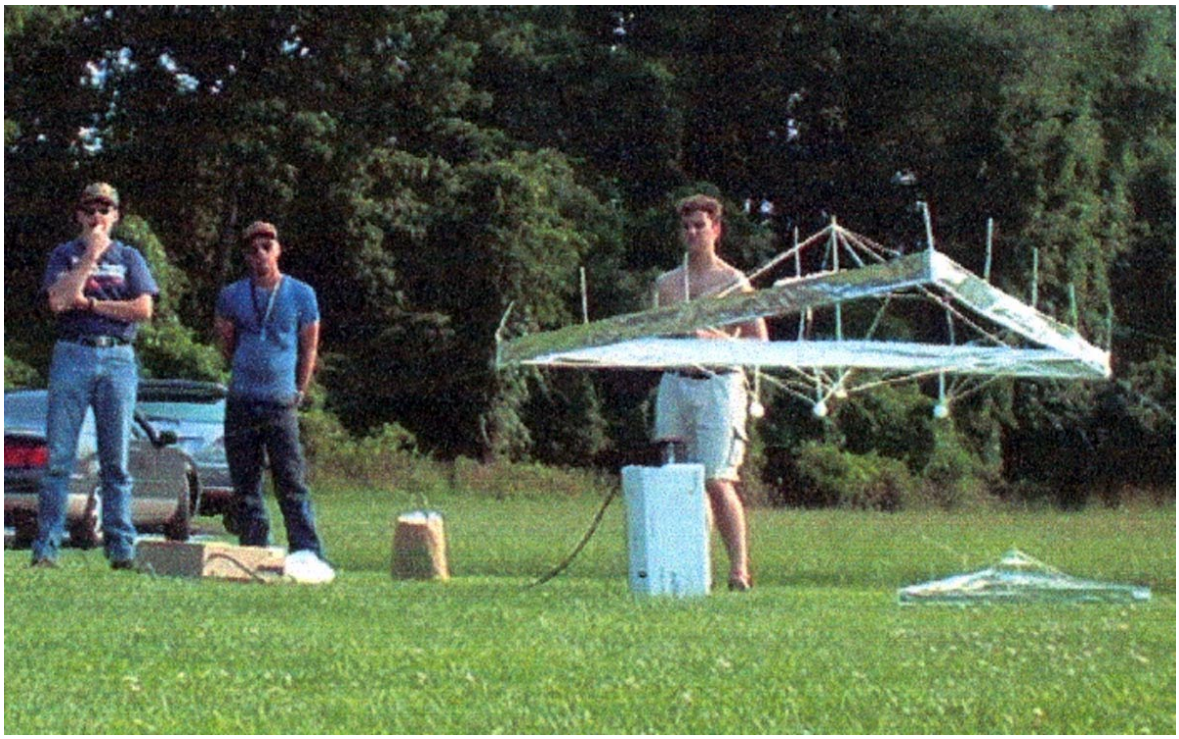

10b

Figures 10a and 10b. High-voltage propulsion device demonstrated at Institute for New Energy 2002 Symposium.

When the voltage on an adjustable high-voltage power supply was increased to approximately 35,000 V [for which the current reading was approximately 1 milliampere (mA)], the device would take off from the floor and rapidly climb vertically (restrained by tether lines).

4.1.3 High-Voltage Propulsion in Vacuum

4.1.3.1–TDT Claim TDT ***claims*** to have achieved high-voltage (propellantless) propulsive thrust in a ***vacuum*** using an electronic component called a "doorknob capacitor." It is the view of MSE that a claim such as this needs to be replicated by others because high-voltage propellantless propulsion in a vacuum is significantly more interesting and potentially more important than such propulsion occurring in air.

4.2 Breakthrough Energy Technologies

Many energy-related technologies are dependent on electric current flowing through conductors and would be more efficient or have a higher weight-basis power density if electric conductors with a significantly lower resistance than copper (at ambient temperatures) were available. The first topic in this section briefly describes an attempt to develop such a technology.

For more than 100 years, a number of inventors have claimed to have discovered methods of producing usable amounts of energy; this energy does not come from a presently known source. Some of these breakthroughs have been well documented, and others have received U.S. patents. Such claims need to be replicated, but a possible source of the "excess" energy is the so-called "zero-point energy," which is believed to exist everywhere and is also believed to have been verified by recent accurate measurements of the Casimir Force.

Concepts related to and current experiments to produce usable energy from zero-point energy are described in this section. Obviously, as zero-point energy does not involve fuels or reaction products; its successful production at a usable level would be of great value for propelling aerospace vehicles.

4.2.1 Ultraconductors

ROOTS, Inc. of Sebastopol, California (ROOTS), has claimed to be developing organic conductors with an electrical conductivity 100,000 times that of copper at normal room temperature (Ref. 35).

This technology is based on a Russian discovery made in the 1980s and uses a controlled irradiation of organic polymers with ultraviolet light. ROOTS has hypothesized that the irradiation aligns oriented dipoles within the polymer around an axial electron "thread" or chain. The result is that microscopic regions of polymer (approximately one-fiftieth the diameter of a human hair and up to 100 microns length) can carry an electric current in excess of 50 A at ambient temperatures. ROOTS is currently seeking funding in order to attempt to scale up this technology from microscopic dimensions to larger sizes.

4.2.2 Zero-Point Energy Concepts

Mr. Moray King has been lecturing on and writing about tapping what is commonly referred to as the "zero-point energy" for more than 28 years (Refs. 36 and 37). Mr. King gave a lecture on this topic at the 2002 Symposium of the INE.

According to the principles of quantum mechanics, the seemingly empty vacuum between atoms, when considered at small enough dimensions (orders of magnitude smaller than atoms), contains an exceedingly high energy density (as large as 10^{94} ergs/cm^3). This energy is referred to as zero-point energy because it is believed to exist even at a temperature of absolute zero. This energy can be thought of as electromagnetic radiation of all frequencies or even as fluctuations of spacetime itself. Because of the totally random characteristic of this energy, it paradoxically appears to cancel itself out or not exist. Most physicists believe that the randomness of this energy does not allow any of it to be tapped for any practical use (one exception is a recent acknowledgment by developers of nanoscale microelectromechanical systems that the zero-point energy (which has been conclusively proven to exert the measurable Casimir Force when micromechanical parts are within 1 micron or less of each other) can prevent such devices from functioning, unless means are introduced to overcome this phenomenon).

As Mr. King explains, zero-point energy is difficult to detect because:

- it is incoherent;
- the energy is everywhere–its detection requires measuring an energy difference;
- less than 1 quantum of energy is cohered at any one mode;
- it flows orthogonally to our space (virtual);
- it rapidly changes frequency–linear detectors cannot resonate coherently with it to follow signal; and
- the very high frequencies do not readily interact with matter.

However, Mr. King contends, that there are a few basic principles that do allow zero-point energy to be tapped and that these principles have been incorporated in technology that inventors have ***claimed*** achieved this result.

One of the principles that Mr. King claims may allow zero-point energy to be tapped is that of the nonequilibrium thermodynamics advanced by Ilya Prigogine who won the Nobel Prize in chemistry for this work in 1977. Mr. King explains Prigogine's work and its importance in the following.

1) The standard scientific belief is that the Second Law of Thermodynamics must cause systems to become more random and disordered.

2) ***Nonlinear systems*** are not restricted to the Second Law of Thermodynamics as it is commonly taught.

3) An example of such a nonlinear system is ionized plasma.

4) The addition of energy to a plasma can sometimes form a metastable vortex ring called a plasmoid. According to Mr. King "such a structure cannot be predicted by a linear thermodynamic model, but it can be predicted by a nonlinear magnetohydrodynamic model. The nonlinear interactions produce macroscopic coherence from random turbulence."

5) The persistence of "ball lightning," which has been modeled as a vortex ring plasmoid, is cited by Mr. King as evidence that such structures are cohering some zero-point energy (which maintains the stability of the structure) and then radiating excess energy as light and heat.

4.2.3 Motionless Electromagnetic Generator

Mr. Tom Bearden is a retired U.S. Army Intelligence Officer who has been presenting his views on advanced energy topics for approximately 25 years.

Mr. Bearden ***claims*** that a paper that he and 14 others have coauthored provides an explanation of an "overunity" (as observed in 3-space) electromagnetic device the coauthors have ***claimed*** to have invented and for which Bearden and four other co-inventors received a U.S. patent (Refs. 38 and 39). According to Bearden, he and his group have a working, bench-scale laboratory model of this device. This invention is referred to as a "Motionless Electromagnetic Generator" because it has no moving (mechanical) parts. Bearden states the functioning of this generator is dependent on:

- toroidal geometry;
- the Aharonov-Bohm effect (Section 4.3.3); and
- the use of nanosized particles of the alloy of which Nd-B-Fe magnets are composed, (which is 15 atom % Nd, 8 atom % B, and 77 atom % Fe).

Other statements by Mr. Bearden are given below.

1) A toroidal-shaped core filled with nanosized particles of Nd-B-Fe has a primary and secondary winding. This is essentially an electrical transformer with a unique core.

2) Due to its toroidal shape, any magnetic field ***within*** the toroid will be confined within that geometry.

3) The nanosized particles of Nd-B-Fe possess the (previously unexpected) property of exhibiting the quantum mechanical effect known as the "Aharonov-Bohm effect," which is formally defined as "an effect manifested when a beam of electrons is split into two beams that travel in opposite directions around a region containing magnetic flux and are then recombined, whereby the intensity of the resulting beam oscillates periodically as the enclosed magnetic field is changed" (Ref. 40).

4) When one unit of electrical energy is then introduced through the primary winding (in the form of electrical spikes), two units of electrical energy can be extracted from the secondary winding. Mr. Bearden claims the "active vacuum" operating through the Aharonov-Bohm effect provides the extra unit of energy.

It will of course be very significant ***if*** Mr. Bearden and his colleagues can publicly demonstrate their device and ***if independent researchers can replicate it***.

4.2.4 Longitudinal Electric Waves

More than 100 years ago, Nikola Tesla discovered, investigated, and wrote about longitudinal electric waves and patented technology based upon their characteristics (Ref. 41).

James Clerk Maxwell's ***original*** electrical wave equations (not taught in universities at this time) described both longitudinal and transverse electric waves (caused by moving electric charges). Heaviside and others changed Maxwell's equations to a "simpler form" (as it is presently taught) by eliminating all reference to longitudinal electric waves but retaining transverse electric waves. Exact definitions are:

- transverse electric waves = transverse electromagnetic waves; and
- longitudinal electric waves = longitudinal magnetodielectric waves.

Thus, strictly speaking, longitudinal electric waves are, by definition, not "electromagnetic."

The potential importance of longitudinal electric waves is that (in contrast to electromagnetic waves and according to the claims of Tesla and present day researchers) they are believed to:

- have a velocity greater than light;
- readily penetrate matter; and
- be a key to extracting useable energy that is otherwise inaccessible (e.g., zero-point energy).

A more thorough investigation of these waves is planned for future work.

4.3 Breakthrough Physics

NASA-LaRC has also asked MSE to investigate and report on possible breakthroughs in physics that are even more fundamental than (but clearly related to) breakthroughs in propulsion and energy.

As an example, breakthroughs in physics would occur when there is an explanation of gravity that allows this universal force to be explained and mastered. No such conclusive theory presently exists. However, there are some concepts and observations that warrant further investigation.

Obviously, if gravity could be selectively modified without the expenditure of high energy, it could lead to forms of transportation that are very energy efficient.

This section presents a sampling of such breakthrough physics concepts.

4.3.1 Background

NASA-LaRC requested that MSE comment on how nonelectromagnetic waves (gravity waves are one example) may possibly be used for communications, imaging, and propulsion applications. Such questions are obviously in the realm of fundamental science; however, it is believed the answers will lead to practical breakthroughs in areas including air and space transportation.

4.3.2 Gravity and Gravitational Waves

The first topic addressed in this section is that of gravity and gravitational waves (GW).

4.3.2.1–Lecture by Dr. Robert Baker Dr. Robert Baker includes a literature survey (covering 40 years) related to attempts researchers have made to generate and/or detect GWs (Ref. 42). The generation of GWs (by any nonastronomical-sized system) is expected to produce waves that would be extremely weak.

Dr. Baker proposes a third derivative approach to generating GWs. (The third derivative is the time-derivative of acceleration.) Dr. Baker's equation is:

$$P = 1.76 \times 10^{-52} (2r\Delta f_{cf}/\Delta t)^2$$

for which:

P = gravitational wave power in watts
f_{cf} = a component of centrifugal force
Δt = time interval
r = system radius

The factor of 10^{-52} illustrates the extreme weakness of GWs that would be generated (in anything less than an astronomical-sized system).

Dr. Baker discusses potential applications of high frequency gravitational waves (HFGW), which include those given below.

1) Propulsion—using HFGW beamed from a spaceship to create a distortion of spacetime, which in effect acts as a source of propulsion.

2) Communication—HFGW would use the property of penetrating matter to achieve a communication system not blocked by any depth of the Earthís crust or water. Such a communications system would obviously be useful. (Note that if matter was ***totally*** transparent to gravity waves, such a communication system would not be possible.)

3) Imaging—Dr. Baker states that others have claimed that the refractive properties of HTS materials (Section 3.3.3.1) allow HFGW to be used for imaging. (This seems to be a reference to Podkletnov's (not yet substantiated) claims that the strength of the Earth's gravity field is reduced approximately 2% above a spinning HTSC disk while the disk is also acted on by electromagnetic fields (of an unstated frequency.)

4.3.2.2–Paper by J. Cameron Mr. J. Cameron (of TDT in Huntsville, Alabama) delivered a paper explaining his concept for gravity wave propulsion at the AIAA July 2001 Joint Propulsion Conference (Ref. 43).

The important points of Mr. Cameron's paper are stated below.

1) "Gravitational wave radiation is generated by the quadrupole moment of matter that is in motion." [Whereas electromagnetic waves are radiated from an oscillating dipole, the generation of GWs requires an oscillating quadrupole that can be represented as an oscillating three-dimensional surface (e.g., a body oscillating between the shape of a sphere and the shape of an ellipsoid)].

2) Theories indicate matter that is stressed and strained will generate GW at right angles to the stress-strain vector, but the radiated power would be extremely weak ($\approx 10^{-29}$ W).

3) Mr. Cameron suggests using high-power laser diodes to photoacoustically drive thin-film resonators in order to produce GWs.

4) Mr. Cameron's first key idea is to use a ***phased array*** of many laser diodes (placed along a 1-ft piece of quartz) timed to act coherently to produce a narrow GW beam. According to equations presented by Mr. Cameron, the phase coherence and narrowness of the beam cause the beam to contain a power level of GWs greater than a kilowatt. (Actually, there are two equal power beams, one emitted from each end of the quartz rod.)

5) Mr. Cameron's second key idea is to alter pulse timing, materials, and pulse rate so the two beams are ***asymmetric***. The two diametrically opposed beams then carry different amounts of power and momentum, which means they exert ***different*** amounts of force on the opposite ends of the quartz rod. The quartz rod would then experience an ***unbalanced*** force ($\approx 10^{-5}$ N), which would be important because a propulsion system based on this phenomenon would not require propellant.

4.3.2.3–Article on the Speed of Gravity by Tom Van Flandern In his article *The Speed of Gravity – What the Experiments Say*, Mr. Tom Van Flandern states that ***experimental evidence*** shows that gravity is propagated at a velocity much greater than the velocity of light, "c" (Ref. 44). According to Mr. Van Flandern, "observational evidence and experiments" show that the force of gravity is propagated at a velocity "not less than 2×10^{10} c."

Mr. Van Flandern's background is professional astronomy. He relates that even though he was taught the Einstein ***postulate*** that nothing could have a velocity greater than that of light, he was also taught that in order to use celestial mechanics to correctly calculate the orbits of

astronomical bodies, it had to be assumed that the force of gravity was transmitted ***instantaneously***. Mr. Van Flandern has investigated this paradox and further claims that "it is widely accepted, even if less widely known, that the speed of gravity in Newton's Universal Law is unconditionally infinite." Mr. Van Flandern carefully presents and explains the following three pieces of evidence to support his claim that the force of gravity is propagated at a velocity much greater than the speed of light.

The first fact is that gravity has no "aberration." Astronomical aberration of light was discovered in 1728. Aberration is defined and its consequences are explained as given below.

1) The speed of light in a vacuum is approximately 186,000 miles per second (mi/s) or 300,000 km/s.

2) At this velocity, light requires approximately 8.3 minutes to traverse the distance from the Sun to the Earth. Thus, an observation of the Sun using visible light (or other waves in the normal electromagnetic spectrum) is seeing the Sun 8.3 minutes in the ***past***.

3) During that 8.3 minutes, the Earth (with orbital velocity approximately 18 mi/s or 30 km/s, has traversed approximately 20 arc seconds of its orbit.

4) Thus, "the true, instantaneous position of the Sun is about 20 arc seconds east of its visible position."

5) The orbital velocity of the Earth also causes star positions to be displaced from their average position by up to 20 arc seconds (depending on the orbital position of the Earth).

6) ***If*** gravity was a force that propagated at the speed of light, then aberration (analogous to the optical case) would introduce a tangential force component equal to 0.000l times the radial force component (this factor is the Earth's orbital velocity divided by the speed of light).

7) This small force, acting continuously, would cause the Earth's distance from the Sun to double in approximately 1,200 years.

8) Such an effect does not occur; therefore, gravity aberration must not exist (or is too small to measure), which proves that gravity force has a velocity much greater than light.

A second type of evidence supporting the high velocity of gravity is determined with pulsars, whose pulses provide a very precise reference system throughout the sky. Mr. Van Flandern claims that when the Earth's orbit is precisely calculated with respect to the distant pulsars, it is found that the Earth is accelerating "toward a point 20 arc seconds in front of the visible Sun, where the Sun will appear to be in 8.3 minutes. In other words, the acceleration now is toward the true, instantaneous direction of the Sun now and is not parallel to the direction of the arriving solar photons now."

Thirdly, binary pulsars (coupled by gravity) do not experience an increase in orbital speed. According to Mr. Van Flandern, this also can only be explained if gravity propagates at a velocity much faster than the speed of light. The reason is the same (lack of aberration) as applies to the Sun-Earth example explained above.

Finally, Mr. Van Flandern claims that calculations based upon binary pulsar data allow the speed of the force of gravity (whose cause is still unknown) to be determined to be equal to or greater than $2x10^{10}$ times the speed of light.

Mr. Van Flandern explains that even though the force of gravity propagates at a velocity much greater than the speed of light, GWs (caused by changes in gravitational fields), are assumed to propagate at the speed of light. However, note that the detection of such waves has never been confirmed, nor has the velocity of such waves ever been measured. It is more correct to regard the velocity of GWs (if they exist) as unknown.

4.3.3 Aharonov-Bohm Effect

Based on the mathematics of quantum theory and the ability of fundamental particles to manifest in some experiments as waves, Yakir Aharonov and David Bohm made the extraordinary hypothesis in 1959 that a ***totally shielded*** magnet could nevertheless change the phase of the electron wave function of a beam of electrons traveling in the vicinity of the magnet (Ref. 45).

In 1986, Akira Tonomura and his colleagues successfully demonstrated this effect at Hitachi Ltd. in Tokyo, Japan, by observing shifts in electron wave interference patterns for an electron beam going through a toroidal magnet that was carefully shielded so all of the magnetic field would be contained within the enclosure of the toroid. The explanation of this effect is that the magnetic ***vector potential*** of the magnetic field (more fundamental than the magnetic field) changes the momentum of the electron waves (but not their energy). The result is a phase change in the electron wave, which is observed as an interference effect with respect to part of the same electron beam that has not traveled in the vicinity of the shielded toroidal magnet.

As an analogy with the ***magnetic*** Aharonov-Bohm effect, there is an ***electrostatic*** Aharonov-Bohm effect in which the electric ***scalar potential*** (more fundamental than the electric field) can be used to influence the flow of electrons. This effect has been used to alter output voltages of electrons flowing through nanoscale semiconductor circuits.

It is important to note that the Aharonov-Bohm effect is the basis of a unique communication system patented by Dr. Harold E. Puthoff of the Institute for Advanced Studies at Austin, located in Austin, Texas (Ref. 46). The patent abstract reads, "Information that changes as a function of time is communicated from a transmitting site to a receiving site by transmitting a signal comprising scalar and vector potentials without including any electromagnetic field. The potentials vary as a function of time in accordance with the information." The patent diagrams depict alternating voltage from a signal generator coupled to two essentially square metal plates at right angles to each other and alternating current from the same signal generator coupled to an electric coil located where the two metal plates would intersect.

The receiver is ***electromagnetically shielded*** and uses a cryogenic superconductor device known as a "Josephson Junction." The Josephson Junction converts the electrostatic scalar and magnetic vector potentials that ***do*** penetrate the shielding into conventional electromagnetic waves that can then be subsequently detected by an ordinary radio receiver.

The importance of this invention is that it is a nonelectromagnetic communication system and cannot be shielded.

In response to specific questions from MSE, Dr. Puthoff stated the following:

- as the patent states, only ***potential*** is being transmitted and received;
- ***no energy*** is transferred from the transmitter to the receiver. (Energy would be the sum of the squares of the individual electrostatic and magnetic fields, and these fields cannot be transferred, as they are shielded); and
- the system has been built and tested "as part of a classified project."

4.3.4 Theoretical Electrodynamics

At the Symposium of the INE in Salt Lake City, Utah, in August 2002, Professor Domina Spencer presented a brief overview of some areas of her work in theoretical physics, which began with studies jointly conducted with her late husband (Dr. Parry Moon) at the Massachusetts Institute of Technology (MIT) 60 years ago. (Dr. Spencer now teaches at the University of Connecticut.) The focus of this work has been to understand and calculate electrical and magnetic forces between moving electrons. The important points and highlights of the work of Dr. Spencer (and Dr. Moon) can be summarized as given below.

1) Something as mundane and practical as overhead electric arc welding on a horizontal surface can be explained by these theories but not by competing theories. Dr. Spencer claims that the Spencer-Moon electrodynamic theories (but not competing theories) uniquely explain the forces that allow the molten bead of metal occurring in overhead electric arc welding on a horizontal surface to "stick" on something that is being welded. If this electrodynamic effect did not exist, overhead electric welding in this geometric configuration could not be performed.

2) Dr. Spencer claims that the molten metal flow patterns in the Hering Furnace (invented in 1916) can only be explained by the electrodynamic theories, which she co-created with her late husband.

3) The functioning of a unipolar generator is also presented by Dr. Spencer as an example of electrical technology, explainable only by the Spencer-Moon theories.

Electrodynamic theories such as those of Dr. Moon and Dr. Spencer could be important and lead to practical breakthroughs in fields of aircraft and spacecraft propulsion and advanced energy technologies because they uniquely predict experimental findings related to moving electrons.

5. Conclusions

There is now convincing evidence to support observations that water vapor emission into the atmosphere at altitudes above 25,000 ft by conventional hydrocarbon-fueled aircraft is changing climate patterns in local regions, possibly adversely through the formation of contrails. However, the extent of the effect has not been fully determined.

Starting with the guideline that any feasible approach could be investigated and considered, and the research performed to date, MSE has determined that a near-emissionless 300 passenger commercial transport aircraft capable of flying substantial distances is conceptually possible. This conclusion was reached by a logical process of eliminating approaches considered to be impractical and assuming there will be modest gains made in areas of technology such as component weight reduction, energy conversion power density, and advanced aeronautics. A numerical analysis based upon the NASA-LaRC FLOPS code, (modified for this application) was used to calculate estimated maximum ranges of the conceptual emissionless aircraft. This analysis, including the energy conversion and aerodynamic assumptions that went into the calculations as well as the calculated ranges and some of the other parameters that are code outputs, have been reported during the course of this study and included herein.

The emissionless aircraft concept developed by MSE would use a novel combination of the following technologies, all of which have been developed as hardware (to some degree):

- LH_2 fuel carried in insulated tanks;
- high temperature PSOFCs to generate electricity by combining hydrogen with oxygen from ambient air;
- bottoming cycle GTEs coupled to generators to convert heat in the fuel cell exhaust gas into additional electric power;
- ultralight, ultraefficient cryogenic electric motors, coupled to fans, to provide propulsion;
- advanced aeronautical technology to maximize the L/D ratio in order to maximize aircraft range;
- lightweight, high-strength materials to fabricate appropriate aircraft components, to minimize empty weight and therefore maximize aircraft range; and
- novel advanced, lightweight heat transfer technology to remove heat from water vapor produced during flight so that water vapor may be condensed to a liquid and stored onboard for the remainder of a flight mission.

All of the above technologies have been investigated and reported on by MSE and are included in this report.

A tentative geometric configuration of major components and systems of the emissionless aircraft was devised within the constraints of technical parameters as currently known.

If liquid water reaction product could be immediately expelled as liquid droplets of an appropriate size and temperature and would cause no adverse effects either in the atmosphere or on the ground, the resulting weight relief would greatly accelerate the project.

A number of novel concepts and systems were also investigated. Some of these are claimed to possess energy densities orders of magnitude greater than the state of the art. MSE determined that the evidence supporting such claims ranged from questionable in some cases to promising in others but that these technologies typically require extensive development before they could potentially be used in practical applications. A partial list of these include:

- LENRs;
- IEC fusion;
- nanofusion;
- Thermal Diodes;
- heat superconductivity (Supertubes); and
- SMES.

MSE also investigated even more revolutionary concepts that are currently the subject of laboratory research and may never prove to be feasible but warrant further monitoring in the event any are successfully developed. A partial list of these potential breakthrough concepts includes:

- high-voltage propulsion;
- zero-point energy;
- longitudinal electric waves; and
- gravity-related phenomena.

References

1. Stenger, Richard, *9/11 Study: Air Traffic Affects Climate*, CNN.com/SCI-TECH, posted Aug. 8, 2002.

2. Dhar, Manmohan, *Stirling Space Engine Program, Volume 1-Final Report,* NASA/CR-1999-209164, Vol. 1, Aug. 1999.

3. Dhar, Manmohan, *Stirling Space Engine Program, Volume 2-Appendices A, B, C, D,* NASA/CR-1999-209164, Vol. 2, Aug. 1999.

4. *Space Power Free-Piston Stirling Engine Scaling Study*, NASA/CR-182218, Oct. 1, 1989.

5. Coutts, Timothy J. and Mark C. Fitzgerald, "Thermophotovoltaics," *Scientific American*, pp. 90-95, Sept. 1998.

6. The JX Crystals website: www.jxcrystals.com.

7. Bushnell, Dennis, NASA Langley Research Center, *Frontiers of the "Responsibly Imaginable" in Aeronautics*, presented at Aero India, Bangalore, India, Dec. 1996.

8. Lindemann, Margrethe A., "Turbulent Reynolds Analogy Factors for Nonplanar Surface Microgeometries," *AIAA Journal of Spacecraft and Rockets*, Vol. 22, pp. 581-582, Sept.-Oct. 1985.

9. Mecham, Michael, "3M Thin Skin Tested by Airbus," *Aviation Week & Space Technology*, p. 34, Dec. 2, 1996.

10. Kramer, Brian R. et al., *Drag Reduction Experiments Using Boundary Layer Heating*, AIAA Paper, AIAA-99-0134, 1998.

11. Joslin, Ronald D., NASA Langley Research Center, *Overview of Laminar Flow Control*, NASA/TP-1998-208705, Oct. 1998.

12. Dornheim, Michael A., "Low Fatigue Material Saves Weight on A380," *Aviation Week & Space Technology*, pp. 126-128, June 18, 2001.

13. "Composite Six Times Stiffer Than Steel," *Aviation Week & Space Technology*, pp. 88-89, Oct. 15, 2001.

14. Brewer, Daniel G., *Hydrogen Aircraft Technology*, CRC Press, 1991.

15. "Boeing Plans to Select Industry Partners…," World News Roundup, *Aviation Week & Space Technology*, p. 18, Dec. 3, 2001.

16. JPL website: http://sec353.jpl.nasa.gov/apc/Chemical/00.html.

17. NASA-GRC website: http://www.lerc.nasa.gov/WWW/TU/launch/foctopsb.htm.

18. www.blacklightpower.com

19. Collins, C. B. et al., "Accelerated Emission of Gamma Rays from the 31-yr Isomer of ^{178}Hf Induced by X-Ray Irradiation," *Physical Review Letters*, Vol. 82, No. 4, January 25, 1999.

20. Turner, James E., *Atoms, Radiation, and Radiation Protection*, John Wiley & Sons, Inc., Second Edition, pp. 451-454, 1995.

21. Bussard, R.W., "Fusion as Electric Propulsion," *Journal of Propulsion and Power*, 6, 5, pp. 567-574, Sept.-Oct., 1990.

22. Bussard, R.W. and L.W. Jameson, "Inertial-Electrostatic-Fusion Propulsion Spectrum: Air-Breathing to Interstellar Flight," *Journal of Propulsion and Power*, 11, 2, pp. 365-372, 1995.

23. Burton, R. et al., *High Performance Manned Interplanetary Space Vehicle Using D-^{3}He Inertial Electrostatic Fusion*, Space Technology & Applications International Forum Conference, January 2002.

24. Miley, George H. et al., "Experimental Status and Potential Applications of a Thin-Film Low Energy Nuclear Reaction (LENR) Power Cell," *Proceedings of ICONE 8*, Baltimore, MD, April 2-6, 2000.

25. Miley, G.H., "Emerging Physics For a Breakthrough Thin-Film Electrolytic Cell Power Unit," *Proceedings of Space Technology & Applications International Forum (STAIF-99)*, Albuquerque, NM, January 31-February 4, 1999.

26. Graham-Rowe, Duncan, "Microchip Can Turn Heat into Electricity," *NewScientist*, February 5, 2002.

27. Hagelstein, P.L. and Y. Kucherov, "Enhanced Figure of Merit in Thermal to Electrical Energy Conversion using Diode Structures," *Applied Physics Letters*, Vol. 81, No. 3, July 15, 2002.

28. Qu, Yuzhi, *Superconducting Heat Transfer Medium*, U.S. Patent No. 6,132,823, October 17, 2000.

29. Wilson, Martin N., "Superconducting Magnets," Scurlock, R.G. (Ed.), *Oxford Science Publications*, 1983.

30. Furth, H.P. et al., "Production and Use of High Transient Magnetic Fields II," *The Review of Scientific Instruments*, Vol. 28, No. 11, November 1957.

31. LyTec LLC, Final Technical Report, Phase I SBIR, *Flight Weight Magnets Using Carbon Nanotubes*, Contract No. NAS8-01181, Report No. LyTec R-02-012, November 2, 2001 through March 2, 2002.

32. Valone, Thomas, *Inertial Propulsion: Concept and Experiment Parts 1 & 2.* Part 1 is the same as the paper published in the 28th Intersociety Energy Conversion Engineering Conference Proceedings, IECEC 1993, Vol. 2, pp. 303-308.

33. Thornson, *Apparatus for Developing a Propulsion Force*, U.S. Patent No. 4,631,971, Issued Dec. 30, 1986.

34. Davis, Dr. William O., "The Fourth Law of Motion," *Analog*, pp. 84-104, May 1962.

35. Grigorov et al., *Materials Having High Electrical Conductivity at Room Temperatures and Methods for Making Same*, U.S. Patent No. 5,777,292, July 7, 1998.

36. King, Moray B., *Quest for Zero-Point Energy*, Adventures Unlimited Press, Kempton, IL, 2001.

37. King, Moray B., *Tapping the Zero-Point Energy*, Adventures Unlimited Press, Kempton, IL, 2002.

38. Anastasovski, P.K. et al., "Explanation of the Motionless Electromagnetic Generator with 0(3) Electrodynamics," *Foundations of Physics Letters*, Vol. 14, No. 1, pp. 87-94, 2001.

39. Patrick, Stephen L. et al., *Motionless Electromagnetic Generator*, U.S. Patent No. 6,362,718, March 26, 2002.

40. "Aharonov-Bohm Effect," *McGraw-Hill Dictionary of Scientific and Technical Terms*, Fifth Edition, pg. 48, 1994.

41. Internet address: http://jnaudin.free.fr/html/lmdtem.htm.

42. Baker, Robert M.L., Jr., Ph.D., *High-Frequency Gravitational Waves*, Lecture Delivered to The Max Planck Institute for Astrophysics (MPA), Gauching, Germany, May 9, 2002, and The National Institute for Nuclear Physics (INFN) Genoa, Italy, May 28, 2002.

43. Cameron, J., *An Asymmetric Gravitational Wave Propulsion System*, AIAA Paper No. 2001-3913, Joint Propulsion Conference, Salt Lake City, Utah, July 8-11, 2001.

44. Internet address: http://www.ldolphin.org/vanFlandern/gravityspeed.html.

45. Imry, Yoseph and Richard A. Webb, "Quantum Interference and the Aharonov-Bohm Effect," *Scientific American*, Vol. 260, No. 4, pp. 56-62, April 1989.

46. Puthoff, Harold E., *Communication Method and Apparatus With Signals Comprising Scalar and Vector Potentials Without Electromagnetic Fields*, U.S. Patent No. 5,845,220, Dec. 1, 1998.

REPORT DOCUMENTATION PAGE

Form Approved
OMB No. 0704-0188

1. REPORT DATE *(DD-MM-YYYY)*	2. REPORT TYPE	3. DATES COVERED *(From - To)*
01- 02 - 2003	Contractor Report	

4. TITLE AND SUBTITLE
Advanced Energetics for Aeronautical Applications

5a. CONTRACT NUMBER

5b. GRANT NUMBER
NAG1-02048

5c. PROGRAM ELEMENT NUMBER

6. AUTHOR(S)
Alexander, David S.

5d. PROJECT NUMBER

5e. TASK NUMBER

5f. WORK UNIT NUMBER
282-10-01-01

7. PERFORMING ORGANIZATION NAME(S) AND ADDRESS(ES)
MSE Technology Applications, Inc.
200 Technology Way
P.O. Box 4078
Butte, MT 59702

NASA Langley Research Center
Hampton, VA 23681-2199

8. PERFORMING ORGANIZATION REPORT NUMBER
NASA-43

9. SPONSORING/MONITORING AGENCY NAME(S) AND ADDRESS(ES)
National Aeronautics and Space Administration
Washington, DC 20546-0001

10. SPONSOR/MONITOR'S ACRONYM(S)
NASA

11. SPONSOR/MONITOR'S REPORT NUMBER(S)
NASA/CR-2003-212169

12. DISTRIBUTION/AVAILABILITY STATEMENT
Unclassified - Unlimited
Subject Category 44
Availability: NASA CASI (301) 621-0390 Distribution: Standard

13. SUPPLEMENTARY NOTES
An electronic version can be found at http://techreports.larc.nasa.gov/ltrs/ or http://techreports.larc.nasa.gov/cgi-bin/NTRS
Langley Technical Monitor: Dennis M. Bushnell

14. ABSTRACT

NASA has identified water vapor emission into the upper atmosphere from commercial transport aircraft, particularly as it relates to the formation of persistent contrails, as a potential environmental problem. Since 1999, MSE has been working with NASA-LaRC to investigate the concept of a transport-size emissionless aircraft fueled with liquid hydrogen combined with other possible breakthrough technologies. The goal of the project is to significantly advance air transportation in the next decade and beyond. The power and propulsion (P/P) system currently being studied would be based on hydrogen fuel cells (HFCs) powering electric motors, which drive fans for propulsion. The liquid water reaction product is retained onboard the aircraft until a flight mission is completed. As of now, NASA-LaRC and MSE have identified P/P system components that, according to the high-level analysis conducted to date, are light enough to make the emissionless aircraft concept feasible. Calculated maximum aircraft ranges (within a maximum weight constraint) and other performance predictions are included in this report. This report also includes current information on advanced energy-related technologies, which are still being researched, as well as breakthrough physics concepts that may be applicable for advanced energetics and aerospace propulsion in the future.

15. SUBJECT TERMS
Aerodynamics; Aircraft propulsion and power; Propellants and fuels; Energy production and conversion; Environment pollution; Meteorology and climatology; Physics

16. SECURITY CLASSIFICATION OF:			17. LIMITATION OF ABSTRACT	18. NUMBER OF PAGES	19a. NAME OF RESPONSIBLE PERSON
a. REPORT	b. ABSTRACT	c. THIS PAGE			STI Help Desk (email: help@sti.nasa.gov)
					19b. TELEPHONE NUMBER *(Include area code)*
U	U	U	UU	105	(301) 621-0390